A bio-hybrid DNA rotor–stator nanoengine that moves along predefined tracks

Julián Valero[1,2], Nibedita Pal[3], Soma Dhakal[3,4], Nils G. Walter[3] and Michael Famulok [1,2]*

Biological motors are highly complex protein assemblies that generate linear or rotary motion, powered by chemical energy. Synthetic motors based on DNA nanostructures, bio-hybrid designs or synthetic organic chemistry have been assembled. However, unidirectionally rotating biomimetic wheel motors with rotor–stator units that consume chemical energy are elusive. Here, we report a bio-hybrid nanoengine consisting of a catalytic stator that unidirectionally rotates an interlocked DNA wheel, powered by NTP hydrolysis. The engine consists of an engineered T7 RNA polymerase (T7RNAP-ZIF) attached to a dsDNA nanoring that is catenated to a rigid rotating dsDNA wheel. The wheel motor produces long, repetitive RNA transcripts that remain attached to the engine and are used to guide its movement along predefined ssDNA tracks arranged on a DNA nanotube. The simplicity of the design renders this walking nanoengine adaptable to other biological nanoarchitectures, facilitating the construction of complex bio-hybrid structures that achieve NTP-driven locomotion.

Nature provides several examples of highly effective biological motors that consume chemical energy for rotation, movement or power transmission[1]. Living organisms require motors for essential functions such as cargo transport, cell locomotion and division, chemotaxis, ATP synthesis[2] or flagellar movement[3], with the latter two consisting of interacting stator and rotor components that generate torque. Despite the complexity of most natural motors, it has been possible to assemble artificial motor systems by employing DNA nanostructures[4–7] or bio-hybrid designs[8–10], or based entirely upon synthetic organic chemistry[11–13]. Apart from synthetic small-molecule motors[14], however, unidirectionally rotating biomimetic wheel motors with rotor–stator units that consume chemical energy have not yet been described.

Here, we describe a supramolecular bio-hybrid rotor composed of a catalytic stator that unidirectionally rotates an interlocked double-stranded (ds) DNA wheel, powered by the hydrolysis of nucleotide triphosphates (NTPs). The design of the engine consists of a static building block with an engineered T7 RNA polymerase (T7RNAP) fused to a DNA-binding Zn²⁺-finger (ZIF) motif (T7RNAP-ZIF). T7RNAP-ZIF attaches firmly to a dsDNA nanoring, thus constituting a stator unit that is interlocked with a rigid rotating dsDNA wheel (the rotor unit) to form a catenane. The wheel motor operates continuously and thereby produces long, repetitive RNA transcripts by rolling circle transcription (RCT). Because this RNA byproduct remains attached to the bio-hybrid nanoengine, it can be used to guide the movement of the entire engine along predefined single-stranded (ss) DNA tracks arrayed on a DNA nanotube.

Design, assembly and characterization of the nanoengine

Integrating T7RNAP as a power generator for our wheel motor offered several design opportunities (Fig. 1). First, because torque generation requires defined stator–rotor interactions, T7RNAP had to be firmly attached to a stationary chassis, otherwise the rotational motion would become undefined, as is the case in classical

RCT[15], where either the polymerase or the circular template can be regarded as the moving part. Second, interlocking of the rings, each containing a different recognition motif for T7RNAP-ZIF, promotes cooperative binding, reducing the probability of polymerase detachment and thereby boosting processivity. Third, we integrated means for quantification of the motor rotation (Fig. 1).

The stator chassis is a 168-base-pair (bp) dsDNA circle containing the 10 bp sequence that binds the three Zn²⁺-finger motif of the Zif268 protein (Fig. 1a)[16]. This sequence has previously been used for site-specific positioning of Zn²⁺-finger-containing proteins on DNA origami[17,18]. Here, it serves as a high-affinity docking site for a T7RNAP N-terminally fused with Zif268 (T7RNAP-ZIF; Supplementary Fig. 1a). The rotor ring contains a T7 promoter (red) and a sequence that allows hybridization of a complementary molecular beacon (MB, green) to the RNA transcript for fluorescence monitoring of product formation. Assembly of the interlocked catenane was performed as described previously (Supplementary Figs. 1b and 2 and Supplementary Table 1)[19]. Gel electrophoresis showed that the mechanically interlocked catenane^mec migrates slightly faster than the corresponding hybridized catenane^hyb (Supplementary Fig. 1c, Cat^hyb), consistent with previous observations on similar DNA nanostructures[19–22].

The Zif268 fragment of T7RNAP-ZIF binds sequence-specifically to the 168 bp stator ring with a dissociation constant K_d of 1.6 nM, as determined by surface plasmon resonance (SPR) (Supplementary Fig. 1d), whereas the T7RNAP fragment recognizes the T7 promoter in the 126 bp rotor ring, completing the bio-hybrid nanoengine. In vitro transcription using a non-interlocked circular DNA template showed that T7RNAP-ZIF performs just like wild-type (wt) T7RNAP (Supplementary Fig. 1e), thus binding to its corresponding T7 promoter, which dictates the direction of transcription on the circular dsDNA template. Atomic force microscopy (AFM) of the isolated catenane (Fig. 1b), T7RNAP-ZIF (Fig. 1c) and the assembled nanoengine (Fig. 1d and Supplementary Figs. 3 and 4) demonstrated the structural integrity
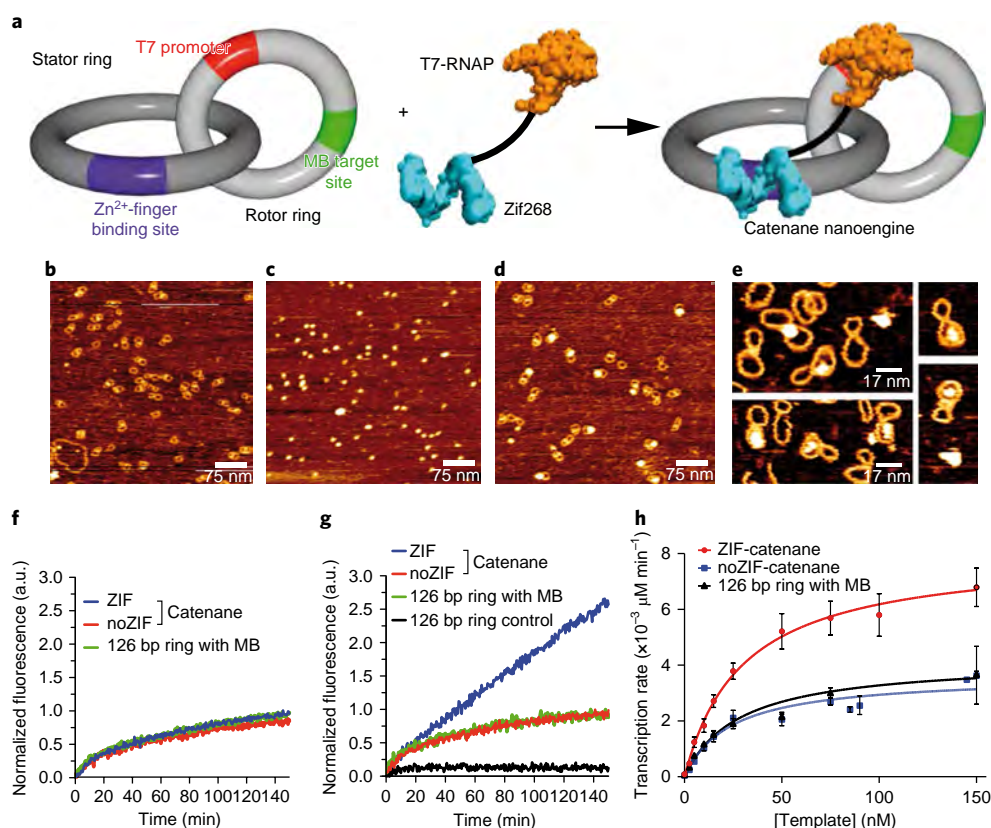
Fig. 1 | Assembly of the DNA catenane rotary motor. a, Schematic representation of T7RNAP-ZIF protein assembled on the DNA catenane. **b–d**, AFM imaging (in tapping mode in air) of the catenane (**b**), T7RNAP-ZIF (**c**) and the catenane–T7RNAP-ZIF assembly (**d**). **e**, High-resolution atomic force microscopy images of the catenane–T7RNAP-ZIF nanoengine in tapping mode in liquid. **f,g**, Fluorescence kinetics of the RCT performed by the catenane (blue), the control catenane lacking the Zif268 binding site (red), a positive control double-stranded 126 bp ring (green) and a negative control 126 bp ring (black) in the presence of wild-type T7RNAP (**f**) and T7RNAP-ZIF (**g**), respectively. **h**, Transcription rate analysis at different concentrations of catenane (red), catenane control (blue) and ring positive control (black) after 150 min of transcription. Data presented as mean ± standard deviation (s.d.), $n = \geq 5$. MB, molecular beacon.

of each sample. Most T7RNAP-ZIF molecules co-localize with the catenane, indicating effective complex formation (Fig. 1d,e). In contrast, without the ZIF-binding DNA sequence (noZIF-catenane, Supplementary Fig. 1f,i), most mica-deposited T7RNAP-ZIF molecules were washed away, or did not co-localize with catenane molecules (Supplementary Fig. 1i, right panel). MB fluorescence analysis of the RNA generated in situ by the wtT7RNAP (Supplementary Fig. 5) revealed comparable transcription activity (Fig. 1f) for the ZIF-containing catenane (ZIF-catenane, Fig. 1a), the noZIF-catenane and the 126 bp ring control containing the MB (Supplementary Fig. 1f,g). Conversely, when using T7RNAP-ZIF, the ZIF-catenane showed a linear increase of RCT during the entire 160 min time course (Fig. 1g, blue), whereas the transcription levels of the noZIF-catenane and MB-containing 126 bp ring controls (Fig. 1g, red and green) were similar to those of T7RNAP on the ZIF-catenane (Fig. 1f). A 126 bp ring lacking the MB-binding site (Supplementary Fig. 1h) showed negligible fluorescence (Fig. 1g, black). Increasing amounts of linear dsDNA containing the ZIF motif (Supplementary Fig. 1d) efficiently competed for T7RNAP-ZIF, decreasing the RCT levels (Supplementary Fig. 1j, blue) to those of the noZIF-catenane (Supplementary Fig. 1j, red). Transcription rate constants measured at different concentrations of catenane and ring-templates (Fig. 1h) confirmed the elevated RCT efficiencies of the ZIF-catenane compared to controls. Taken together, these results support the formation of the fully functional nanoengine as designed.

MB calibration and RCT kinetics

We next calibrated the MB fluorescence signal using its complementary DNA (cDNA) sequence, plotting fluorescence levels against increasing cDNA concentrations (Supplementary Fig. 6), which allowed us to quantify the RNA transcribed from the ZIF-catenane, noZIF-catenane and MB-ring at 5 and 10 nM template concentrations (Supplementary Fig. 7). This analysis revealed speeds of 0.23 rotations per minute (r.p.m.) or 0.48 nucleotides per second (nt s^{-1}) for the ZIF-catenane, 0.08 r.p.m. (0.17 nt s^{-1}) for the noZIF-catenane, and 0.11 r.p.m. (0.23 nt s^{-1}) for the MB-ring control (Supplementary Fig. 6). The cooperative binding of T7RNAP-ZIF to the ZIF-catenane results in an increased transcription efficiency compared to T7RNAP, the noZIF-catenane or the MB-ring. The overall reduced transcription rate observed for our circular dsDNA rings has previously been described for other tightly looped DNA rings compared to linear templates[23]: an elongating T7RNAP on a highly bent circular DNA template similar to ours shows highly unidirectional processivity over ~8,000 bp, or ~40 and ~60 cycles for the 210 bp and 126 bp rotors, respectively. Together, our data suggest that the stator-bound T7RNAP-ZIF drives the unidirectional rotation of the rotor.

Single-molecule FRET studies

To assess the rotary motion of individual nanoengines, we conceived a series of single-molecule fluorescence resonance energy transfer (smFRET) experiments. The design required labelling[24] of
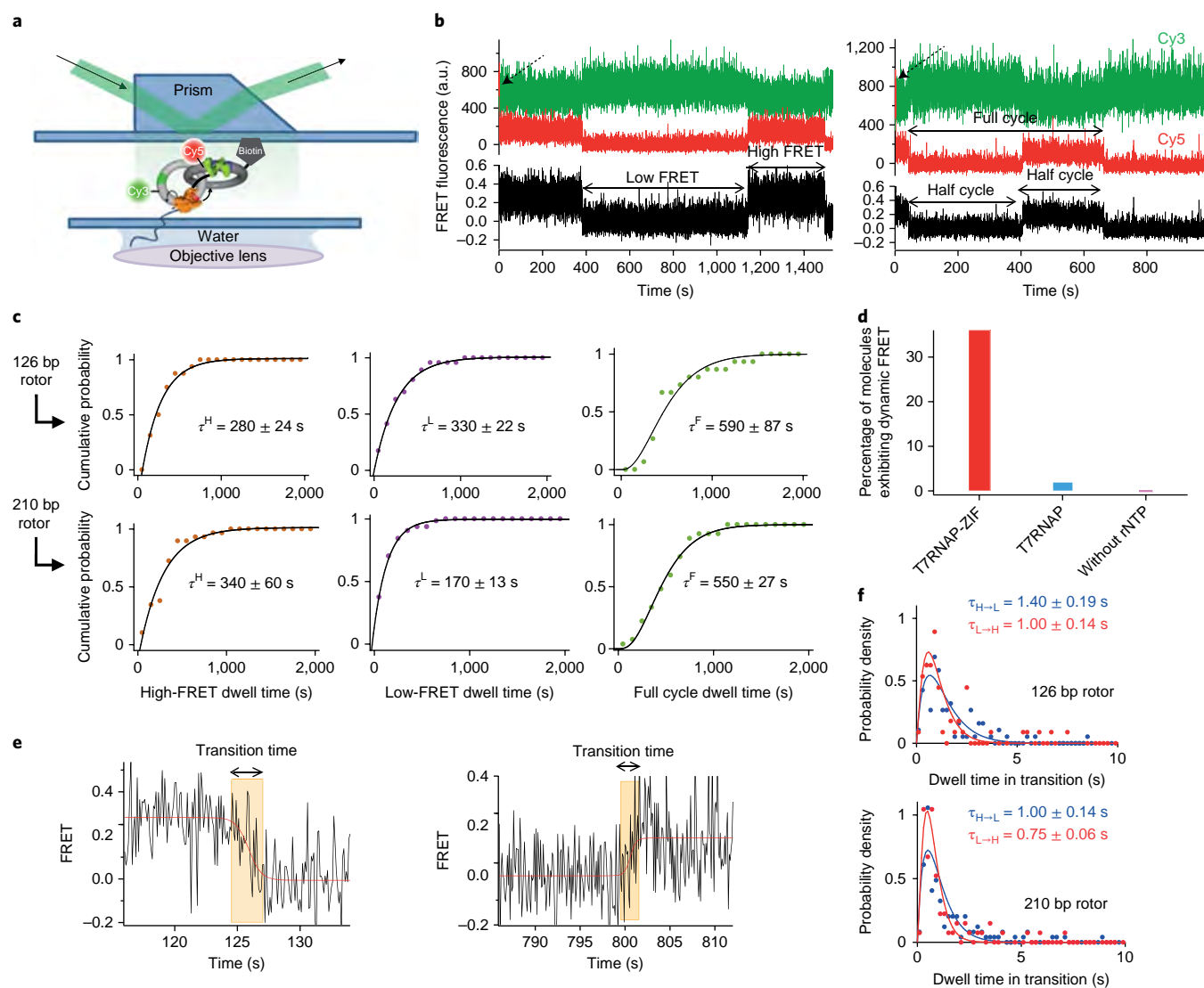
Fig. 2 | Single-molecule FRET studies of the DNA catenane rotatory motor. a, Schematic representation of the experimental set-up used for smFRET studies. **b**, Representative dynamic trajectories from smFRET experiments showing low- and high-FRET states (left) and full and half transcription cycles (right). Green and red lines represent the fluorescence intensity of the Cy3 donor and Cy5 acceptor, respectively, and the black line represents the resulting FRET signal. The presence of Cy5 was confirmed at the very beginning of data collection by direct excitation with a 640 nm laser (black broken arrow). **c**, Transcription cycle kinetics were obtained from the smFRET data for the nanoengine with the 126 bp rotor (upper panels) and the 210 bp rotor (lower panels) by exponential fitting of the cumulative distribution of the dwell times in the high- and low-FRET states (left and middle panels), whereas that for the full transcription cycle (right panels) was calculated from a fit with a Gamma function assuming n irreversible steps with identical rates. The dwell times were corrected for the limited observation time window. The dwell times in the high- and low-FRET states were calculated from 15–44 molecules. **d**, Percentage of molecules exhibiting dynamic FRET in the presence of T7RNAP-ZIF (red) and wtT7RNAP (blue), and in the absence of NTPs (magenta). **e**, Representative trajectories of the transition times from the high- to low-FRET state and vice versa (left and right, respectively). The time each transition covers was extracted, and probability densities of these transition times were calculated. Red lines serve as visual guides. **f**, Probability density distributions of the transition times obtained from 30 and 90 smFRET trajectories for catenanes with the 126 bp rotor and the 210 bp rotor, respectively, were fitted with Gamma functions to obtain the underlying time constants.

the non-coding strands of rotor and stator with a donor Cyanine 3 (Cy3) and an acceptor Cyanine 5 (Cy5) FRET pair, respectively. For surface immobilization of the nanoengine, the stator ring was modified with a protruding 5′-biotinylated dsDNA strand (Fig. 2a and Supplementary Fig. 8a–c). During rotation of the rotor over the stator ring, the relative distance between the fluorophores changes periodically, generating an oscillating FRET signal that we monitored using total internal reflection fluorescence microscopy (TIRFM, Fig. 2a). The oscillation frequency should reflect the rotational cycle and therefore should help assess the rotational frequency of an individual nanoengine. Indeed, smFRET time traces during

transcription showed periodic oscillatory FRET signals with donor and acceptor intensities changing in an anti-correlated fashion (Fig. 2b and Supplementary Fig. 9). Kinetic analysis of the full FRET cycles (Fig. 2c, upper right; for details see Methods), which each entail a dwell time in the high-FRET state (Fig. 2c, upper left panel) and one in the low-FRET state (Fig. 2c, upper middle panel), yielded an average rotation time of 590 ± 87 s (0.10 r.p.m.), consistent with the sum of the low- and high-FRET half-cycle dwell times analysed separately (610 ± 33 s). The average r.p.m. of 0.10 (0.21 nt s⁻¹) determined by smFRET matches, within twofold, the value obtained by bulk fluorescence, consistent with the difference
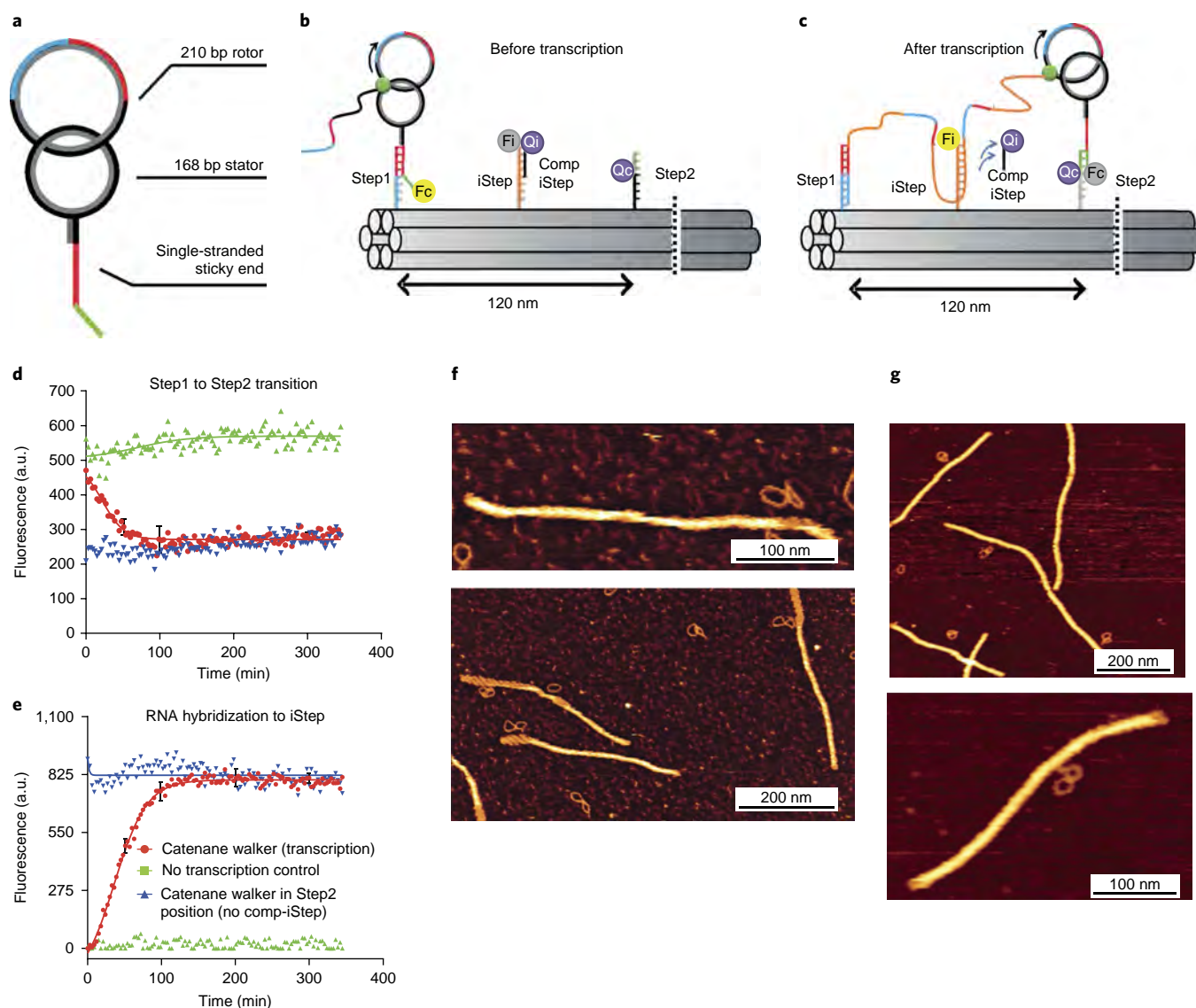
Fig. 3 | The nanoengine moves along predefined tracks. a, Scheme of the DNA catenane walker bearing a single-stranded sticky end for specific hybridization to Step1 or Step2 on a predefined DNA path. **b,c**, Scheme of the working principle of the DNA catenane walker on a six-helix-bundle DNA origami path before (**b**) and after (**c**) transcription. Fc: TAMRA; Fi: Cy5; Qi and Qc: Black hole quencher 2 (BHQ2). Green circle: T7RNAP-ZIF. **d,e**, Kinetic fluorescence analysis of the catenane:DNA path assembly in the presence or absence of transcription (red and blue lines, respectively) and the corresponding controls (green lines) for the TAMRA fluorophore (Fc) attached to the DNA walker (**d**) or the Cy5 fluorophore (Fi) attached to the intermediate step (**e**). Data are presented as mean ± s.d. $n = 2$. **f,g**, AFM imaging in tapping mode in liquid of the DNA catenane walker attached to the initial Step1 (**f**) and final Step2 (**g**) positions of the DNA origami path.

in temperature of the two experiments (25 °C and 37 °C, respectively; Supplementary Fig. 8d).

The fraction of DNA nanoengines exhibiting these dynamic FRET transitions was more than 35% (Fig. 2d), attesting to a reasonable assembly yield. This percentage dropped to 2% when T7RNAP instead of T7RNAP-ZIF was used, and was <1% in the absence of NTPs (Fig. 2d), with the remaining traces showing either zero or static FRET throughout, demonstrating that unidirectional rotation is enabled only on T7RNAP-ZIF-based transcription. The T7RNAP transcription control produced a static average FRET signal close to zero, consistent with random Brownian motion of one ring versus the other as the FRET pairs can move arbitrarily through the interlocked space in the absence of the ZIF-based stator attachment, with an average distance of 15.9 nm, far beyond the FRET detection range of up to ~10 nm (Supplementary Fig. 10).

Similarly, in a T7RNAP-ZIF control experiment without NTP, zero FRET trajectories were observed (Supplementary Fig. 11); transition occupation density plots (TODPs) of the experiments without and with NTPs illustrate the dynamic transitions only in the latter case (Supplementary Fig. 12).

It was previously found that T7RNAP transcription accelerates with decreasing ring strain[23]. We therefore performed smFRET experiments using a 210 bp rotor catenane instead of the 126 bp rotor. Although the average full rotation time of the 210 bp rotor remained almost unchanged (550 ± 27 s ≈ 0.11 r.p.m., Fig. 2c lower panels), the nucleotide incorporation rate was 1.8-fold higher (0.38 nt s^{-1}, Fig. 2c, lower panels) than that of the 126 bp rotor, as expected. When detected by MB fluorescence the 210 bp rotor catenane similarly showed 2.8-fold faster nucleotide incorporation than the 126 bp rotor (Supplementary Fig. 8e).
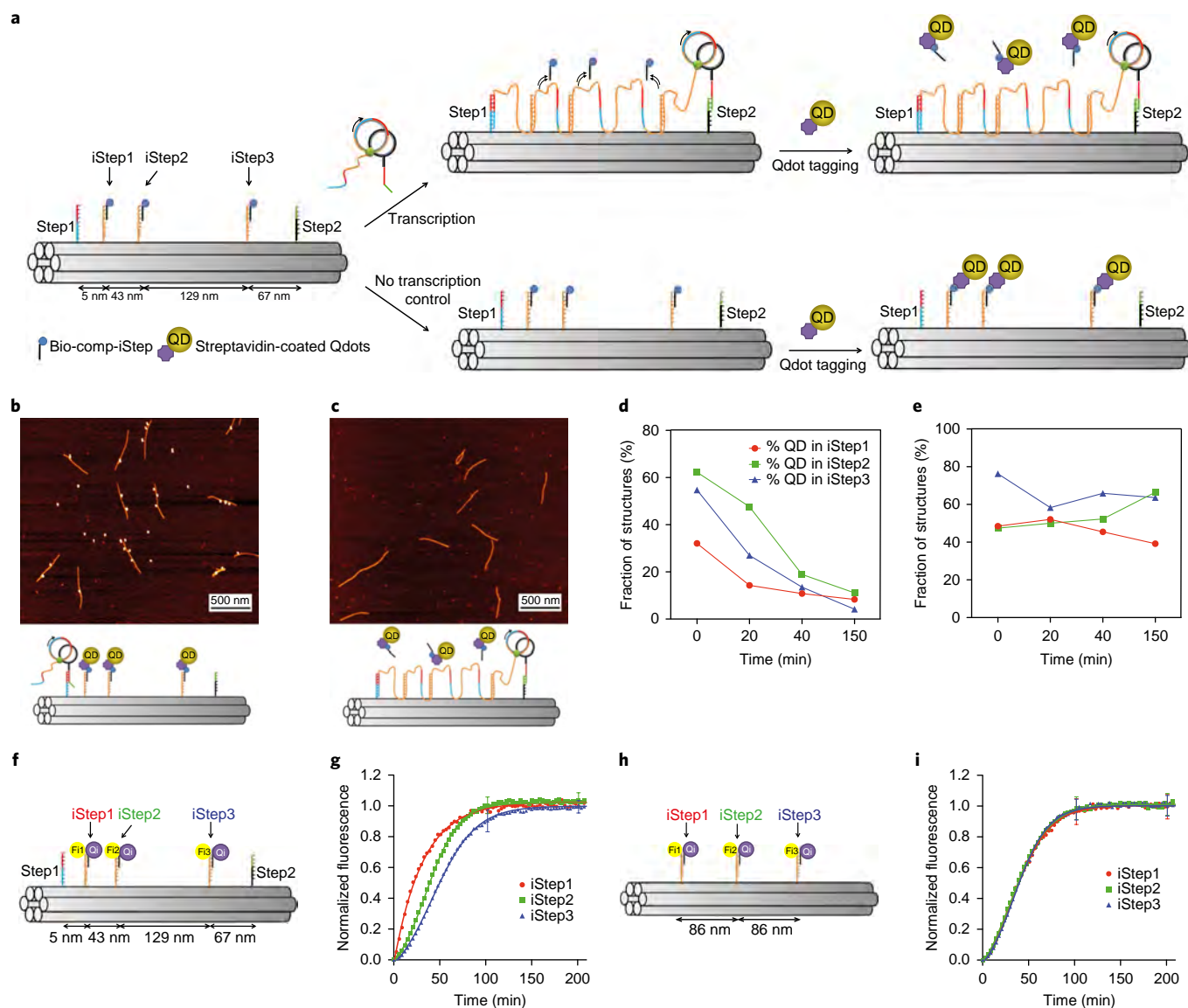
Fig. 4 | Analysis of the RNA sequential hybridization to iSteps during RCT of the catenane walker. a, Scheme of the origami design, the position and relative distances between iSteps for Qdot tagging. After incubation (37 °C) at different time points in the presence or absence (no transcription control) of the catenane nanoengine, samples were tagged with strep-Qdots and analysed by AFM. **b,c**, Overall AFM images of the origami tagged with Qdots in the presence of the catenane walker before (**b**, $n = 443$) and after (**c**) transcription. **d,e**, Qdot occupancy for each origami position at 0, 20, 40 and 150 min on an average of $n = 76$ structures for each time point in the presence (**d**) or absence (non-transcription control) (**e**) of the catenane walker. **f**, Representation of the DNA origami path labelled with three different fluorophores for each iStep position (Fi1:HEX; Fi2:Cy5; Fi3:Texas Red). **g**, Fluorescence kinetic data of the RNA hybridization to iStep1 (red), iStep2 (green) and iStep3 (blue) positions upon RCT of the catenane walker. Data are presented as mean ± s.d. $n = 4$. **h**, Representation of corresponding DNA origami control having equidistant iSteps and lacking Step1 and Step2 (Fi1:HEX, Fi2:FAM, Fi3:Cy5). **i**, Fluorescence kinetic data of the RNA hybridization to iStep1 (red), iStep2 (green) and iStep3 (blue) positions in a control DNA origami lacking Step1 and Step2 (**h**), upon RCT of the catenane walker. Half-life (τ) values were obtained by exponential fitting of the kinetic fluorescence data. Data are presented as mean ± s.d. $n = 4$.

In our smFRET traces of both the 126 bp and 210 bp rotors, we observed multiple transitions (Supplementary Fig. 9), representative of repetitive transcription cycles. For the 210 bp rotor, 43% of smFRET trajectories showed more than one and a half full transcription cycles before photobleaching, compared to 28% for the 126 bp rotor (Supplementary Fig. 13). This observation supports the notion that dissociation of both ZIF and T7RNAP is negligible within our long observation time window (~20 min). It is also consistent with the known high processivity of an elongating T7RNAP on a highly bent circular DNA template[23]. This high processivity is probably further enhanced by the tight binding of ZIF with a known dissociation rate constant of $2 \times 10^{-4}\,\text{s}^{-1}$ (ref. [25]). This high processivity reaches far beyond our smFRET observation window of just a few cycles.

The smFRET trajectories showed strikingly gradual, monotonous changes when transitioning from the high- to the low-FRET state and vice versa (Fig. 2e and Supplementary Fig. 14). The probability densities of the resulting transition times were not single-exponential, suggesting that more than one rate constant arises from the underlying molecular processes (Fig. 2f). This observation fits the facts that a single NTP incorporation itself involves multiple steps, including DNA unwinding, NTP binding, a conformational
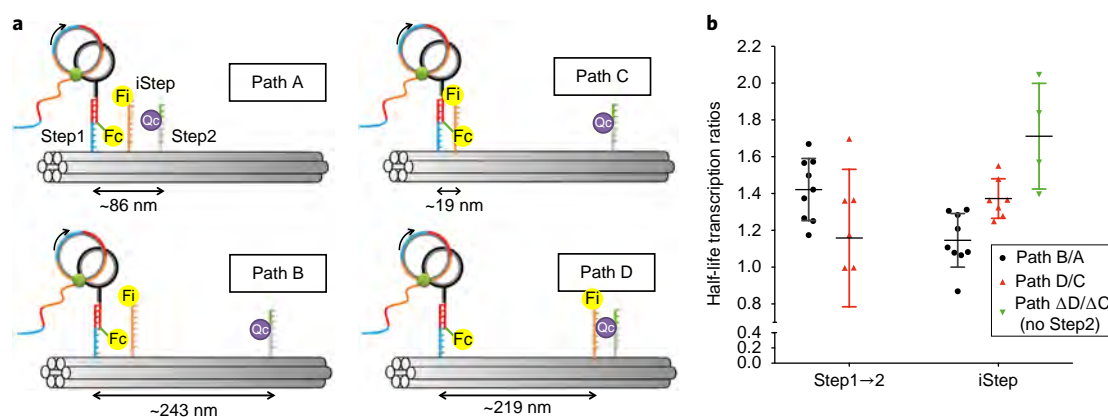
Fig. 5 | Kinetics of nanoengine walking on a path with varying distances between steps. a, Schematic representation of different six helix-bundle DNA origami paths used to evaluate the kinetics of the catenane walker by varying the relative distances between iSteps and Step2 with respect to initial Step1. **b**, Half-life transcription ratios of the Step1→2 transition and the RNA hybridization to iStep measured for different origami paths. Half-life (τ) values were calculated by exponential fitting of the kinetic fluorescence data. Data are presented as mean ± s.d. $n = 9$ for paths A and B, $n = 7$ for paths C and D and $n = 4$ for paths ΔC and ΔD.

change upon pyrophosphate release, and enzyme translocation, and that it may take multiple NTP incorporations to move the fluorophores out of or into FRET distance. To extract the number of steps involved, we fitted the probability densities with Gamma functions and obtained 2.3 steps for the 126 bp rotor and 2.6 steps for the 210 bp rotor, with transition times of ~1 s in both cases (Fig. 2f and Supplementary Table 2). The similar transition rates and general symmetry of the high-to-low and low-to-high FRET transitions (Supplementary Fig. 14) support that they reflect the action of a processive T7RNAP rather than mere Brownian rotation. Given that our full cycle times predict an NTP incorporation rate of ~0.2–0.5 s^{-1}, this leaves two possible interpretations—our Gamma function steps represent the sub-steps of a single NTP incorporation, or elongation is fast where the fluorophores leave and enter FRET distance but is slowed at other segments of the rotation, such as when topological or sterical stress is encountered. Given that previous measurements of T7RNAP on similarly bent, uncatenated substrates found an incorporation rate of ~4 nt s^{-1} at 37 °C (ref. [23]), we favour the model wherein our Gamma function steps relate to the number of NTP incorporations needed to bring the fluorophores out of or into FRET range, and an occasional topological strain release slows the cycle elsewhere. It may also be possible that the donor fluorophore and the promoter segment slow down the rotation, explaining the slow progress in the high and low FRET states. Taken together, our single-molecule results strongly support the NTP-fuelled unidirectional rotation of the rotor in the fully assembled DNA nanoengine.

Nanoengine-based walker design

Transcription by T7RNAP-ZIF generates a long, repetitive RNA transcript encoded by the rotor ring template, which remains bound to the nanoengine and can be harnessed to guide the movement of the nanoengine along predefined DNA tracks. We used the 210 bp ring as the rotor and added an ssDNA branch with two different domains (Fig. 3a, red and green line, bottom, Supplementary Fig. 15) to the stator ring, to allow hybridization of the nanoengine to two distinct complementary ssDNAs, Step1 and Step2 (Supplementary Fig. 16). The path consists of a rigid DNA-origami nanotube containing different protruding ssDNA sequences serving as steps for hybridization of the nanoengine at various stages of transcription (Fig. 3b,c, Supplementary Figs. 17 and 18, Supplementary Table 3). Spatiotemporally controlled strand-displacement reactions and hybridization of the

RCT-generated RNA to the protruding steps are expected to guide the motion of the nanoengine along the path. Prior to transcription, the nanoengine preferentially hybridized to Step1 (Fig. 3b, red). Upon transcription, the growing RNA strand is expected to displace it from Step1 by forming a thermodynamically more stable DNA/RNA heteroduplex over the entire Step1 sequence (Fig. 3b,c, red/blue). As transcription proceeds, the growing RNA can eventually reach the intermediate Step(s) (iStep). Once a sufficient length of RNA is produced, the nanoengine finally is expected to reach Step2 (Fig. 3c), located 120 nm from Step1. iSteps serve as additional anchoring points that assist in guiding the nanoengine along the path, thereby endowing it with processivity. To monitor this directed locomotion, we labelled the 5′-position of the catenane's single-stranded sticky end with TAMRA (5-carboxytetramethylrhodamine) (Fc, Fig. 3b,c). Accordingly, when reaching the quencher-labelled (Qc) Step2 the Fc fluorescence is quenched (Fig. 3d, red). By contrast, fluorescence remained unchanged (Fig. 3d, blue) both in the non-transcription control and in a control where the catenane was hybridized to Step2 by blocking Step1 (Fig. 3d, green).

In parallel, the iStep was labelled with a Cy5 fluorophore (Fi) quenched by a complementary oligonucleotide (comp-iStep) bearing quencher BHQ2 (Qi). RNA hybridization displaces comp-iStep Cy5 and fluorescence increases (Fig. 3e, red) to the level of a control experiment lacking comp-iStep (Fig. 3e, blue). The fluorescence signal of the non-transcription control remained quenched (Fig. 3e, green).

Preferential binding of the catenane to Step1 prior to transcription was further confirmed by high-resolution (HR)-AFM (Fig. 3f and Supplementary Fig. 19). When mimicking the presence of the transcribed RNA by adding a release oligodeoxynucleotide (ODN) (RO) that blocks Step1, the catenane selectively hybridized to Step2 (Fig. 3g and Supplementary Fig. 19). Similarly, AFM analysis after transcription showed the catenane positioned on Step2 (Supplementary Fig. 20), consistent with the fluorescence experiments (Fig. 3d,e).

Walking of the nanoengine

To investigate binding of the RCT-produced RNA to the iSteps, we assembled a path containing three iSteps located ~5, 48 and 177 nm from Step1. By displacing biotinylated complementary iSteps (bio-comp-iSteps) that could be detected by tagging with streptavidin-coated quantum dots (Qdots), we were able to monitor

RNA attachment to the different iSteps by AFM. The fraction of iSteps occupied with Qdots should decrease gradually during RCT as the transcribed RNA displaces the bio-comp-iSteps (Fig. 4a). Before transcription, an average of ~51% of all available positions had a Qdot attached (Fig. 4b), consistent with previously reported efficiencies[26]. The distinct positioning of the iSteps allowed their discrimination, facilitating the assessment of bio-comp-iStep attachment at each site. AFM analysis of the path before and after transcription revealed efficient displacement of each bio-comp-iStep upon transcription, as visualized by the absence of Qdot tagging (Fig. 4b,c). By counting the number of attached Qdots for each iStep at different time points we verified that Qdot occupancy progressively decreased during transcription (Fig. 4d, Supplementary Figs. 21–25 and Supplementary Tables 4 and 5), but remained stable in the absence of the catenane walker (Fig. 4e and Supplementary Figs. 26–29). Similar results were obtained with the 126 bp rotor catenane walker (Supplementary Figs. 21b–d, 30–33).

Each iStep was then labelled with a different fluorophore (Fig. 4f) to determine the half-lives τ for the RNA hybridization to each individual iStep by progressive release of quencher-labelled comp-iSteps (Fig. 4g). The τ values were 25 ± 4 min (iStep1), 32 ± 6 min (iStep2) and 40 ± 7 min (iStep3), consistent with the expectation that the nanoengine directionally walks from one end to the other. In contrast, a control path lacking Step1 and Step2 with the three iSteps equidistantly positioned at 86 nm (Fig. 4h,i) showed identical half-lives of 36 ± 11 min for all iSteps, reflective of the random attachment of the RCT transcript upon loss of spatiotemporal control due to diffusion of the nanoengine in solution. These results confirmed progressive and highly processive walking of the nanoengine only if initially attached to Step1.

Walking kinetics and processivity

To further study the kinetics and processivity of the nanoengine, we assembled tracks that contained a single iStep at varying positions between the two Steps (Fig. 5a). The catenane, all iSteps and Step2 were labelled with fluorophores and quenchers, respectively, as before (Fig. 3b), to monitor τ of the Step1→2 transition and RNA binding to the iSteps. We first assembled paths A and B with distances between Step1 and Step2 of 86 nm and 243 nm, respectively (Fig. 5a). In both paths, the distance between Step1 and the iStep was 48 nm. The value of τ of the Step1→2 transition was ~40% slower in path B than in A (half-life ratio $\tau_{(B/A)} \sim 1.4$, Fig. 5b), whereas the iSteps were reached almost simultaneously with $\tau_{(B/A)}$ close to 1 ($\tau_{(B/A)} \sim 1.1$). In paths C and D, Step2 was at the same distance from Step1 but the iSteps were placed 19 nm and 219 nm from Step1. Here, $\tau_{(D/C)}$ for the Step1→2 transition was ~1.0, while the comp-iStep displacement was 30% slower for path D than for C ($\tau_{(D/C)} \sim 1.3$). These ratios are consistent with the expected dependence of walker kinetics on the distance between steps, strongly supporting processive nanoengine walking rather than detachment and random diffusion to another path.

For the Step1→2 transition, paths C and D showed average half-lives of $\tau_C = 21 \pm 11$ and $\tau_D = 22 \pm 10$ min, whereas the half-lives for reaching the iStep were $\tau_C = 32 \pm 10$ and $\tau_D = 43 \pm 13$ min. The average Step1→2 transition speed in these paths was ~0.2 nm s^{-1}. Although still slower than the biological motors kinesin or dynein, the nanoengine is among the fastest DNA nanowalkers described so far[27–31]. The slower kinetics for RNA hybridization to the iSteps compared to the Step1→2 transition may be due to differences in the kinetics of strand displacement and hybridization. RNA binding to the iSteps involves displacement of the quencher-labeled comp-iStep, a process that can considerably slow down the kinetics[32]. Strand-displacement kinetic control experiments independent of RCT and the relative positioning of the catenane and the steps on the path (Supplementary Fig. 34a) showed that the average half-life for the Step1→2 transition was 0.7 ± 0.2 min, whereas the displacement

of comp-iStep from iStep was ~10-fold slower (6.5 ± 1.7 min, Supplementary Fig. 34b,c). These data support the faster kinetics observed with the nanoengine for the Step1→2 transition compared with the displacement of comp-iStep from iStep. The hybridized comp-iStep only serves the purpose of tracking the nanoengine's walking. In absence of comp-iStep, RNA binding to the iSteps should occur before the walker reaches Step2.

To study the kinetics and processivity of RNA hybridization to the iStep without the influence of Step2 we assembled paths ΔC and ΔD lacking Step2. The half-life kinetics of comp-iStep displacement in path ΔD was ~70% slower than in path ΔC (Fig. 5b, green; $\tau_{(\Delta D/\Delta C)} \sim 1.7$, $\tau_{\Delta C} = 38 \pm 8$ and $\tau_{\Delta D} = 66 \pm 24$ min). Due to its proximity to the iStep, Step2 in path D can act as an anchoring point for catenane walker hybridization, synergistically favouring the RNA interaction with the corresponding iStep ($\tau_D = 43 \pm 13$ min versus $\tau_{\Delta D} = 66 \pm 24$ min). These results indicate that the relative positioning of Steps 1 and 2, as well as the location and number of iSteps, can be used to rationally modulate the nanoengine's walking kinetics and processivity (Fig. 5).

Conclusion

The nanoengine described here constitutes a unidirectionally rotating molecular motor fuelled by chemical energy that employs an unprecedented autonomous walking mechanism. Its guided walking depends on interlocking of the stator with the rotor ring to allow its free movement during RCT on the one hand, and mechanical anchoring of the entire nanoengine to the programmable path on the other. The straightforward design of this nanoengine differs from synthetic walkers created to date[12,33], including molecules that walk step by step along predefined tracks[34], convert light[35], electricity[36], fuel/antifuel inputs[37–39] or cleavage energy[40,41] into unidirectional motion, or transmission of force[42]. Our walker is among the fastest artificial molecular walkers described so far[43–46]. A compelling feature of the design is the fact that a multistep path, once taken, cannot be used a second time, driving directionality. Unlike 'burnt-bridges' walkers, where used steps are irretrievably destroyed[28,40,41,47], our design retains the potential to regenerate its steps after RNA hydrolysis. This property is attractive for the design of future walkers on prescriptive landscapes to study, for example, swarm-like behaviour on the nanoscale.

The continuous, unidirectional rotation fuelled by triphosphate hydrolysis and the rotor–stator design also sets our bio-hybrid rotor apart from rotors generated by organic synthesis[14,36] or DNA nanotechnology[7,37,48]. Random Brownian motion usually drives the latter, and unidirectional rotation is achieved by selective blockade of the reverse direction. These rotors thus cannot exert torque. We foresee that further optimization of the nanoengine will improve its efficiency, speed and processivity to approach those of natural protein rotors and walkers. Our nanoengine already combines a multitude of features that we anticipate will facilitate the creation of nanoscale robots capable of performing ever more sophisticated tasks.

Methods

References

1. Schliwa, M. & Woehlke, G. Molecular motors. *Nature* **422**, 759–765 (2003).
2. Spetzler, D. et al. Single molecule measurements of F1-ATPase reveal an interdependence between the power stroke and the dwell duration. *Biochemistry* **48**, 7979–7985 (2009).
3. Macnab, R. M. How bacteria assemble flagella. *Annu. Rev. Microbiol.* **57**, 77–100 (2003).

4. Krishnan, Y. & Simmel, F. C. Nucleic acid based molecular devices. *Angew. Chem. Int. Ed.* **50**, 3124–3156 (2011).

5. Zhang, D. Y. & Seelig, G. Dynamic DNA nanotechnology using strand-displacement reactions. *Nat. Chem.* **3**, 103–113 (2011).

6. Bath, J. & Turberfi ld, A. J. DNA nanomachines. *Nat. Nanotech.* **2**, 275–284 (2007).

7. Ketterer, P. Willner, E. M. & Dietz, H. Nanoscale rotary apparatus formed from tight-fitting 3D DNA components. *Sci. Adv.* **2**, e1501209 (2016).

8. van den Heuvel, M. G. & Dekker, C. Motor proteins at work for nanotechnology. *Science* **317**, 333–336 (2007).

9. Goel, A. & Vogel, V. Harnessing biological motors to engineer systems for nanoscale transport and assembly. *Nat. Nanotech.* **3**, 465–475 (2008).

10. Giselbrecht, S., Rapp, B. E. & Niemeyer, C. M. The chemistry of cyborgs–interfacing technical devices with organisms. *Angew. Chem. Int. Ed.* **52**, 13942–13957 (2013).

11. Feringa, B. L. In control of motion: from molecular switches to molecular motors. *Acc. Chem. Res.* **34**, 504–513 (2001).

12. von Delius, M. & Leigh, D. A. Walking molecules. *Chem. Soc. Rev.* **40**, 3656–3676 (2011).

13. Fletcher, S. P., Dumur, F., Pollard, M. M. & Feringa, B. L. A reversible, unidirectional molecular rotary motor driven by chemical energy. *Science* **310**, 80–82 (2005).

14. Wilson, M. R. et al. An autonomous chemically fuelled small-molecule motor. *Nature* **534**, 235–240 (2016).

15. Daubendiek, S. L., Ryan, K. & Kool, E. T. Rolling-circle RNA synthesis: circular oligonucleotides as effici t substrates for T7 RNA polymerase. *J. Am. Chem. Soc.* **117**, 7818–7819 (1995).

16. Elrod-Erickson, M., Rould, M. A., Nekludova, L. & Pabo, C. O. Zif268 protein–DNA complex refi ed at 1.6 Å: a model system for understanding zinc fi ger–DNA interactions. *Structure* **4**, 1171–1180 (1996).

17. Nakata, E. et al. Zinc-fi ger proteins for site-specific protein positioning on DNA-origami structures. *Angew. Chem. Int. Ed.* **51**, 2421–2424 (2012).

18. Ngo, T. A., Nakata, E., Saimura, M. & Morii, T. Spatially organized enzymes drive cofactor-coupled cascade reactions. *J. Am. Chem. Soc.* **138**, 3012–3021 (2016).

19. Lohmann, F., Valero, J. & Famulok, M. A novel family of structurally stable double stranded DNA catenanes. *Chem. Commun.* **50**, 6091–6093 (2014).

20. Ackermann, D., Jester, S. S. & Famulok, M. Design strategy for DNA rotaxanes with a mechanically reinforced PX100 axle. *Angew. Chem. Int. Ed.* **51**, 6771–6775 (2012).

21. Ackermann, D. et al. A double-stranded DNA rotaxane. *Nat. Nanotech.* **5**, 436–442 (2010).

22. Weigandt, J., Chung, C.-L., Jester, S.-S. & Famulok, M. A daisy chain rotaxane interlocked DNA nanostructure. *Angew. Chem. Int. Ed.* **55**, 5512–5516 (2016).

23. Lionberger, T. A. & Meyhofer, E. Bending the rules of transcriptional repression: tightly looped DNA directly represses T7 RNA polymerase. *Biophys. J.* **99**, 1139–1148 (2010).

24. Lee, W., von Hippel, P. H. & Marcus, A. H. Internally labeled Cy3/Cy5 DNA constructs show greatly enhanced photo-stability in single-molecule FRET experiments. *Nucleic Acids Res* **42**, 5967–5977 (2014).

25. Yang, W. P., Wu, H. & Barbas, C. F. 3rd Surface plasmon resonance based kinetic studies of zinc fi ger–DNA interactions. *J. Immunol. Methods* **183**, 175–182 (1995).

26. Ko, S. H., Gallatin, G. M. & Liddle, J. A. Nanomanufacturing with DNA origami: factors affecting the kinetics and yield of quantum dot binding. *Adv. Funct. Mater.* **22**, 1015–1023 (2012).

27. Abendroth, J. M., Bushuyev, O. S., Weiss, P. S. & Barrett, C. J. Controlling motion at the nanoscale: rise of the molecular machines. *ACS Nano* **9**, 7746–7768 (2015).

28. Pan, J. et al. Visible/near-infrared subdiffraction imaging reveals the stochastic nature of DNA walkers. *Sci. Adv.* **3**, e1601600 (2017).

29. Pan, J., Li, F., Cha, T. G., Chen, H. & Choi, J. H. Recent progress on DNA based walkers. *Curr. Opin. Biotechnol.* **34**, 56–64 (2015).

30. Yehl, K. et al. High-speed DNA-based rolling motors powered by RNase H. *Nat. Nanotech.* **11**, 184–190 (2016).

31. Tomov, T. E. et al. DNA bipedal motor achieves a large number of steps due to operation using microfluidics-based interface. *ACS Nano* **11**, 4002–4008 (2017).

32. Zhang, D. Y. & Winfree, E. Control of DNA strand displacement kinetics using toehold exchange. *J. Am. Chem. Soc.* **131**, 17303–17314 (2009).

33. Jung, C., Allen, P. B. & Ellington, A. D. A stochastic DNA walker that traverses a microparticle surface. *Nat. Nanotech.* **11**, 157–163 (2016).

34. Omabegho, T., Sha, R. & Seeman, N. C. A bipedal DNA Brownian motor with coordinated legs. *Science* **324**, 67–71 (2009).

35. Berna, J. et al. Macroscopic transport by synthetic molecular machines. *Nat. Mater.* **4**, 704–710 (2005).

36. Kudernac, T. et al. Electrically driven directional motion of a four-wheeled molecule on a metal surface. *Nature* **479**, 208–211 (2011).

37. Lu, C. H., Cecconello, A., Elbaz, J., Credi, A. & Willner, I. A three-station DNA catenane rotary motor with controlled directionality. *Nano Lett.* **13**, 2303–2308 (2013).

38. Venkataraman, S., Dirks, R. M., Rothemund, P. W., Winfree, E. & Pierce, N. A. An autonomous polymerization motor powered by DNA hybridization. *Nat. Nanotech.* **2**, 490–494 (2007).

39. Turberfi ld, A. J. et al. DNA fuel for free-running nanomachines. *Phys. Rev. Lett.* **90**, 118102 (2003).

40. Bath, J., Green, S. J. & Turberfi ld, A. J. A free-running DNA motor powered by a nicking enzyme. *Angew. Chem. Int. Ed.* **44**, 4358–4361 (2005).

41. Lund, K. et al. Molecular robots guided by prescriptive landscapes. *Nature* **465**, 206–210 (2010).

42. Eelkema, R. et al. Molecular machines: nanomotor rotates microscale objects. *Nature* **440**, 163–163 (2006).

43. Liu, M. H. et al. Biomimetic autonomous enzymatic nanowalker of high fuel effici cy. *ACS Nano* **10**, 5882–5890 (2016).

44. Cheng, J. et al. Bipedal nanowalker by pure physical mechanisms. *Phys. Rev. Lett.* **109**, 238104 (2012).

45. Loh, I. Y., Cheng, J., Tee, S. R., Efremov, A. & Wang, Z. From bistate molecular switches to self-directed track-walking nanomotors. *ACS Nano* **8**, 10293–10304 (2014).

46. Bath, J., Green, S. J., Allen, K. E. & Turberfi ld, A. J. Mechanism for a directional, processive, and reversible DNA motor. *Small* **5**, 1513–1516 (2009).

47. Tian, Y., He, Y., Chen, Y., Yin, P. & Mao, C. A DNAzyme that walks progressively and autonomously along a one-dimensional track. *Angew. Chem. Int. Ed.* **44**, 4355–4358 (2005).

48. Yang, Y. et al. A photoregulated DNA-based rotary system and direct observation of its rotational movement. *Chemistry* **23**, 3979–3985 (2017).

Acknowledgements

Authors contributions

M.F. and J.V. developed the concepts of interlocked bio-hybrid nanoengines and the walking principle. J.V. performed and designed, with M.F., most of the included studies. M.F. supervised the research project. N.P., S.D. and N.G.W. planned and performed the single-molecule fluorescence experiments. All authors discussed the experimental results and contributed to writing the manuscript (J.V. and M.F. performed the bulk of the writing).

Competing interests

The authors declare no competing interests.

Additional information

Supplementary information is available for this paper at https://doi.org/10.1038/s41565-018-0109-z.

Reprints and permissions information is available at www.nature.com/reprints.

Correspondence and requests for materials should be addressed to M.F.

Publisher's note: Springer Nature remains neutral with regard to jurisdictional claims in published maps and institutional affiliations.

Methods

Buffer systems. 1× TAE buffer: 40 mM Tris·HCl, 20 mM AcOH, 1 mM EDTA at pH 8.3.
1× DNA buffer: 10 mM Tris·HCl, 50 mM NaCl, 10 mM MgCl$_2$ at pH 7.5.
1× origami buffer: 5 mM Tris·HCl, 1 mM EDTA, 18.5 mM MgCl$_2$ at pH 7.9.
1× ligase buffer: 40 mM Tris·HCl, 10 mM MgCl$_2$, 10 mM dithiothreitol (DTT), 5 mM ATP at pH 7.8.
WAX buffer A: 20 mM Tris·HCl at pH 9.0.
WAX buffer B: 20 mM Tris·HCl, 1 M NaCl at pH 9.0.
5× transcription buffer: 200 mM Tris·HCl (pH 7.9 at 25 °C), 50 mM DTT, 50 mM NaCl and 10 mM spermidine.

ODNs. Oligodeoxynucleotides (ODNs) used for rings and catenane assemblies were purchased from Ella Biotech (HPLC-purified). ODN staples used for the assembly of the DNA origami nanotube were purchased from Eurofins Genomics (high-purity salt free (HPSF) grade) and the M13mp18 scaffold was obtained from Tilibit.

Assembly of 126 and 210 bp rotor rings. The oligonucleotides (4 μM) used for assembly of the rings (Supplementary Fig. 1 and Supplementary Table 1) and NaCl (40 mM) in 1× ligase buffer were annealed from 60 °C to 15 °C over 75 min. Ligase (1 μl/100 μl, 10 U) was added and ligated overnight at 15 °C. The products were purified by HPLC and concentrated using Amicon Ultra-30K centrifugal filters.

Assembly of partial ¾-168 bp stator rings. The partial ¾-168 bp stator rings containing all ODNs for the different stator rings (Supplementary Fig. 1 and Supplementary Table 1), except for the threading ODN, which was assembled and purified as described for the rotor rings.

Synthesis of catenanes. Assembly of the DNA catenanes described in this work was performed as previously reported[19]. Briefly, 1 equiv. of rotor ring was mixed with 1.1 equiv. of threading ODN (in 1× DNA buffer and 1× ligase buffer) and threaded at 4 °C for 1 h. The ¾-168 bp stator ring (1.3 equiv.) was then added, allowed to hybridize for 15 min before ligase (2 μl/100 μl) was added, and ligated for 4 h at 15 °C. To convert the hybridized catenane (Cat^{hyb}) to the mechanically interlocked catenane (Cat^{mec}; Fig. 1a), 5 equiv. of 'RO-rotor' was added together with more ligase (0.5 μl/100 μl) and incubated for 30 min at 15 °C before adding 10 equiv. of 'RO-stator' (Supplementary Fig. 1). The sample was incubated for 4 h at 15 °C, purified by HPLC, and concentrated using Amicon Ultra-30K centrifugal filters.

HPLC purification of rings and catenane nanostructures. Rings and other catenane precursors were purified by weak anion exchange HPLC using an isocratic gradient from 0 to 0.5 min at 20% of WAX B buffer and then from 45 to 65% in 20 min (0.8 ml min^{-1} flow, column TSKgel DEAE-NPR 4.6 mm × 35 mm (TOSOH)). Catenane structures were similarly purified using an isocratic gradient from 0 to 5 min at 55% of WAX B buffer, and the gradient was increased to 62% from 5 to 25 min (0.5 ml min^{-1} flow, column TSKgel DNA-NPR 4.6 mm × 75 mm (TOSOH)).

T7RNAP-ZIF protein expression and purification. T7RNAP-ZIF protein was expressed in *Escherichia coli* (strain BL21 DE3) using the plasmid pQE80-HT-zf-T7RNAP (H = HisTag; T = TEV (tobacco etch virus protease cleavage site); zf = 268zif; T7RNAP = T7 RNA polymerase). Pre-culture was performed by overnight incubation at 37 °C, using 200 ml of lysogeny broth (LB) medium with 50 μg ml^{-1} kanamycin. The solution was then diluted to an optical density at 600 nm (OD$_{600}$) of 0.4 (1:10) and when cells reached the mid log phase (OD$_{600}$ of ~0.6), isopropyl-β-d-thiogalactoside (IPTG) was added to a final concentration of 0.5 mM. Cells were incubated at 37 °C over 4 h for expression, collected by centrifugation (4,000 r.p.m.) and stored at −80 °C or resuspended in 15 ml of lysis buffer (50 mM Tris, pH 7.8 at 4 °C, 300 mM NaCl, 10% glycerine, 20 mM imidazole and 1 mM ZnCl$_2$). Subsequently, cells were disrupted (French press, 1,000 psi max., two rounds), centrifuged at 4 °C (20,000 r.p.m., 20 min), then the supernatant was incubated with 1.5 ml of Ni-NTA agarose equilibrated bead matrix (Macherey Nagel) for 30 min and washed three times with the lysis buffer. T7RNAP-ZIF construct was expressed with N-terminal His6-tags for its subsequent purification by affinity chromatography, then washed twice and eluted with elution buffer (lysis buffer containing 250 mM imidazole) before incubation with TEV protease to remove the His6-tag (and consequent reverse Ni-NTA chromatography to remove the His-tag). Finally, size exclusion chromatography (SEC) purification of the sample was performed using a Superdex 200 column (GE Healthcare Life Sciences), fractions were collected, and the buffer was exchanged by dialysis (Slide-A-Lyzer Dialysis Cassettes, 10K molecular weight cutoff) to storage buffer (50 mM Tris, pH 8.0 at 4 °C, 0.1 mM EDTA, 1 mM DTT, 0.05% (wt/vol) of 3-[(3-cholamidopropyl)dimethylammonio]-1-propanesulfonate (CHAPS), 50% (vol/vol) glycerol).

SPR measurements. BIAcore 3000 equipment was used to perform SPR measurements. Streptavidin (SA) sensor chips (GE Healthcare Life Sciences) were used to immobilize the corresponding biotinylated ODN (Supplementary Fig. 1) containing the binding sequence for 268Zif protein. To this end, 10 μl injection of the dsDNA (50 nM in 1× DNA buffer) was followed by an additional 10 μl injection of the complementary ssDNA. Typically, 300–500 resonance units (RUs) of this ODN were immobilized on the chip surface. Different concentrations of T7RNAP-ZIF ranging from 32 nM to 300 nM were injected (200 μl injection of protein in binding buffer: 50 mM HEPES, 50 mM NaCl, 5 mM MgCl$_2$, 20 μM ZnCl$_2$, 2 mM DTT, 0.05% (wt/vol) Tween) in kinject mode with a contact time of 600 s for association and an additional 600 s for dissociation, followed by direct injection of 20 μl 0.1% (wt/vol) SDS solution, with a constant flow rate of 20 μl min^{-1}. Dissociation and association kinetic constants (k_{off} and k_{on}, respectively) as well as K_d equilibrium constants were assessed using Biacore evaluation software.

MB fluorescence experiments. To monitor transcription, real-time fluorescence assays with a MB were performed. The corresponding DNA template was incubated at different concentrations (typically 5 or 10 nM) with 31.7 μl of MgCl$_2$ (30 mM), 38 μl of a mastermix containing 2.5× transcription buffer, 5 mM NTPs, RNAsin (1:20 vol/vol), T7RNAP-ZIF (64.5 nM) and 1.5 μM of the MB in a total volume of 95 μl. This volume was split into three samples of 30 μl each, loaded in a 384-well plate (Greiner Fluotrac 200, 384-well plate) and the FAM fluorescence (ex. 491 nm; em. 521 nm) was measured in an Enspire 2300 plate reader (Perkin Elmer) every 3 min at 37 °C for 3 h.

Calibration of the MB. As described for the MB fluorescence experiments, different concentrations of the JVgmblong_RO ODN (replacing the DNA ring and catenane templates) were mixed with mastermix containing the MB, and the resulting fluorescence was recorded over time in an Enspire 2300 plate reader (see previous section for experimental details). JVgmblong_RO is fully complementary to the MB, thus allowing the hairpin to open, resulting in an increase in the fluorescence signal. Linear fitting of fluorescence intensity versus ODN concentration yielded the corresponding calibration curve for the MB (Supplementary Fig. 5), used to assess RNA concentration during RCT.

Sample preparation for smFRET study. Fluorescently labelled nanoengines with protruding 5′-biotinylated dsDNA were immobilized through a biotin−streptavidin interaction onto a quartz slide with a microfluidic channel. The steps of surface functionalization and construction of the microfluidic channel are described elsewhere[49]. An enzymatic oxygen scavenger system (OSS) containing (at 1×) 50 nM protocatechuate-3,4-dioxygenase (PCD), 5 mM protocatechuic acid (PCA) and 2 mM Trolox (6-hydroxy-2,5,7,8-tetramethylchroman-2-carboxylic acid) was added to the imaging buffer to minimize photobleaching and photoblinking of the fluorophores[50]. Before immobilizing the nanoengines on the quartz slide, the sample was incubated at 37 °C for 30 min with a threefold excess of T7RNAP-ZIF over catenane (catenane:T7RNAP-ZIF = ~0.6:1.7 nM) without rNTP for optimal binding of T7RNAP-ZIF to the catenane. After injecting the nanoengine (catenane/T7RNAP-ZIF complex) into the microfluidic channel, excess unbound T7RNAP-ZIF was washed away by flushing with ~300 μl buffer containing 1× TAE-Mg^{2+} buffer (40 mM Tris base, 20 mM acetic acid, 1 mM EDTA, 12.5 mM MgCl$_2$, pH 7.5) and 1× OSS. Following the washing step, a transcription mixture containing 2.0 mM each of rNTP (GTP, ATP, CTP, UTP), 1× transcription buffer, RNasin Ribonuclease Inhibitor (40 U), 25 mM MgCl$_2$, 1× OSS and 5% (vol/vol) DMSO to conformationally relax the DNA double helices was injected and incubated for 3 min before collecting TIRFM movies. All data were collected at ~25 °C.

Monitoring the rotation of individual nanoengines by smFRET using TIRFM. TIRFM was used to monitor the rotation of each nanoengine through smFRET. The particulars of the TIRFM instrumental set-up are described elsewhere[51-53]. Briefly, a 532 nm green laser (CrystaLaser, CL532-050-L) and a 638 nm red laser (Coherent, 1069415/AR) were used to excite Cy3 and Cy5 molecules, respectively, at ~5.0 mW. The presence of Cy5 was confirmed by directly exciting with the red laser at 638 nm for a brief period at the very beginning and end of each movie. The emitted fluorescence was collected through a 60× 1.2 NA water immersion objective (Olympus UplanApo). The fluorescence emission was split into donor and acceptor signals by pairs of dichroic mirrors and reflective mirrors (Thorlabs) and projected onto the two halves of an intensified charged-coupled device (ICCD, I-Pentamax, Princeton Instruments). Fluorescence time traces were collected as movies using the ICCD at 100 ms time resolution. The typical duration of data collection was ~20 min. Data acquisition started 3–4 min after injection of the transcription mixture into the slide to allow the oxygen scavenger system sufficient time to remove molecular oxygen introduced through the perturbation of injection. We chose to pursue continuous observation in our experiments to detect any significant disengagement of the nanoengine from its template, which should lead to spurious fluctuations of either the FRET signal or FRET state dwell time. The upper limit of our observation window arose from inevitable photobleaching of the fluorophores, which was reduced by lowering the excitation laser power to ~5 mW, as low as possible without inappropriately deteriorating either the signal-to-noise ratio or the time resolution needed to distinguish the two quite similar FRET values.

Analysis of smFRET data. Intensity time traces were generated from the recorded movies using IDL (Research Systems) and analysed further using MATLAB scripts as described in ref. [54]. Dwell times in the high- and low-FRET states were extracted from the single-molecule intensity time traces by identifying the transition points from low- to high-FRET and vice versa within the error limit of one frame (0.1 s) using hidden Markov model fit. The cumulative distributions of dwell times in the low- and high-FRET states were fitted with single-exponential functions to extract the most probable dwell times, whereas the cumulative distribution of dwell times for the full transcription cycle was fitted with a Gamma function using MATLAB. The time over which the transitions between the two FRET states occurred was extracted and the probability density of these transition times fitted with a Gamma function using MATLAB to reveal the number of intermediate steps. The probability density describes the likelihood of a random variable (the transition time in this case) falling within a particular range of values. A Gamma function yields a shape factor corresponding to the number n of irreversible states and dwell times in each state[55]. All dwell times were corrected for the limited time window of data collection/trajectory truncation as described in ref. [56] (Supplementary Table 2).

Assembly of the DNA catenane walker. One equivalent of rotor ring was mixed with 1.1 equiv. of threading ODN (in 1× DNA buffer and 1× ligase buffer + 10 mM MgCl$_2$) and threaded at 4 °C for 1 h. Simultaneously, the ¾-168 bp stator ring (1.3 equiv. in 1.5× DNA buffer and 1× ligase buffer) was incubated with the Blocker_Rc2c ODN (1.5 equiv.) at 40 °C for 1 h and then incubated at 4 °C for 5 min before adding it to the rotor ring solution. The mixture was incubated for 15 min before adding the ligase (2 µl/100 µl) and then ligated for 4 h at 15 °C. To convert the hybridized catenane (Cat^{hyb}) to the mechanically interlocked catenane (Cat^{mec}), first 5 equiv. of 'RO-rotor' were added together with more ligase (0.5 µl/100 µl) and incubated for 30 min at 15 °C before 10 equiv. of 'RO-stator' was added. The sample was incubated for 3 h at 15 °C. Finally, the RO-Blocker_Rc2c (3 equiv.) was added to release the Blocker_Rc2c ODN from the ss-region of the stator, incubated for 30 min, purified by HPLC, and concentrated using Amicon Ultra-30K centrifugal filters.

Design and assembly of the six-helix bundle DNA origami. The six-helix bundle DNA origami was designed using the 2.2.0 version of caDNAno[57]. For the assembly, the DNA M13mp18 scaffold (7,429 bp, 20 nM) was mixed with the corresponding DNA staples at 200 nM concentration each, in 1× TAE buffer (40 mM Tris, 20 mM acetic acid, 1 mM EDTA, pH 8), 5 mM NaCl and 20 mM MgCl$_2$. The mixture was subjected to thermal annealing in a Nexus thermocycler (Eppendorf), from 80 to 65 °C at 1 °C min^{-1} and from 65 to 20 in steps of 20 min °C^{-1}. The samples were purified following the PEG precipitation protocol described previously[58]. Briefly, samples were mixed 1:1 (vol/vol) with precipitation buffer (15% PEG 800 (wt/vol) (Carl Roth), 5 mM Tris, 1 mM EDTA and 505 mM NaCl) and spun at 16,000g for 25 min at room temperature using a microcentrifuge (Eppendorf 5424R). The supernatant was discarded and the pellet containing the DNA origami nanotubes dissolved in 1× origami buffer (5 mM Tris·HCl, 1 mM EDTA, 18.5 mM MgCl$_2$ at pH 7.9).

Assembly of the DNA catenane walker to the origami path and monitoring of transcription by bulk fluorescence experiments. A solution of the catenane walker (final concentration 75 nM) was incubated at room temperature for 15 min with 16 µl of mastermix (2.5× transcription buffer, RNAsin (1:20 vol/vol), T7RNAP-ZIF (223 nM), 2.5 mM MgCl$_2$, 18.75% (vol/vol) DMSO) to allow T7RNAP-ZIF (final concentration 86 nM, 1.15 equiv. with respect to catenane) to bind the catenane. In parallel, a solution of the DNA origami nanotube (final concentration 75 nM) was incubated at 37 °C with the comp-iStep (BHQ-2) ODN (1.33 equiv. per each iStep) or the Step1_blocker ODN for the corresponding control (2 equiv.) for 15 min. The catenane and origami solutions were then mixed in 2× DNA buffer (20 mM Tris·HCl, 100 mM NaCl, 20 mM MgCl$_2$ at pH 7.5), the volume adjusted to 40 µl, then incubated for 30 min at 37 °C to allow the catenane walker to hybridize to the Step1 position on the DNA origami. The sample was split in two (20 µl each) and loaded in a 386-well plate (ProxiPlate-384 Plus, PerkinElmer). To each well, the NTPs mixture (25 mM, final concentration 2 mM) was added to start transcription and the plate was covered with a sealing plastic film (Biorad) to prevent evaporation. Finally, the fluorescence (FAM ex. 492 nm, em. 521 nm; HEX ex. 535 nm, em. 556 nm; TAMRA ex. 555 nm, em. 576 nm; Texas Red ex. 593 nm, em. 613 nm; Cy5: ex. 649 nm, em. 670 nm) was measured in a plate reader (Enspire 2300 (Perkin Elmer) or TECAN Infinite M1000 Pro) every 3 min at 37 °C for at least 5 h. Analysis of the kinetic data was performed by exponential fitting (one phase decay for Fc fluorophore (TAMRA) and one phase association for Fi fluorophores) using GraphPad Prism software.

Fitting of the data kinetic analysis. One phase decay:

$$FI = (FI_{max} - FI_{min}) \times e^{(-K * X(\text{time}))} \tag{1}$$

One phase association:

$$FI = FI_{min} + (FI_{max} - FI_{min}) \times (1 - e^{(-K * X(\text{time}))}) \tag{2}$$

Quantum dot attachment after transcription. Assembly of the DNA catenane walker to the origami path and the subsequent transcription reaction were performed as described in the section of Methods above. To allow attachment of the streptavidin-coated Qdots, the comp-iStep (BHQ2) ODN was replaced by a biotinylated version (bio-comp-iStep), which was added to the catenane:origami complex (4 equiv. per binding site/iStep). After adding the NTPs mixture (final concentration 2 mM), aliquots of 5 µl were taken from each sample at different time points (0, 20, 45 and 150 min). These aliquots were further diluted in 400 µl of 2× DNA buffer, filtered in Amicon Ultra-10K centrifugal filters, and washed four times with an extra 300 µl of 2× DNA buffer (3 × 7,500g for 5 min and 1 × 7,500g for 20 min). After concentration, 0.4 µl of sample (~6.25 nM; final concentration 1 nM) was mixed with 0.5 µl of Qdots (Qdot 655 streptavidin conjugate, Thermo Fischer Scientific, 1 µM, final concentration 200 nM) in 1.5× DNA buffer (total volume 2.5 µl). The sample was incubated for 2 h at room temperature (or overnight at 4 °C) before measuring by AFM.

AFM sample preparation and imaging. All AFM images were obtained using a Nanowizard 3 AFM (JPK Instruments). Images of the DNA catenane, T7RNAP-ZIF and catenane motor were recorded in tapping mode (a.c. mode) in air. The structures were absorbed onto freshly cleaved mica surface-coated with 0.001% polyornithine (30–70 kDa; Sigma-Aldrich). For this, 3 µl of polyornithine was deposited on the freshly cleaved mica for ~1 min, washed three times with 200 µl of water and dried with an aero duster. Then, 3 µl of sample (2.5–5 nM) was deposited for 1 min, washed, and dried again. ACTA probes (NanoWorld) with silicon tips were used. The high-resolution images were obtained in HyperDrive mode in liquid (water) following the same protocol, except 400 µl of water was added finally on top of the sample. USC probes with highly dense carbon tips (NanoWorld) were used.

AFM images of the DNA catenane walker attached to the origami path were collected in tapping mode (a.c. mode) in liquid (water). Again, 3 µl of sample (1 nM) was deposited on freshly cleaved mica untreated or coated with 0.001% (wt/vol) polyornithine, washed once with 200 µl of water and then, 400 µl of water was added on top of the sample to allow imaging in liquid. USC probes with high dense carbon tips (NanoWorld) were used.

Images of the DNA origami path labelled with Qdots were taken in tapping mode in air. A 3 µl volume of linear polyethylenimine (PEI, Polysciences) was deposited over 1 min on freshly cleaved mica, washed three times with 200 µl of water and subsequently dried, to coat the surface. Then, 3 µl of sample (0.25 nM) was loaded on the PEI-coated surface for 1 min, washed once (200 µl water), and dried with an aero duster. Imaging was performed using ACTA probes with silicon tips. The position of the quantum dots was determined according to the design of the DNA origami path and the relative distances between iSteps. Incomplete or overlapped structures were not used for Qdot quantification.

Gel electrophoresis. Catenane assemblies were analysed using agarose gel electrophoresis (2.5% agarose gel, 0.5× TAE buffer, 20 min at 180 V). Six-helix bundle DNA origami assemblies were run in 2% agarose gels (0.5× TAE, 10 mM MgCl$_2$) for 1 h at 80 V. All gels were poured from 'agarose high resolution' (ROTH), stained with ethidium bromide and visualized by UV irradiation.

Data availability. The data that support the plots within this paper and other findings of this study are available from the corresponding author upon reasonable request.

References

49. Michelotti, N., de Silva, C., Johnson-Buck, A. E., Manzo, A. J. & Walter, N. G. A bird's eye view tracking slow nanometer-scale movements of single molecular nano-assemblies. *Methods Enzymol.* **475**, 121–148 (2010).
50. Aitken, C. E., Marshall, R. A. & Puglisi, J. D. An oxygen scavenging system for improvement of dye stability in single-molecule fluorescence experiments. *Biophys. J.* **94**, 1826–1835 (2008).
51. Fu, J. et al. Multi-enzyme complexes on DNA scaffolds capable of substrate channelling with an artificial swinging arm. *Nat. Nanotech.* **9**, 531–536 (2014).
52. Suddala, K. C. & Walter, N. G. Riboswitch structure and dynamics by smFRET microscopy. *Methods Enzymol.* **549**, 343–373 (2014).
53. Suddala, K. C., Wang, J., Hou, Q. & Walter, N. G. Mg^{2+} shifts ligand-mediated folding of a riboswitch from induced-fit to conformational selection. *J. Am. Chem. Soc.* **137**, 14075–14083 (2015).
54. Fu, J. et al. Assembly of multienzyme complexes on DNA nanostructures. *Nat. Protoc.* **11**, 2243–2273 (2016).

55. Rashid, F. et al. Single-molecule FRET unveils induced-fit mechanism for substrate selectivity in flap endonuclease 1. *Elife* **6**, e21884 (2017).

56. Rueda, D. et al. Single-molecule enzymology of RNA: essential functional groups impact catalysis from a distance. *Proc. Natl Acad. Sci. USA* **101**, 10066–10071 (2004).

57. Douglas, S. M. et al. Rapid prototyping of 3D DNA-origami shapes with caDNAno. *Nucleic Acids Res.* **37**, 5001–5006 (2009).

58. Stahl, E., Martin, T. G., Praetorius, F. & Dietz, H. Facile and scalable preparation of pure and dense DNA origami solutions. *Angew. Chem. Int. Ed.* **53**, 12735–12740 (2014).

In the format provided by the authors and unedited.

A bio-hybrid DNA rotor–stator nanoengine that moves along predefined tracks

Julián Valero[1,2], Nibedita Pal[3], Soma Dhakal[3,4], Nils G. Walter[3] and Michael Famulok [1,2]*

[1]LIMES Program Unit Chemical Biology & Medicinal Chemistry, c/o Kekulé Institut für Organische Chemie und Biochemie, University of Bonn, Bonn, Germany. [2]Center of Advanced European Studies and Research (CAESAR), Bonn, Germany. [3]Single Molecule Analysis Group, Department of Chemistry, University of Michigan, Ann Arbor, MI, USA. [4]Present address: Department of Chemistry, Virginia Commonwealth University, Richmond, VA, USA. *e-mail: m.famulok@uni-bonn.de

Supplementary Information

A bio-hybrid DNA rotor/stator nanoengine that moves along predefined tracks

Julián Valero, Nibedita Pal, Soma Dhakal, Nils G. Walter, & Michael Famulok
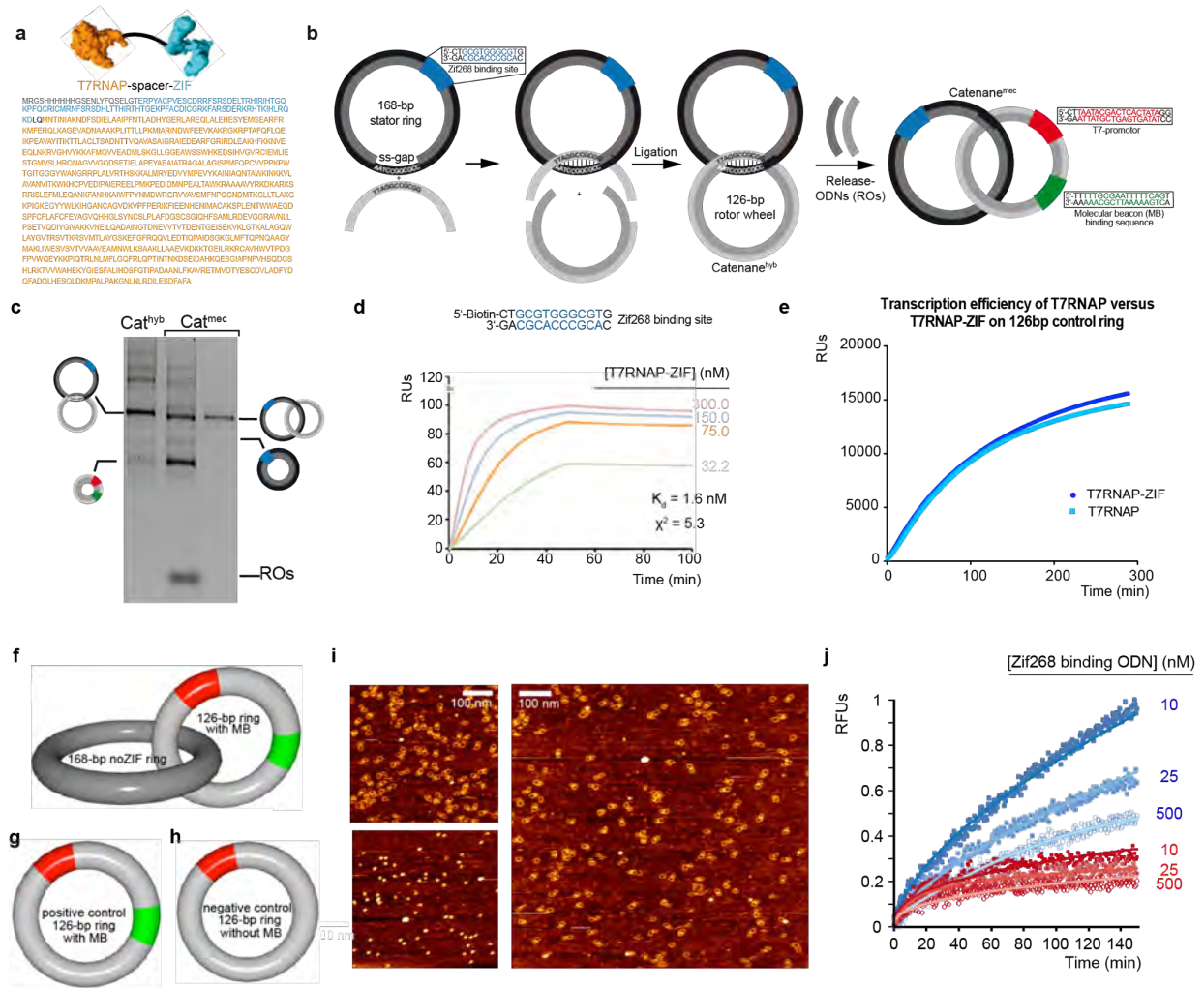
Supplementary Fig. 1. Assembly of the catenane nanoengine, transcription activity, binding affinity, and control experiments (**a**) Amino acid sequence of T7RNAP-ZIF. (**b**) Design, and schematic assembly of the non-symmetrical DNA catenane. (**c**) Analytical agarose gel of the assembled non-symmetric catenane. Lane 1, pseudocatenane, lane 2, catenane after addition of ROs. (**d**) Surface plasmon resonance binding studies of T7RNAP-ZIF in presence of the Zif268 targeting sequence. (**e**) Transcription activity of engineered T7RNAP-ZIF compared with commercial T7RNAP in presence of the circular 126-bp ring rotor template. (**f-h**) Schematic representation of the DNA catenane structure lacking (**f**) the Zif268 binding site and representation of 126-bp rotor rings containing (**g**, positive control) or lacking (**h**, negative control) the sequence encoding the molecular beacon binding site. (**i**) AFM images of the DNA catenane lacking the Zif268 binding domain (upper left), the T7RNAP-ZIF (lower left) and the combination of both (right). (**j**) Fluorescence kinetics of the RCT performed by the catenane (blue) and the control catenane (red) at different equivalents of zinc finger binding motif as indicated (10, 25, 500 nM), in the presence of T7RNAP-ZIF.
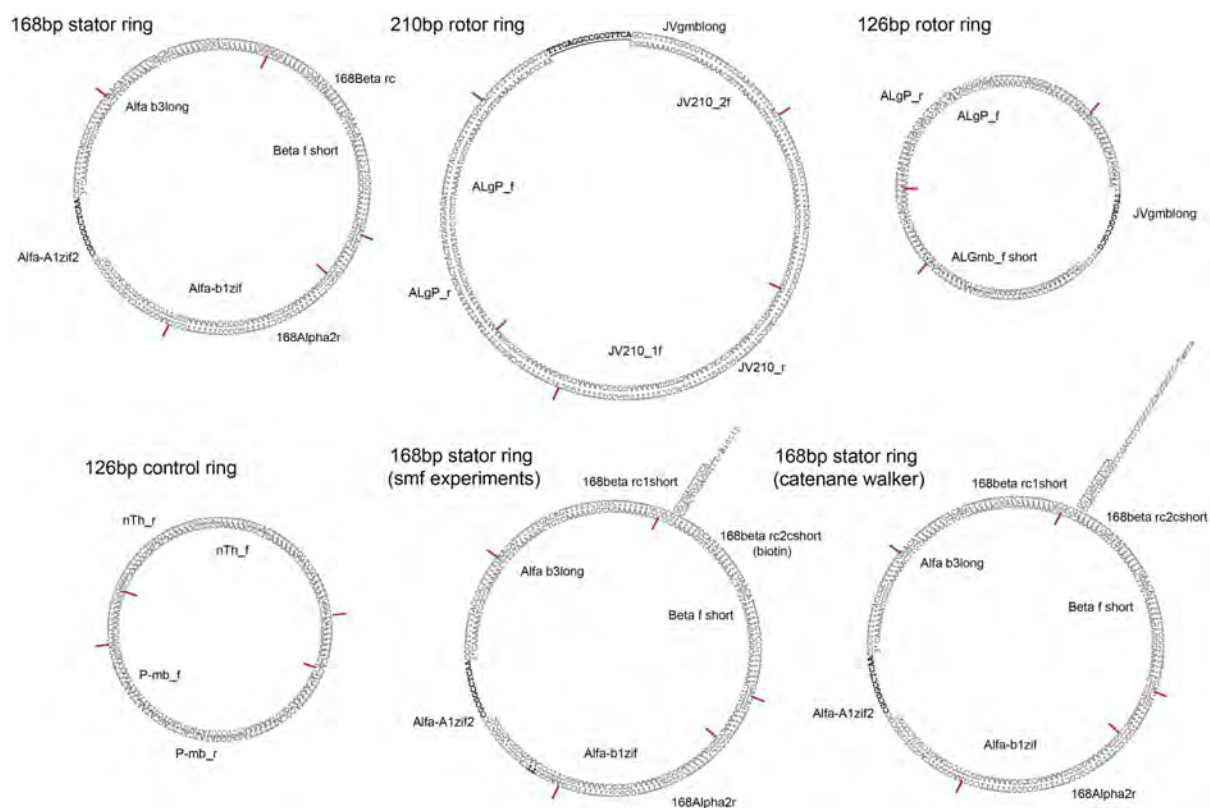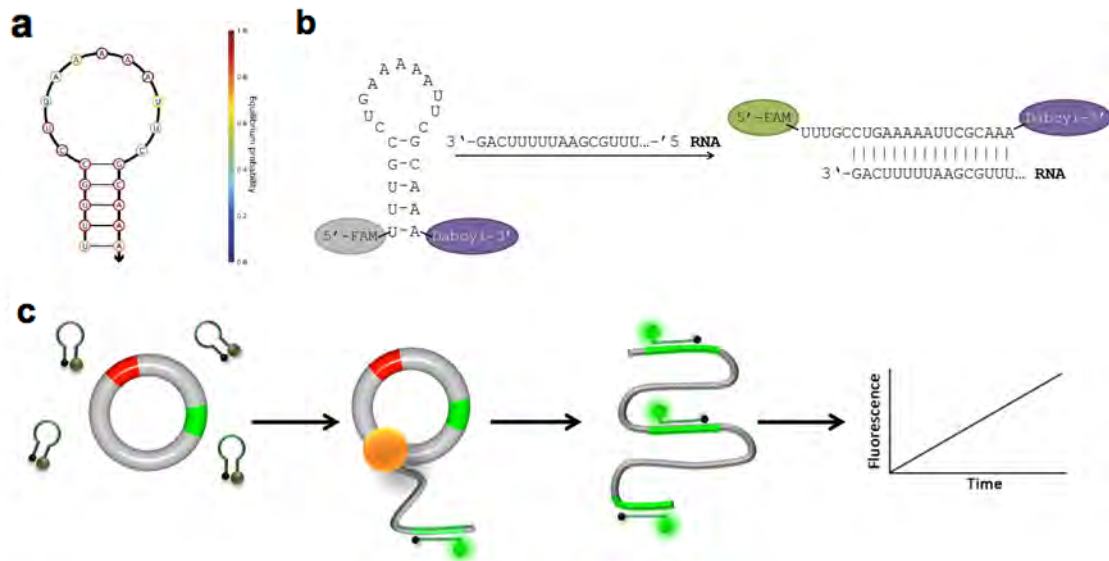
Supplementary Fig. 2. Secondary structure of all DNA rings used in this study, including the names of the ODNs used for the assembly.
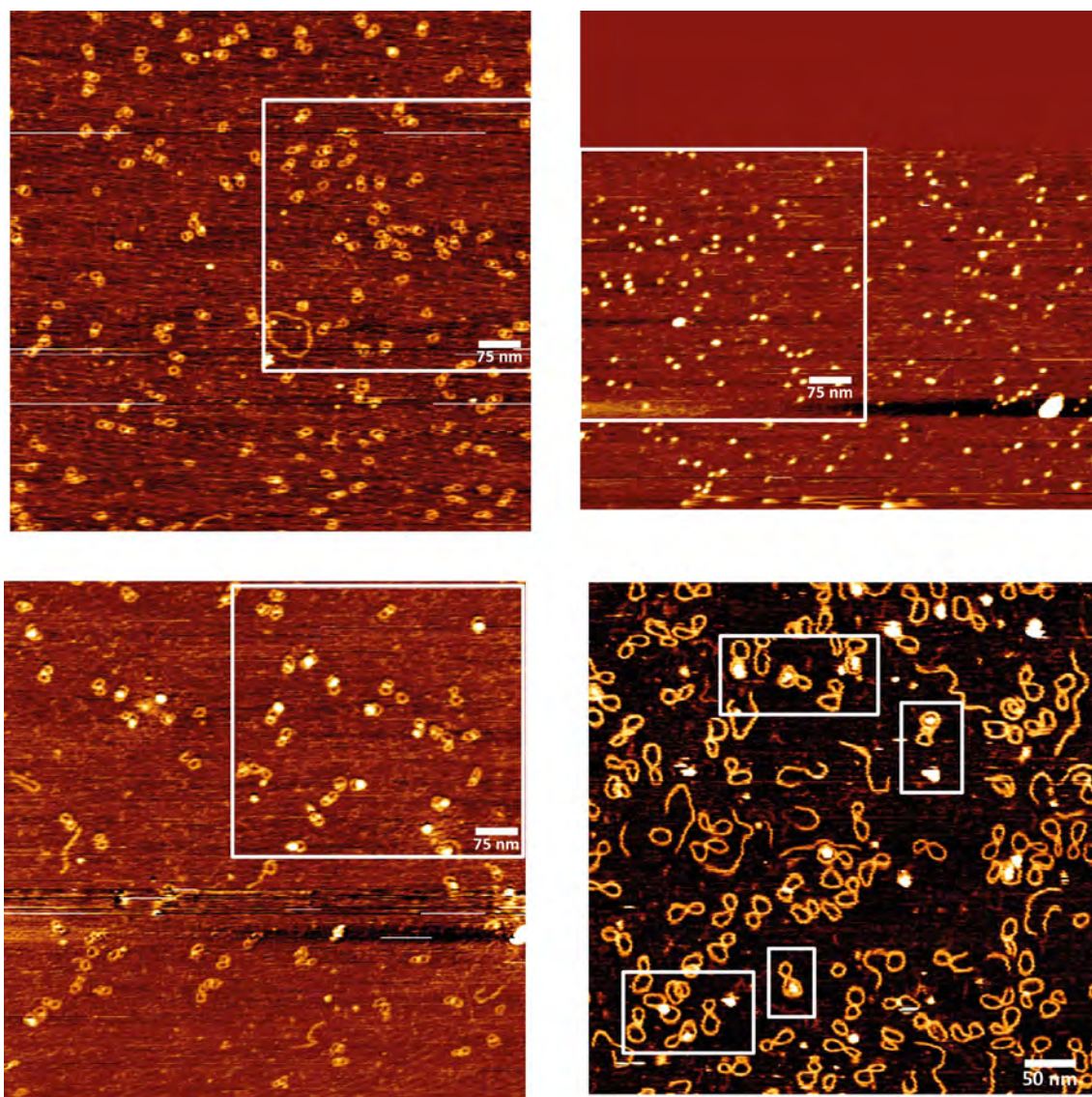
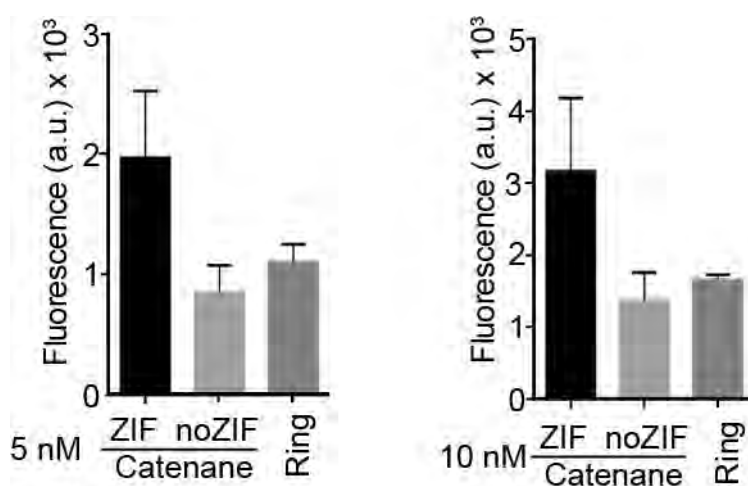**Supplementary Fig. 3.** Larger sections from the uncropped AFM images used for the panels in Figure 1.
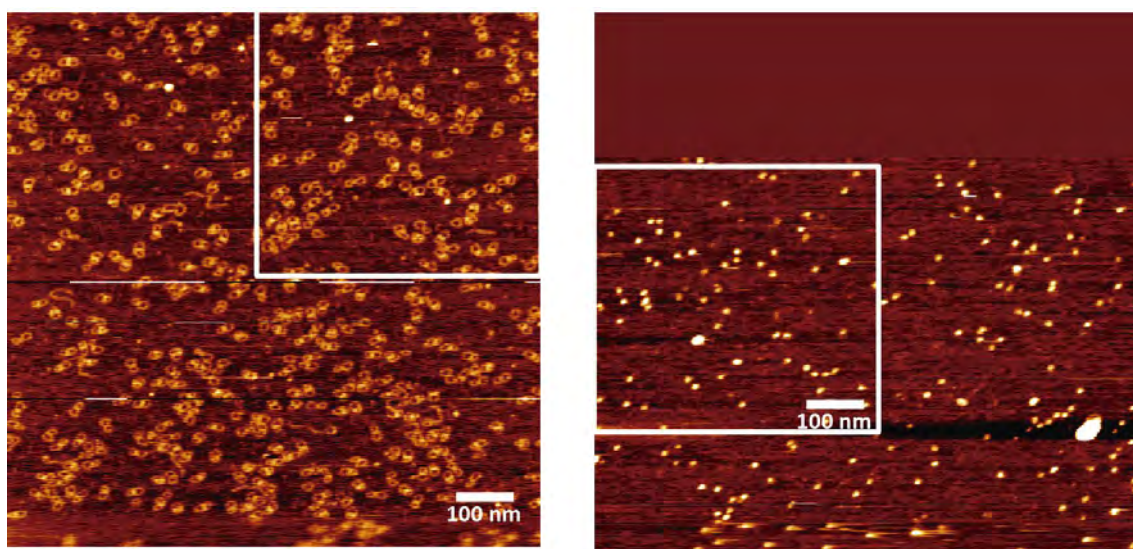
Supplementary Fig. 4. Larger sections from the uncropped AFM images used for the panels in Suppl. Fig. 1.

Supplementary Fig. 5. Folding, structure, and hybridization scheme of the molecular beacon (MB) used in this study. (**a**) Intramolecular folding patter of MB calculated by Nupack[1] (using Mathews et al., 1999 RNA energy parameters)[2] at 37 ºC. The probability of the given configuration at each site is color coded from 0 (blue) to 1 (red). (**b**) Molecular beacon hybridization. An RNA fragment produced during rolling circle transcription opens the hairpin structure of the MB (2'-O-Me-RNA), forms the duplex and thus, gives rise to an increase of FAM fluorescence signal. (**c**) Working principle of the molecular beacon fluorescence assay during rolling circle transcription of a DNA ring template.
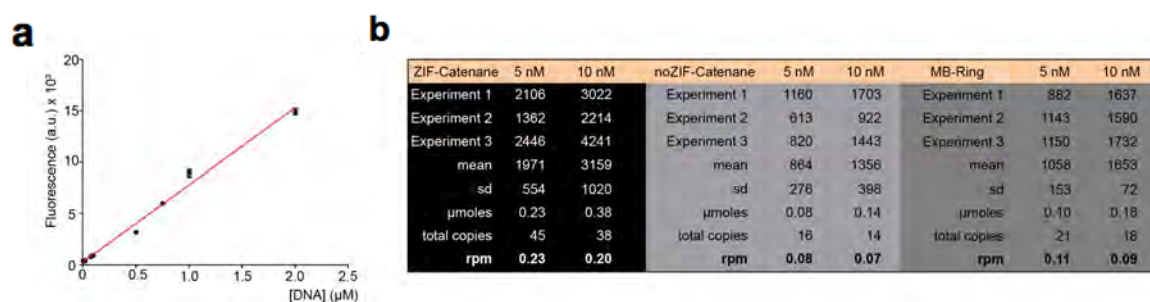
Supplementary Fig. 6. Calibration and quantification of the RNA produced during rolling circle transcription and kinetic analysis by molecular beacon fluorescence experiments. (**a**) Calibration curve for the molecular beacon at increasing concentrations of the complementary ODN (JVgmblong_RO). (**b**) Analysis of the amount of RNA copies generated and the rpm values obtained for ZIF-catenane, the noZIF-catenane, and the MB-ring control (see Suppl. Fig. 7).

The table in panel (b):

ZIF-Catenane	5 nM	10 nM	noZIF-Catenane	5 nM	10 nM	MB-Ring	5 nM	10 nM
Experiment 1	2106	3022	Experiment 1	1160	1703	Experiment 1	882	1637
Experiment 2	1362	2214	Experiment 2	613	922	Experiment 2	1143	1590
Experiment 3	2446	4241	Experiment 3	820	1443	Experiment 3	1150	1732
mean	1971	3159	mean	864	1356	mean	1058	1653
sd	554	1020	sd	276	398	sd	153	72
µmoles	0.23	0.38	µmoles	0.08	0.14	µmoles	0.10	0.18
total copies	45	38	total copies	16	14	total copies	21	18
rpm	0.23	0.20	rpm	0.08	0.07	rpm	0.11	0.09

Supplementary Fig. 7. Kinetic analysis of the molecular beacon transcription assay. Fluorescence signal obtained after the molecular beacon transcription assay for the ZIF-catenane, the noZIF-catenane, and the MB-ring control at 5 and 10 nM template concentrations, respectively. Error bars: n = 9, mean ±SD
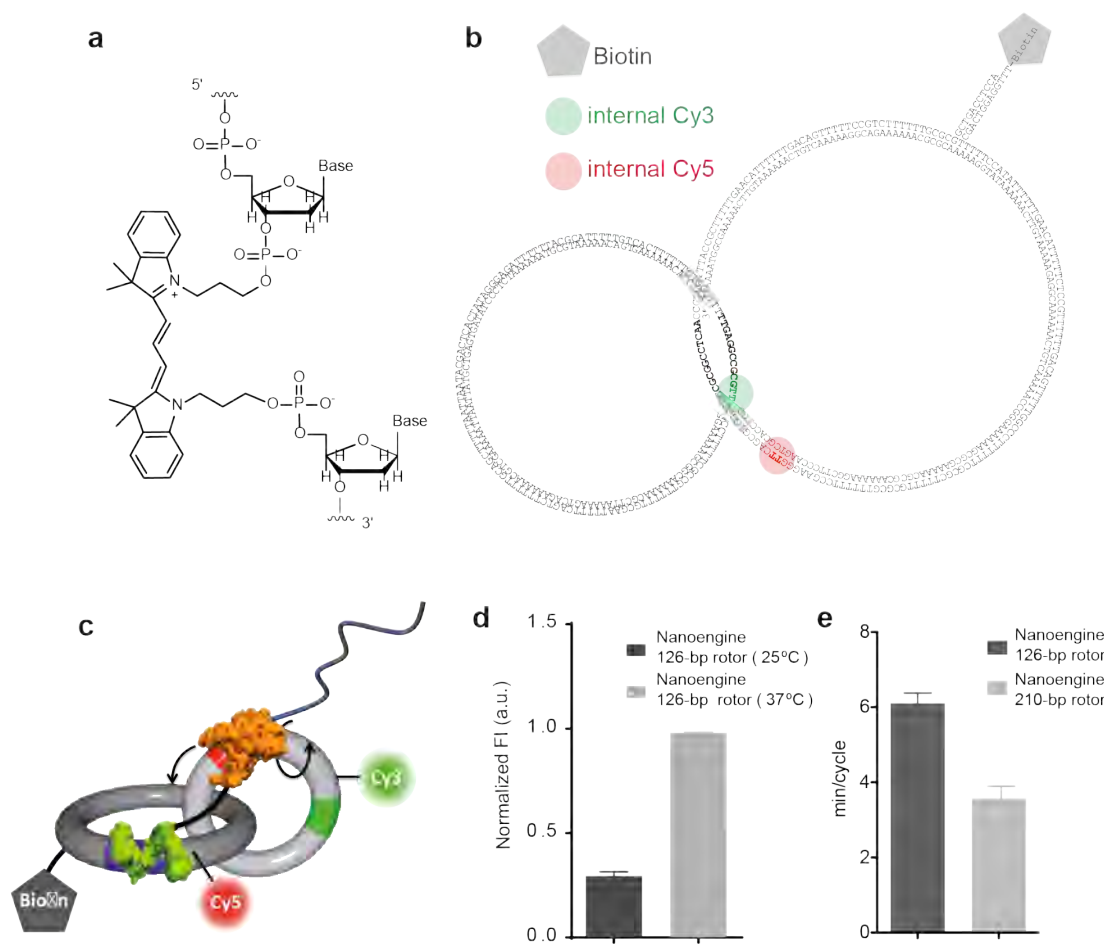
Supplementary Fig. 8. Fluorophore labelling strategy and microscope setup for the sm-FRET experiments (**a**) Chemical structure of the internal Cy3 fluorescent label used in this study, which is located in the DNA backbone between two phosphodiester groups. (**b**) Detailed representation of the DNA catenane used for smFRET experiments and the specific sequence location of the Cy3, Cy5 and biotin labels. (**c**) Scheme of the DNA catenane motor labelled with donor (Cy3, rotor) and acceptor (Cy5, stator) FRET pairs and a biotin molecule for immobilization on a streptavidin-coated glass surface to perform smFRET studies. (**d**) Molecular beacon fluorescence experiment carried out at 25ºC and 37ºC with the nanoengine having the 126-bp rotor ring. (**e**) Rotational speed assessed by bulk fluorescence experiments at 25ºC of the labelled nanoengines containing either 126-bp or 210-bp rotor rings. Error bars: n = 3, mean ±SD
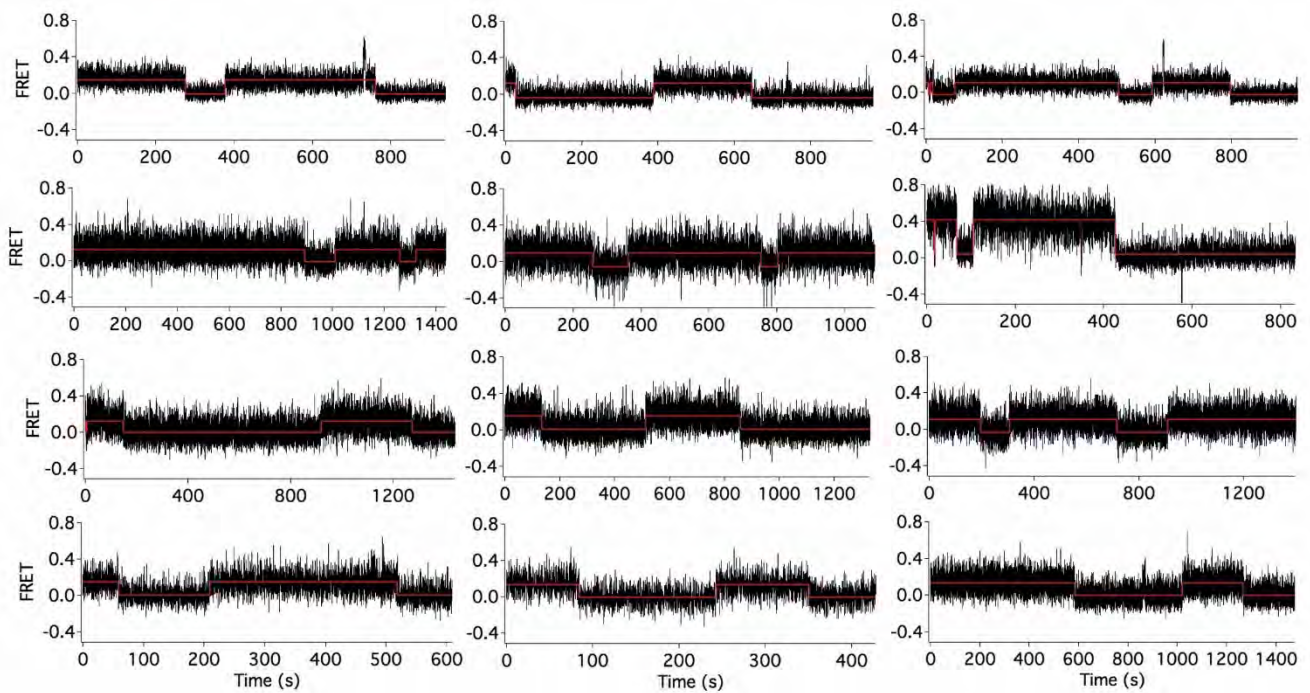
Supplementary Fig. 9. Representative smFRET trajectories with more than one-and-a-half full transcription cycles representing continuous T7RNAP-ZIF operation, consistent with a high processivity. The fitted red lines are hidden Markov model fits. The absence of any significant short-lived FRET state excursions suggests the scarcity of random Brownian rotation events, at least over the time course of the experiment.
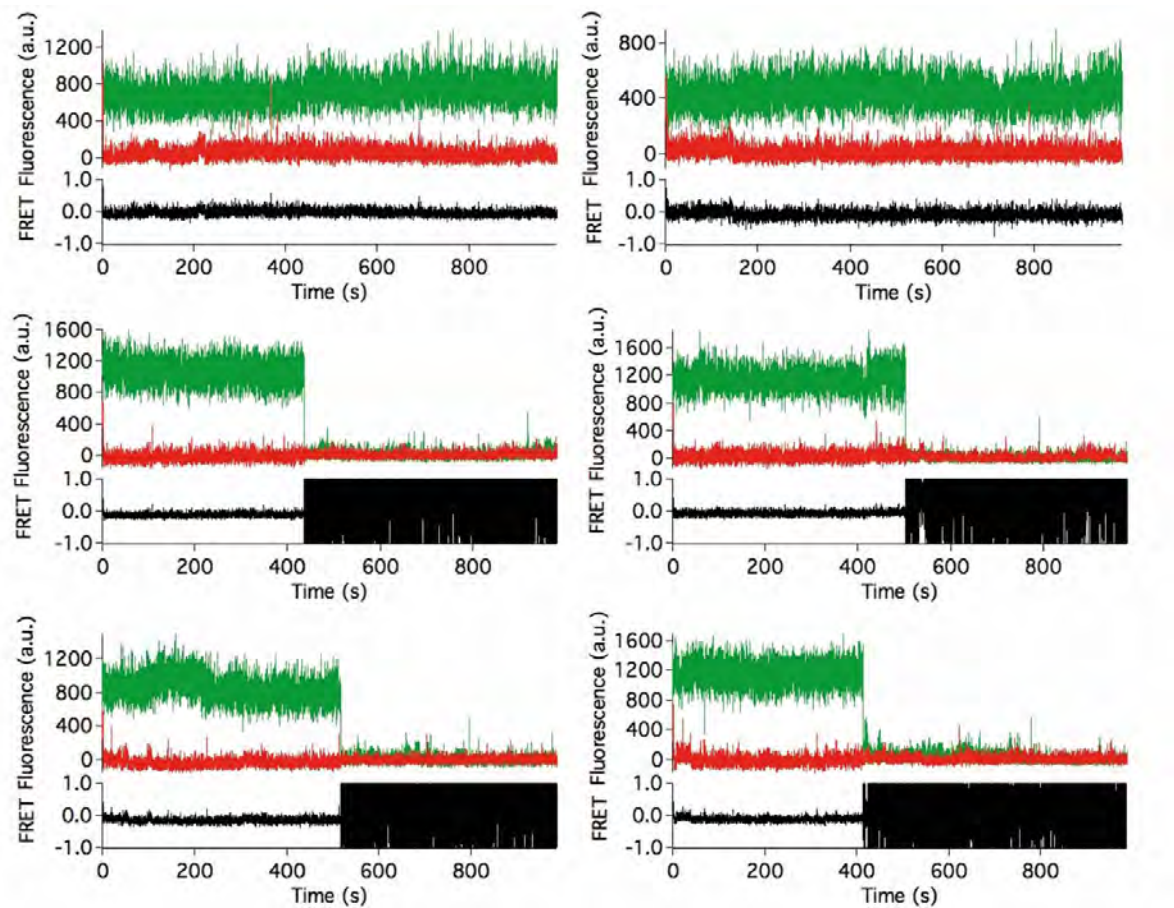
Supplementary Fig. 10. Representative donor (green), acceptor (red) and FRET (black) signal in trajectories from the T7RNAP control experiment for the 126-bp rotor. The brief, high-intensity red signals at the very beginning of each trajectory reflect direct excitation of Cy5, confirming its presence on the stator; the sudden loss of donor signal in the third to sixth trace reflects single-step photobleaching, as expected for a single molecule fluorescence experiment.
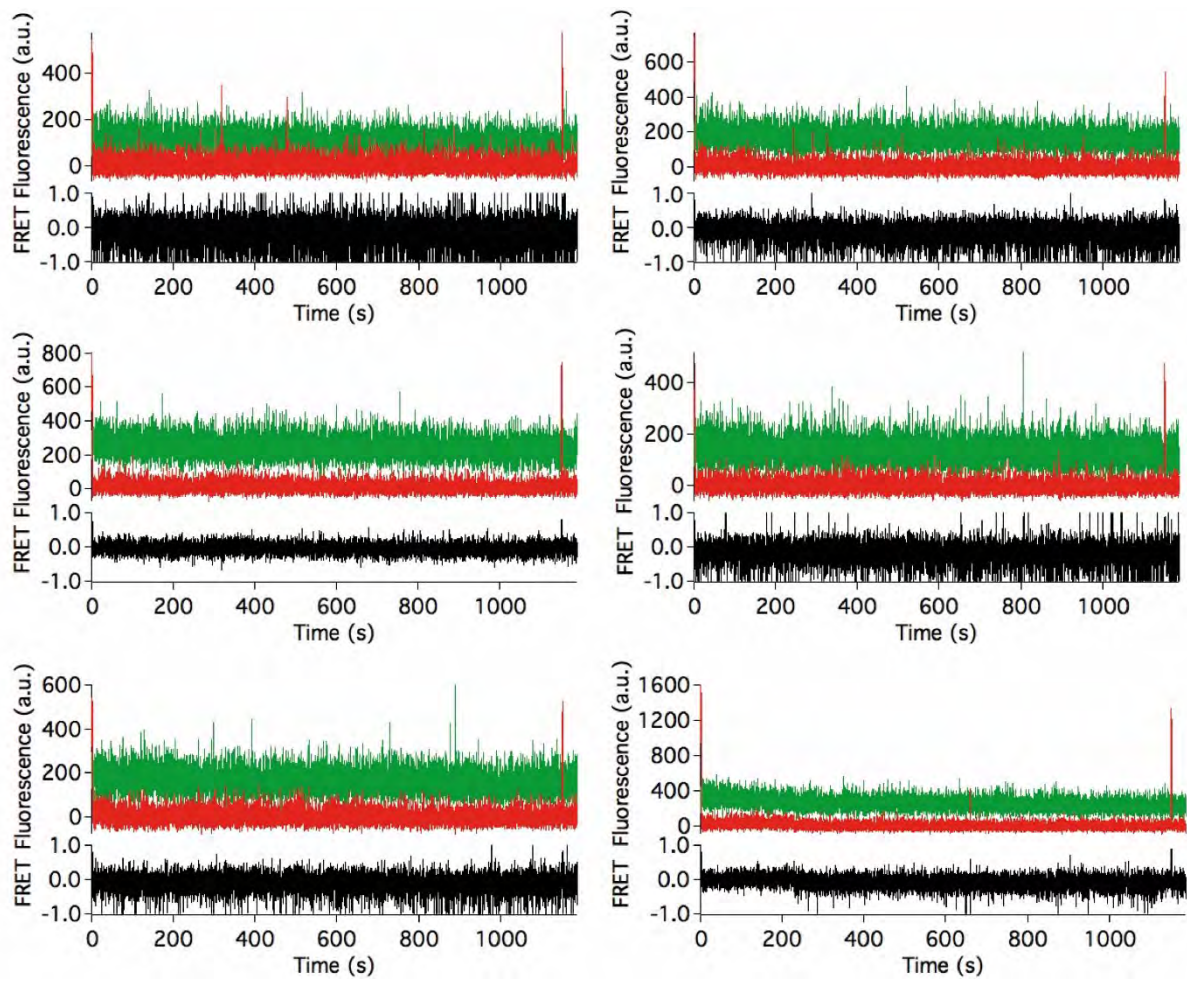
Supplementary Fig. 11. Representative smFRET trajectories from the T7RNAP-ZIF control experiment without NTPs for the 210-bp rotor. The brief, high-intensity red signals at the very beginning and toward the end of each trajectory reflect direct excitation of Cy5, confirming its presence on the stator.
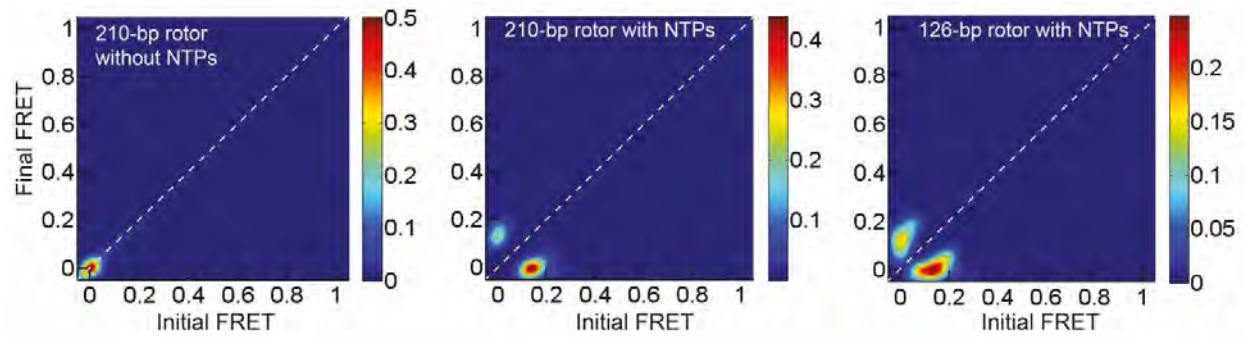
Supplementary Fig. 12. Transition occupation density plots (TODP) for the 210- and 126-bp rotors. The population on the diagonal represents the fraction of static rotors, whereas off-diagonal peaks represent rotors dynamically transitioning between defined FRET states during the observation time windows of individual smFRET trajectories.
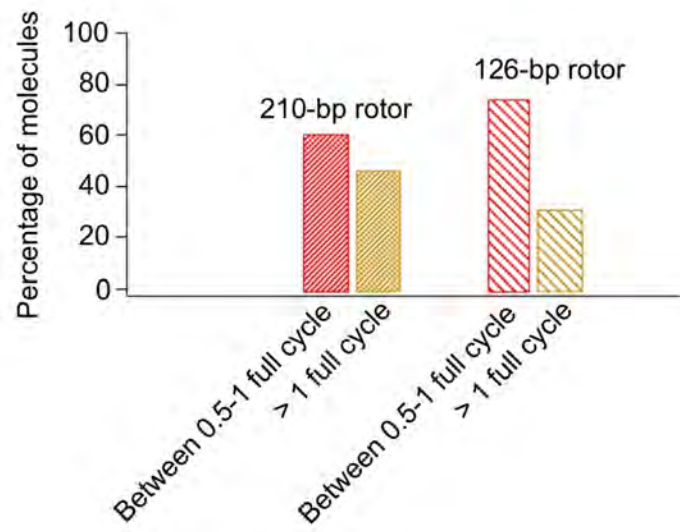
Supplementary Fig. 13. Percentage of single 210- and 126-bp rotor nanoengines exhibiting either partial or more than full transcription cycles within the ~20 min observation time window.
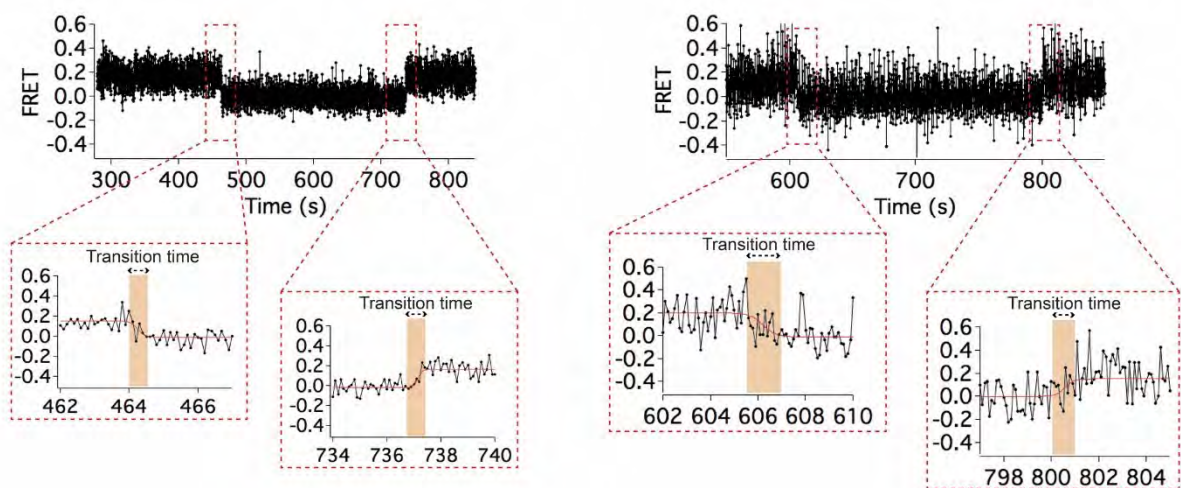

Supplementary Fig. 14. Single molecule FRET trajectories highlighting FRET transitions between high- and low-FRET states. The zoomed insets highlight the gradual changes in FRET value during the transitions from one state to another and their symmetric features.
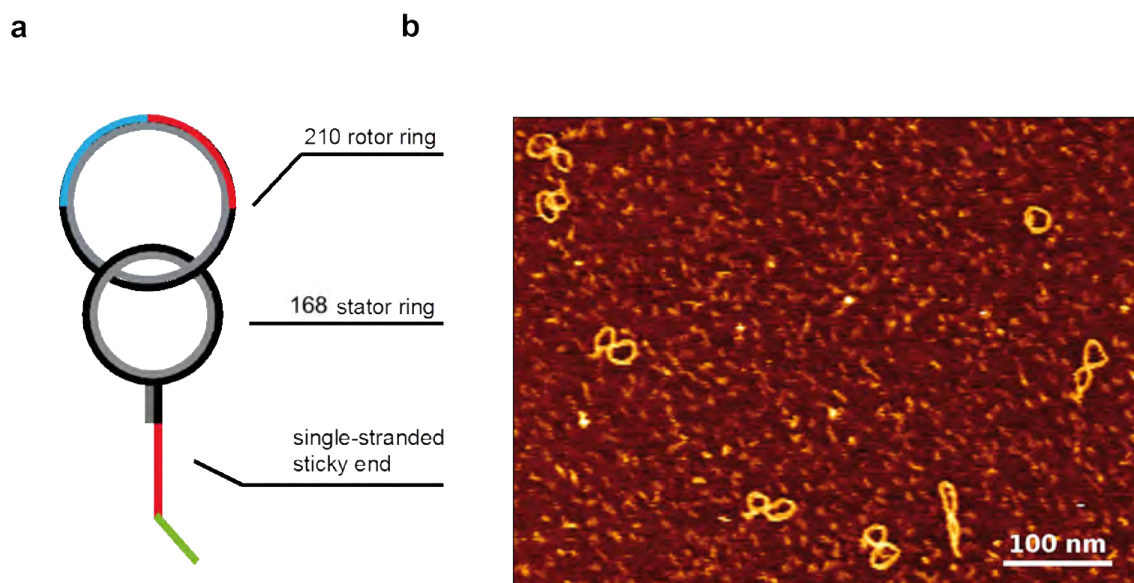
Supplementary Fig. 15. Design and AFM analysis of the catenane walker. (**a**) Scheme of the DNA catenane walker bearing a single stranded sticky end for the specific hybridization to Step1 or Step2 on a predefined DNA path. (**b**) AFM imaging in tapping mode in liquid confirmed the integrity of the DNA catenane walker having a 210-bp ring as rotor.
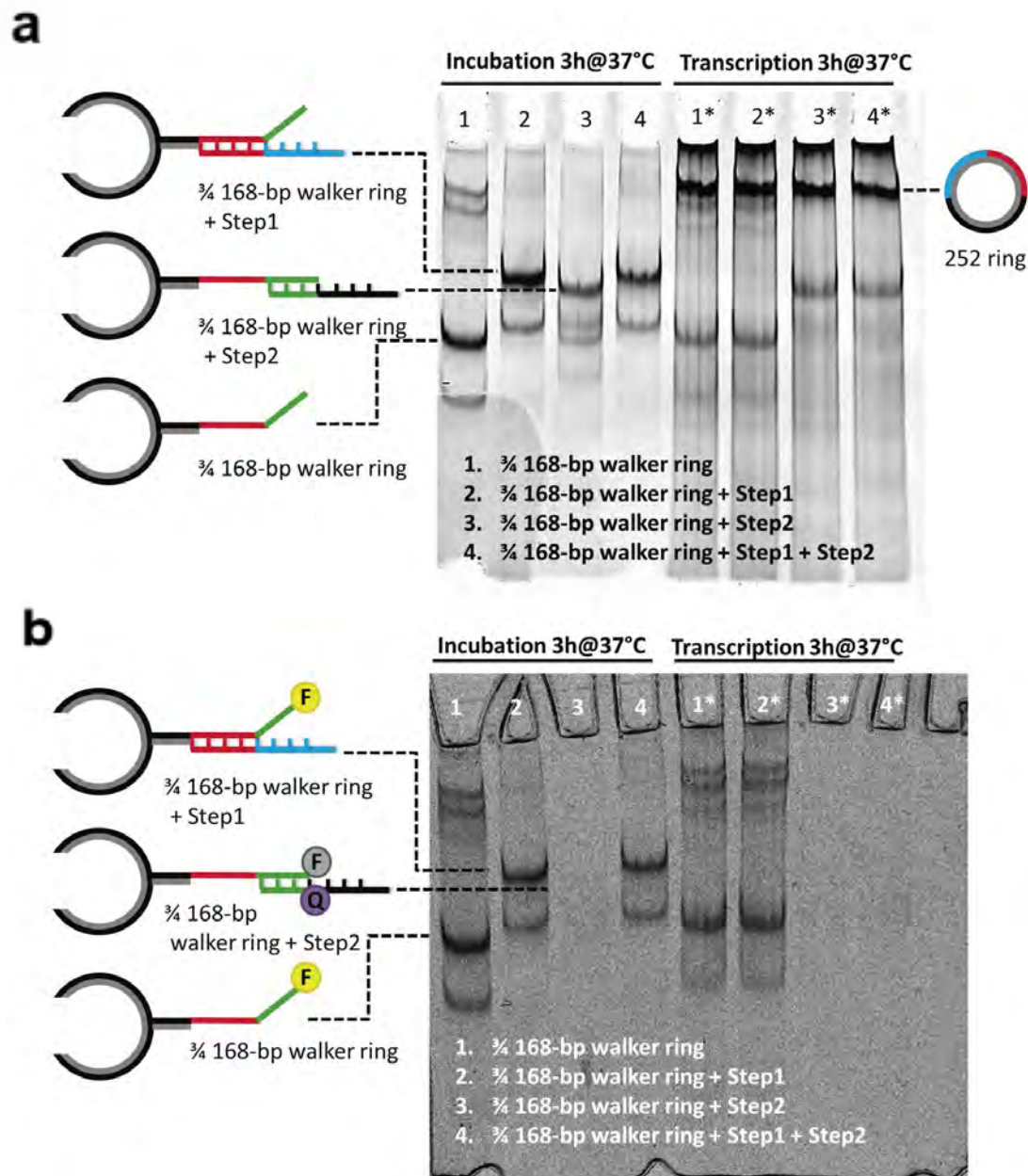
Supplementary Fig. 16. Gel electrophoretic analysis showing selective binding of the 3/4 168-bp walker ring to Steps 1 and 2. (**a**) Lane 1: Unpurified ¾ 168-bp walker ring. Lane 2. Walker ring hybridized to Step1. Lane 3: Walker ring hybridized to Step 2. Lane 4: Walker ring in the presence of both steps, showing selective binding to Step1. Lanes 1-4*. Same sample composition as their corresponding analog lane in which transcription with a 252-bp ring (analog to the 126-bp rotor) has taken place for 3 h. As observed, ring walker is efficiently displaced from Step 1 to Step 2 upon transcription, remaining bound to the last (lane 4*). (**b**) Fluorescence-Electrophoretic Gel Shift Assay (F-EMSA) performed prior ethidium bromide staining. Fluorophore-quencher pairs described in Figure 3 were used to track the different hybridization species. Upon hybridization to Step2 which contains BHQ-2, the band corresponding with the walker ring (fluorescently labelled with TAMRA) is not detectable.
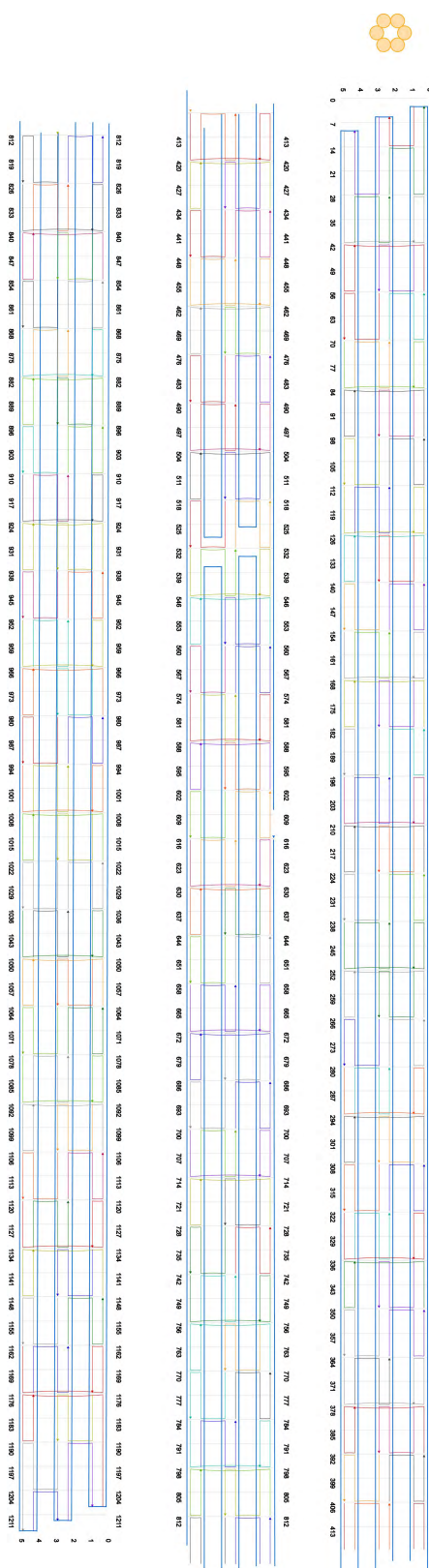
Supplementary Fig. 17. Detailed scheme of the six-helix bundle DNA origami designed using caDNAno[3]. Modified ODNs used for the assembly of the different 6HB DNA origami paths. **Three iSteps path (Qdot attachment)**: Substitute

6HB_JV34, 6HB_JV92, 6HB_JV95, 6HB_JV104 and 6HB_JV51 for Step1_6HB_JV34, iSteplong2_6HB_JV92, iSteplong4_6HB_JV95, iSteplong7_6HB_JV104 and Step2b_6HB_JV51. **Three iSteps path (fluorescence):** Substitute 6HB_JV34, 6HB_JV92, 6HB_JV95, 6HB_JV104 and 6HB_JV51 for Step1_6HB_JV34, iSteplong2_6HB_JV92(HEX), iSteplong4_6HB_JV95, iSteplong7_6HB_JV104(TxR) and Step2b_6HB_JV51. **Three iSteps path (fluorescence control):** Substitute 6HB_JV34, 6HB_JV92, 6HB_JV95, 6HB_JV104 and 6HB_JV51 for Step1_6HB_JV34, iSteplong2_6HB_JV92, iSteplong5_6HB_JV98(FAM), iSteplong7_6HB_JV104(TxR) and Step2b_6HB_JV51. **Path A:** Substitute 6HB_JV34, 6HB_JV95 and 6HB_JV40 for Step1_6HB_JV34, iSteplong4_6HB_JV95 and Step2b_6HB_JV40. **Path B:** Substitute 6HB_JV34, 6HB_JV95 and 6HB_JV51 for Step1_6HB_JV34, iSteplong4_6HB_JV95 and Step2b_6HB_JV51. **Path C:** Substitute 6HB_JV34, 6HB_JV92 and 6HB_JV51 for Step1_6HB_JV34, iSteplong2_6HB_JV92 and Step2b_6HB_JV51. **Path D:** Substitute 6HB_JV34, 6HB_JV107 and 6HB_JV51 for Step1_6HB_JV34, iSteplong8_6HB_JV107 and Step2b_6HB_JV51. **Path ΔC:** Substitute 6HB_JV34 and 6HB_JV92 for Step1_6HB_JV34, and iSteplong2_6HB_JV92. **Path ΔD:** Substitute 6HB_JV34 and 6HB_JV107 for Step1_6HB_JV34 and iSteplong8_6HB_JV107.
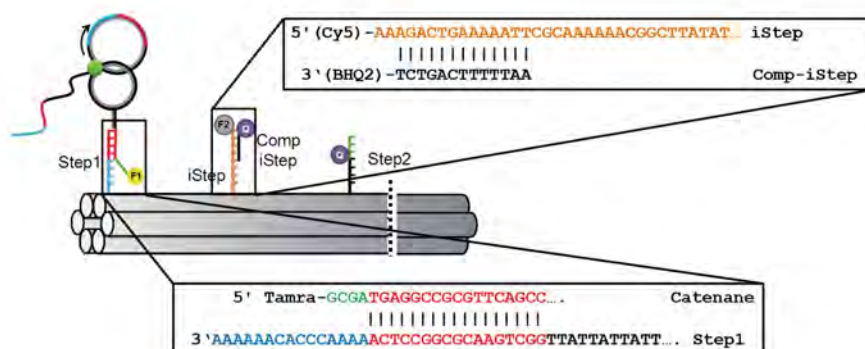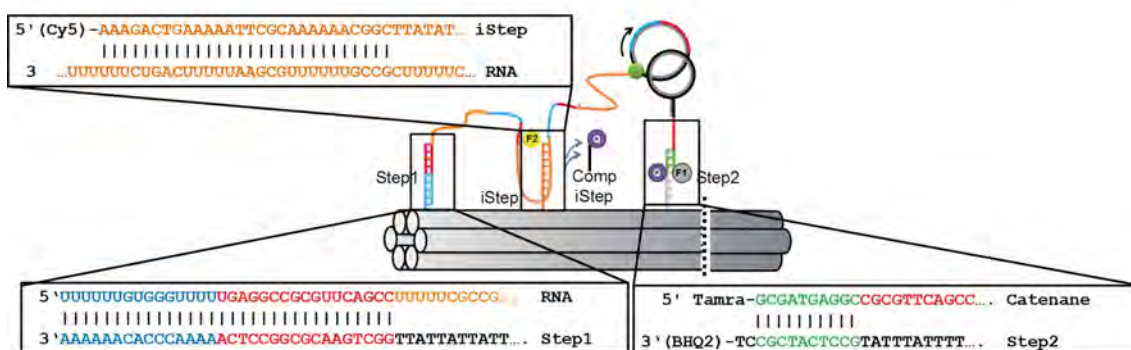
Supplementary Fig. 18. Detailed scheme of the working principle of the DNA catenane walker, showing the specific sequences involved in the hybridization and strand-displacement reactions occurring before (**a**) and after (**b**) transcription. F1: TAMRA; F2: Cy5; Q Black hole quencher 2 (BHQ2). Green circle: T7RNAP-ZIF.
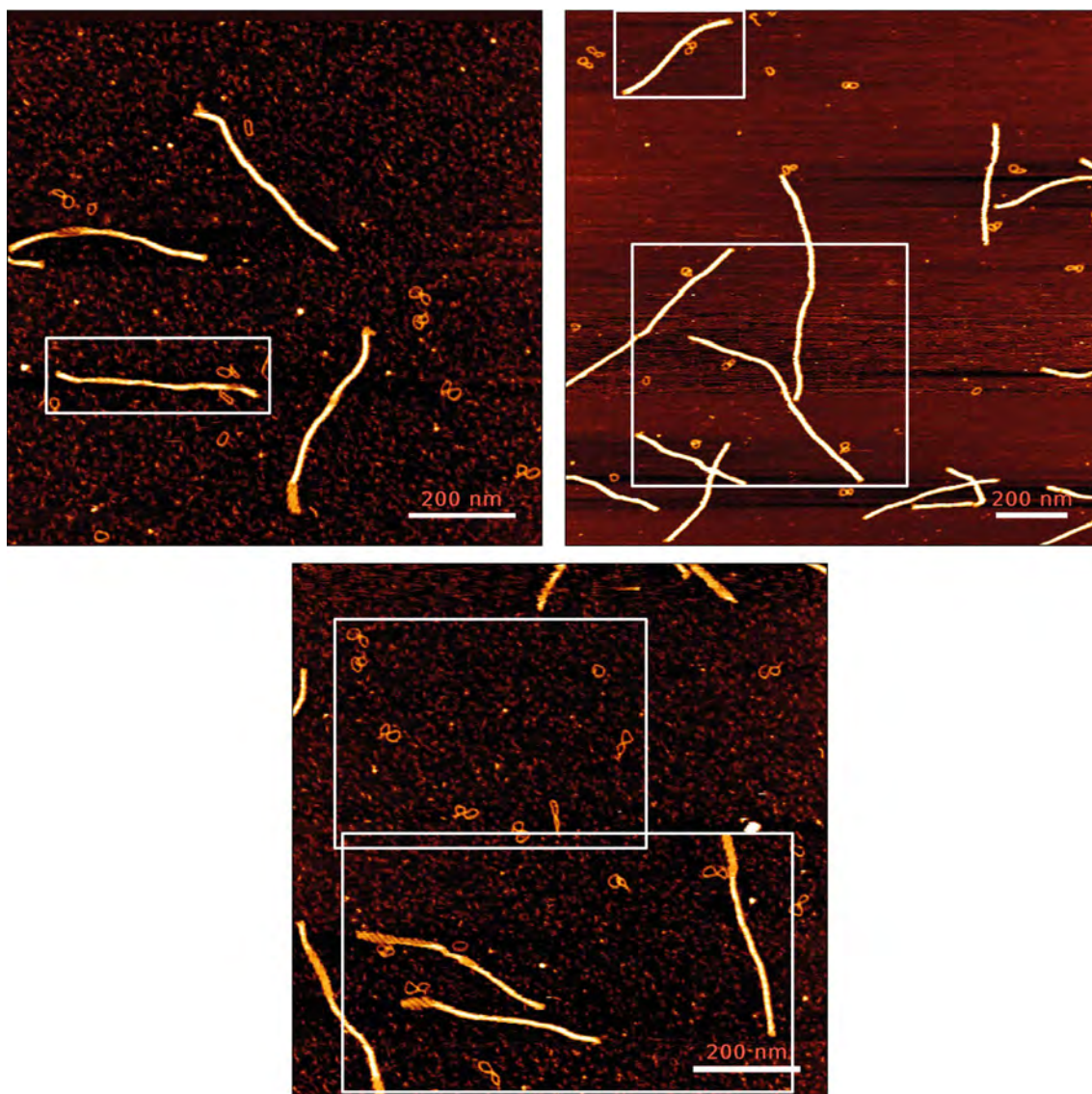
Supplementary Fig. 19. Larger sections from the uncropped AFM images used for the panels in Figure 3f,g and Suppl. Fig. 15b.
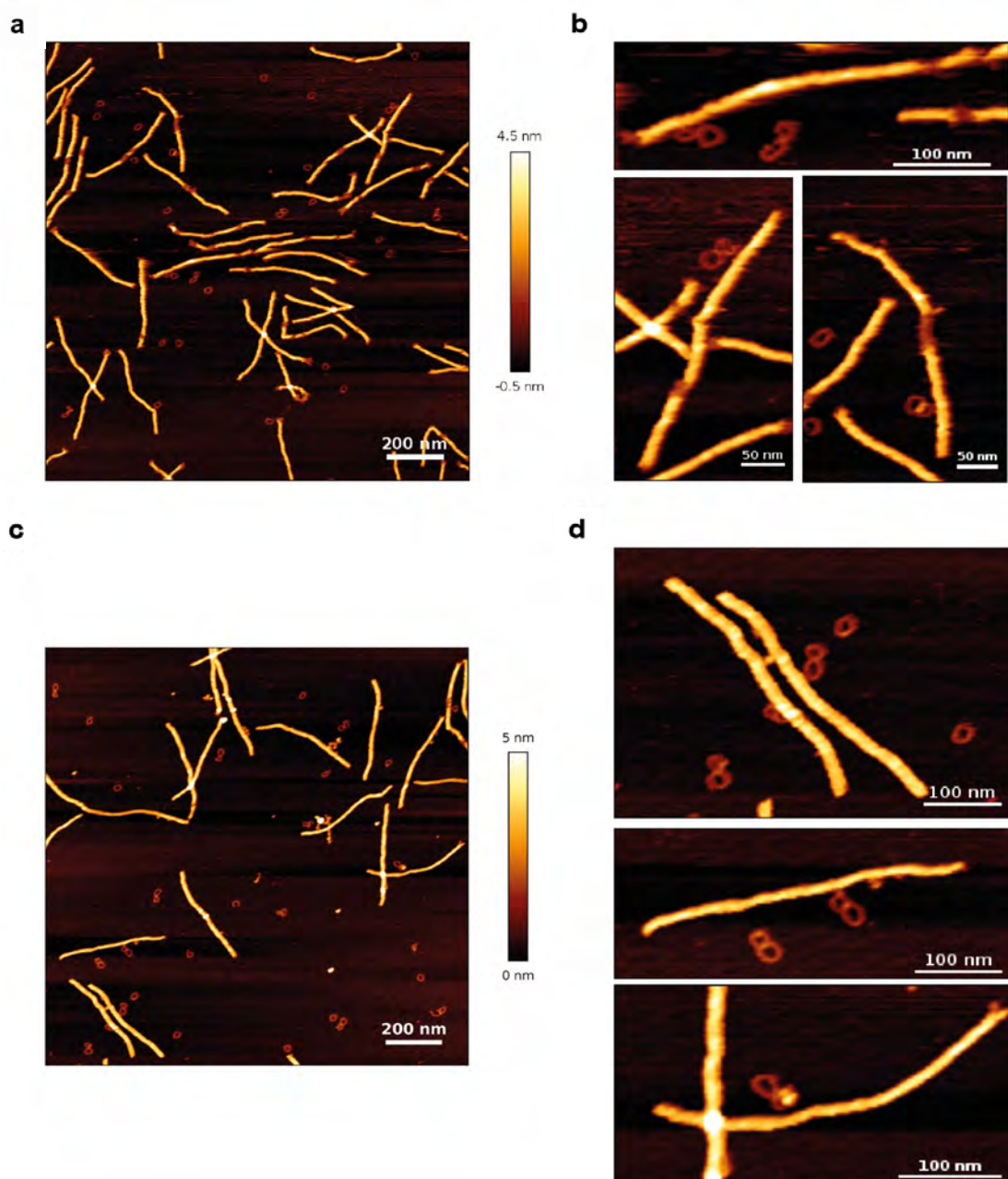
Supplementary Fig. 20. Tapping mode AFM imaging in liquid of the catenane nanoengine together with the DNA path before and after transcription. (**a**) AFM imaging of the catenane nanoengine before transcription in the presence of the DNA origami path. Despite AFM conditions were not optimal for hybridization, all assembled structures, i.e. where the catenane is interacting with the DNA origami path, show the catenane positioned in Step1. (**b**) Detailed pictures of catenane nanoengines before transcription assembled to the Step1 position of the DNA path. (**c**) AFM imaging of the catenane nanoengine after transcription in the presence of the DNA origami path. All assembled structures, i.e. where the catenane is interacting with the DNA origami path, show the catenane positioned in Step2. (**d**) Detailed pictures of catenane nanoengines after transcription assembled to the Step2 position of the DNA path.
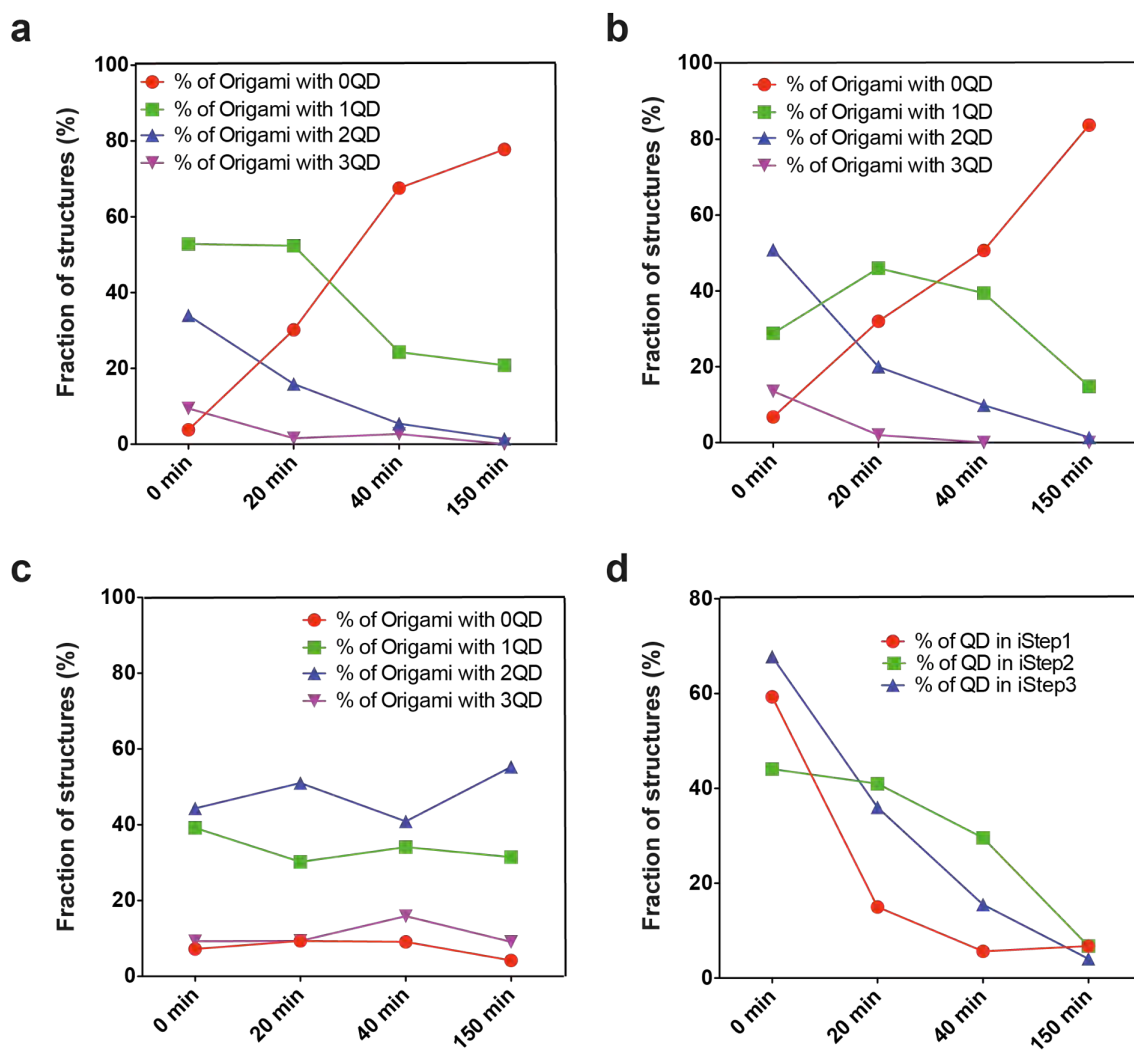
Supplementary Fig. 21. Qdot attachment upon transcription by AFM analysis (**a-c**) Fraction of structures found by AFM analysis with diverse number of Qdots at different time points in the presence of the catenane walker with the 210-bp rotor ring (**a**), the 126-bp rotor ring (**b**) and in absence of catenane walker (**c**, non transcription control). (**d**) Qdot occupancy for each origami position at different time points in presence of the catenane walker containing the 126-bp rotor ring (iStep1 [red], iStep2 [green], iStep3 [blue]).
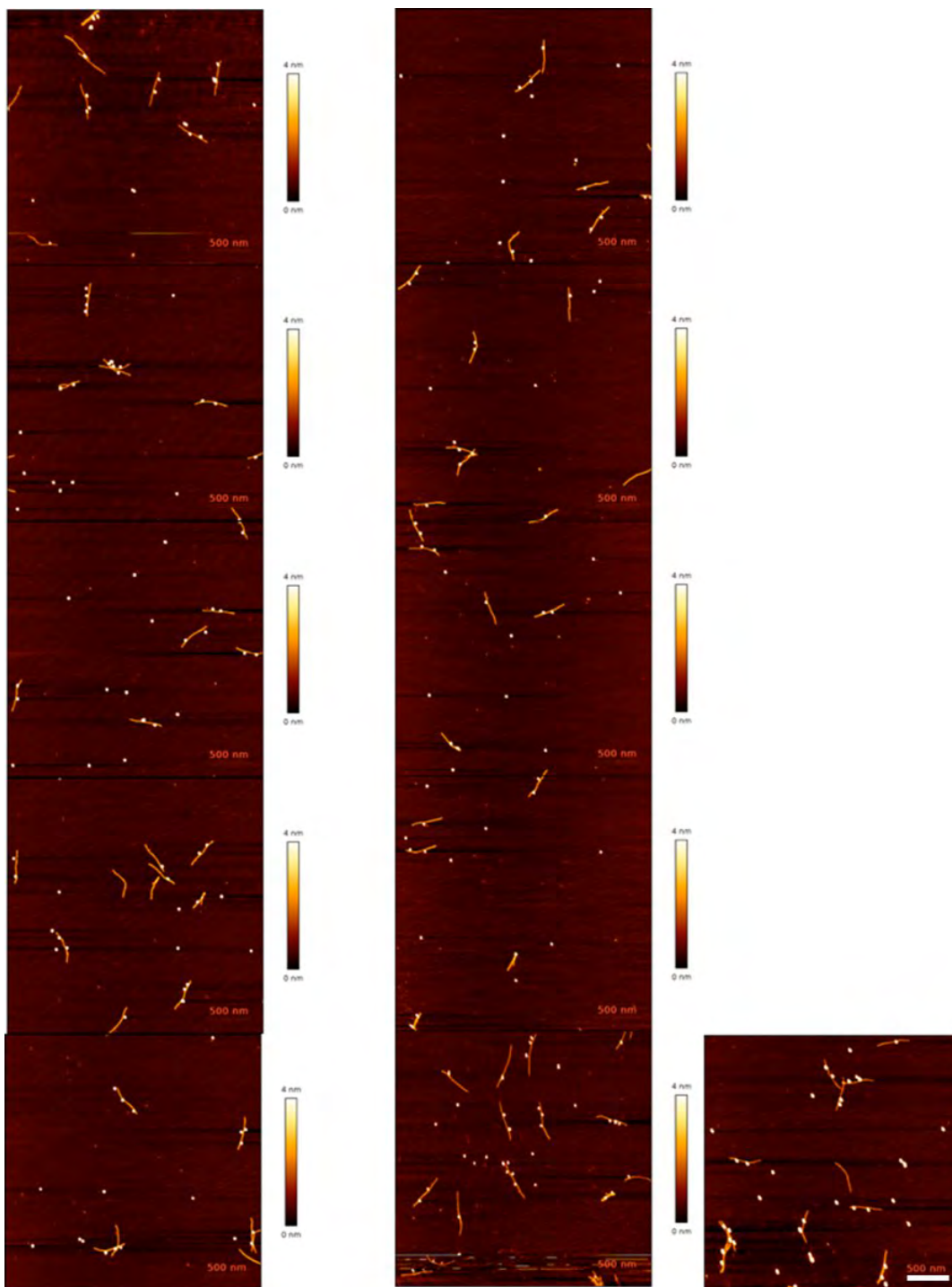
Supplementary Fig. 22. AFM images corresponding with the Qdot tagging of the bio-comp-iSteps on the DNA origami path upon transcription with Catenane walker (210-bp rotor). Time 0 min. The scans reflect a continuous surface, but images were measured subsequently and then re-aligned.
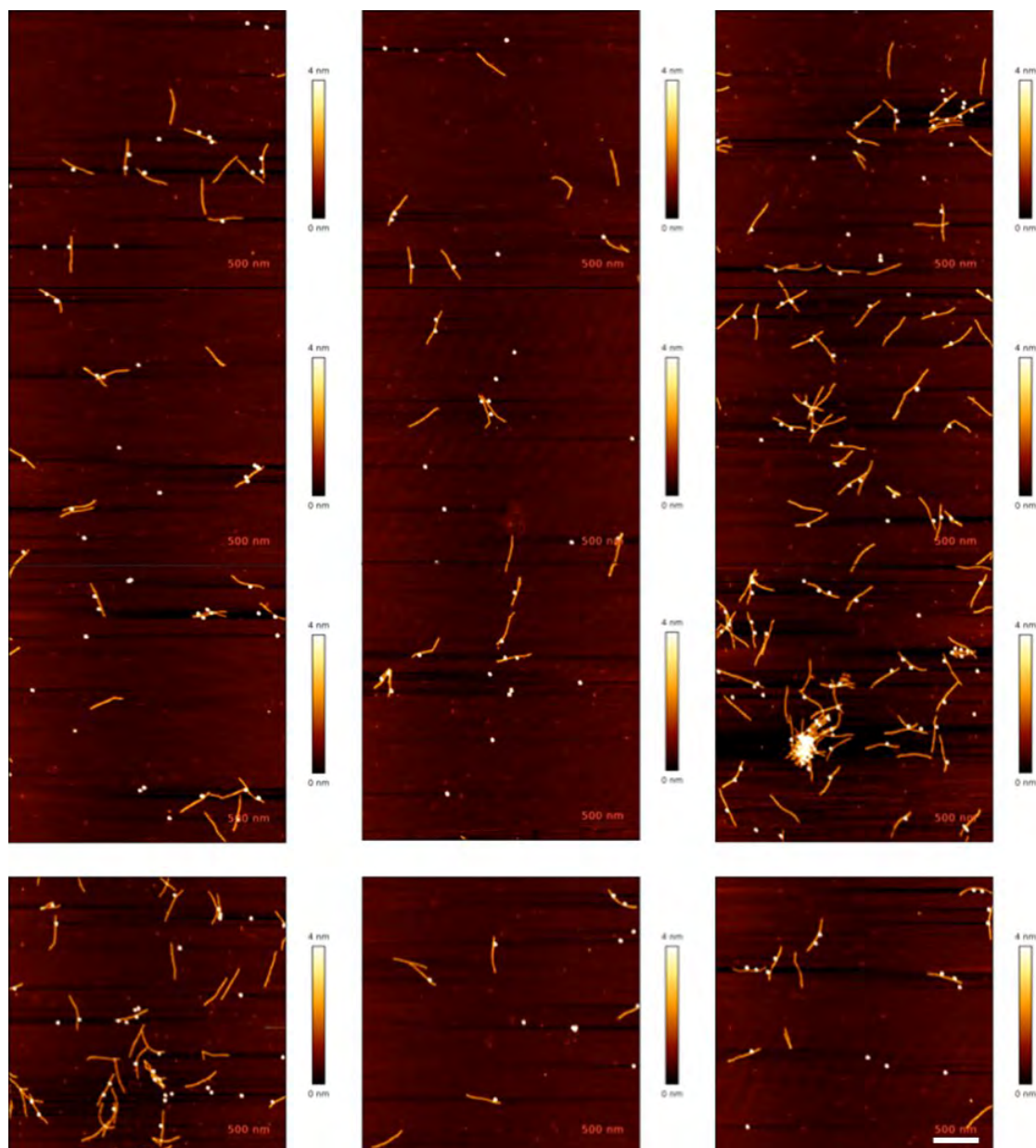
Supplementary Fig. 23. AFM images corresponding with the Qdot tagging of the bio-comp-iSteps on the DNA origami path upon transcription with Catenane walker (210-bp rotor). Time 20 min. The scans reflect a continuous surface, but images were measured subsequently and then re-aligned.
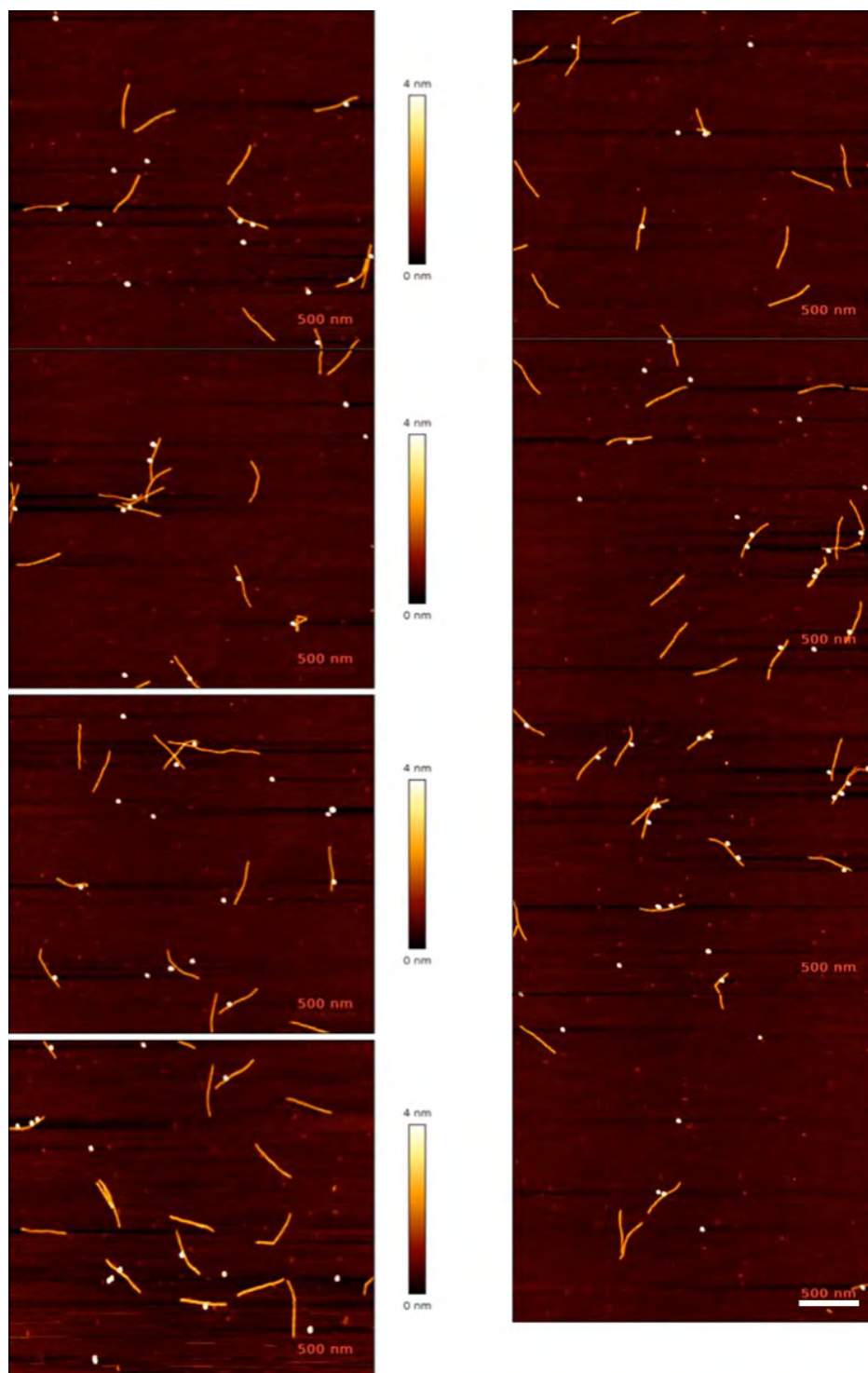
Supplementary Fig. 24. AFM images corresponding with the Qdot tagging of the bio-comp-iSteps on the DNA origami path upon transcription with Catenane walker (210-bp rotor). Time 40 min. The scans reflect a continuous surface, but images were measured subsequently and then re-aligned.

Supplementary Fig. 25. AFM images corresponding with the Qdot tagging of the bio-comp-iSteps on the DNA origami path upon transcription with Catenane walker (210-bp rotor). Time 150 min. The scans reflect a continuous surface, but images were measured subsequently and then re-aligned.

Supplementary Fig. 26. AFM images corresponding with the Qdot tagging of the bio-comp-iSteps on the DNA origami path for the no transcription control. Time 0 min. The scans reflect a continuous surface, but images were measured subsequently and then re-aligned.

Supplementary Fig. 27. AFM images corresponding with the Qdot tagging of the bio-comp-iSteps on the DNA origami path for the no transcription control. Time 20 min. The scans reflect a continuous surface, but images were measured subsequently and then re-aligned.
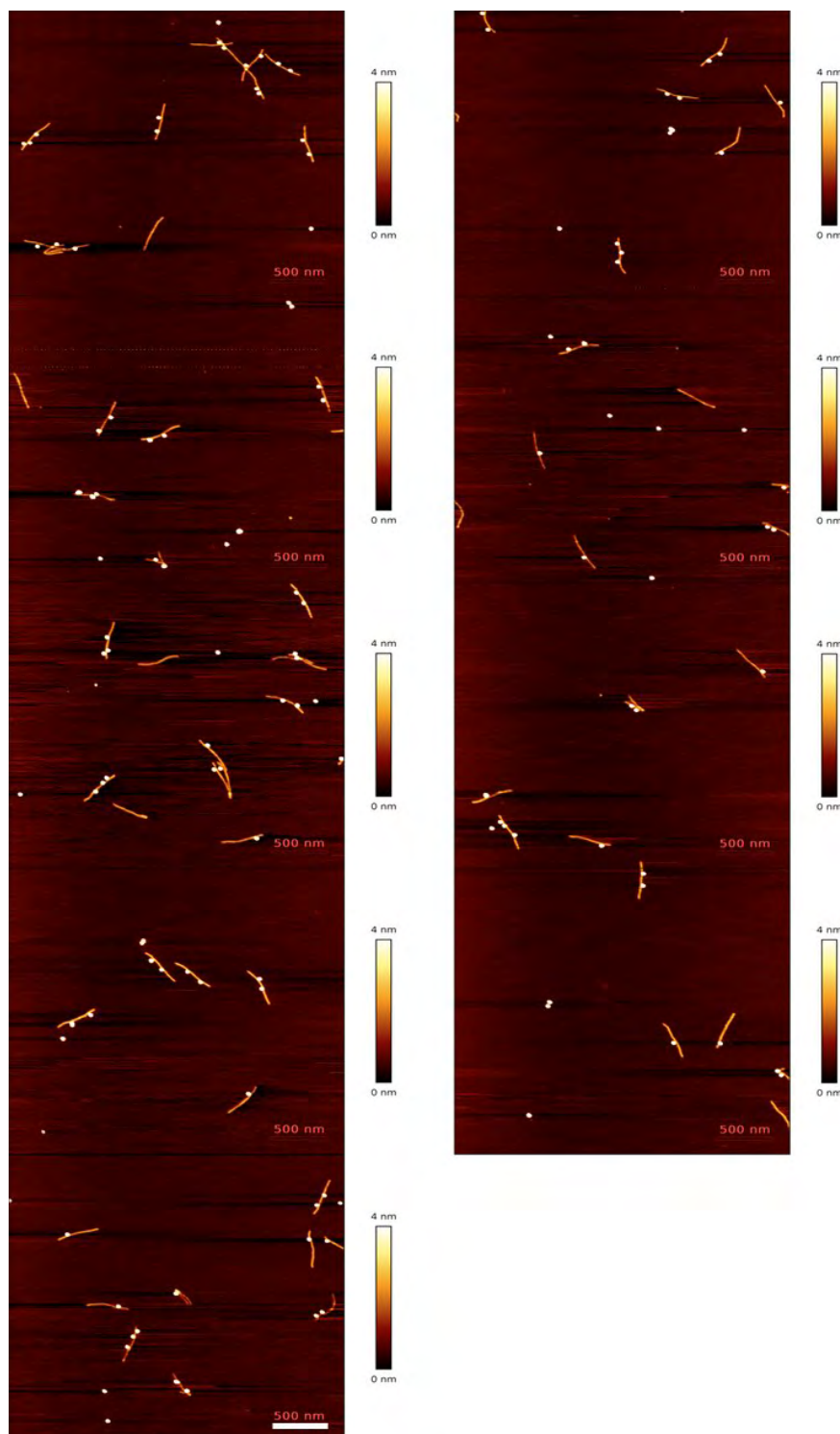
Supplementary Fig. 28. AFM images corresponding with the Qdot tagging of the bio-comp-iSteps on the DNA origami path for the no transcription control. Time 40 min. The scans reflect a continuous surface, but images were measured subsequently and then re-aligned.
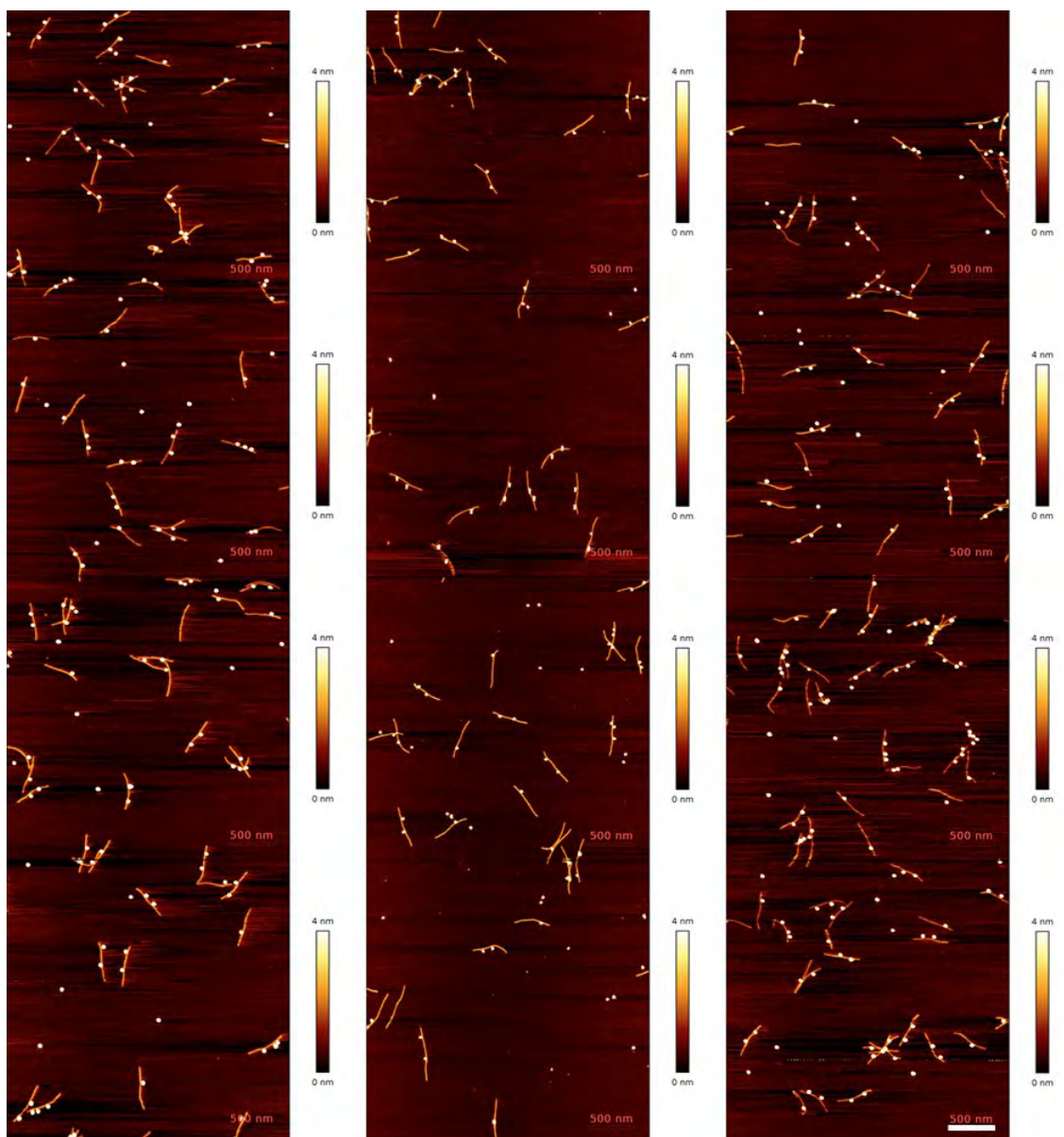
Supplementary Fig. 29. AFM images corresponding with the Qdot tagging of the bio-comp-iSteps on the DNA origami path for the no transcription control. Time 150 min. The scans reflect a continuous surface, but images were measured subsequently and then re-aligned.
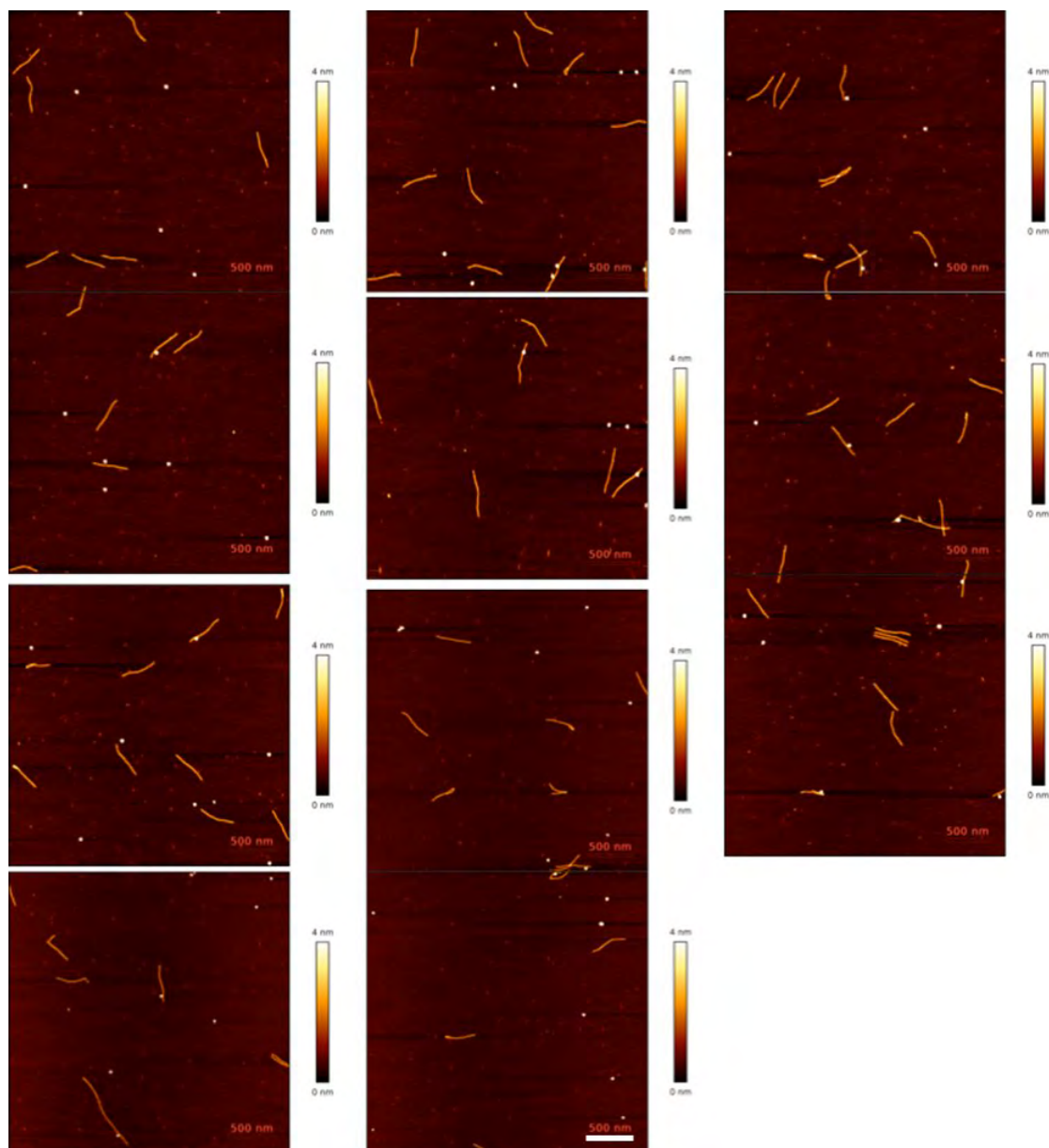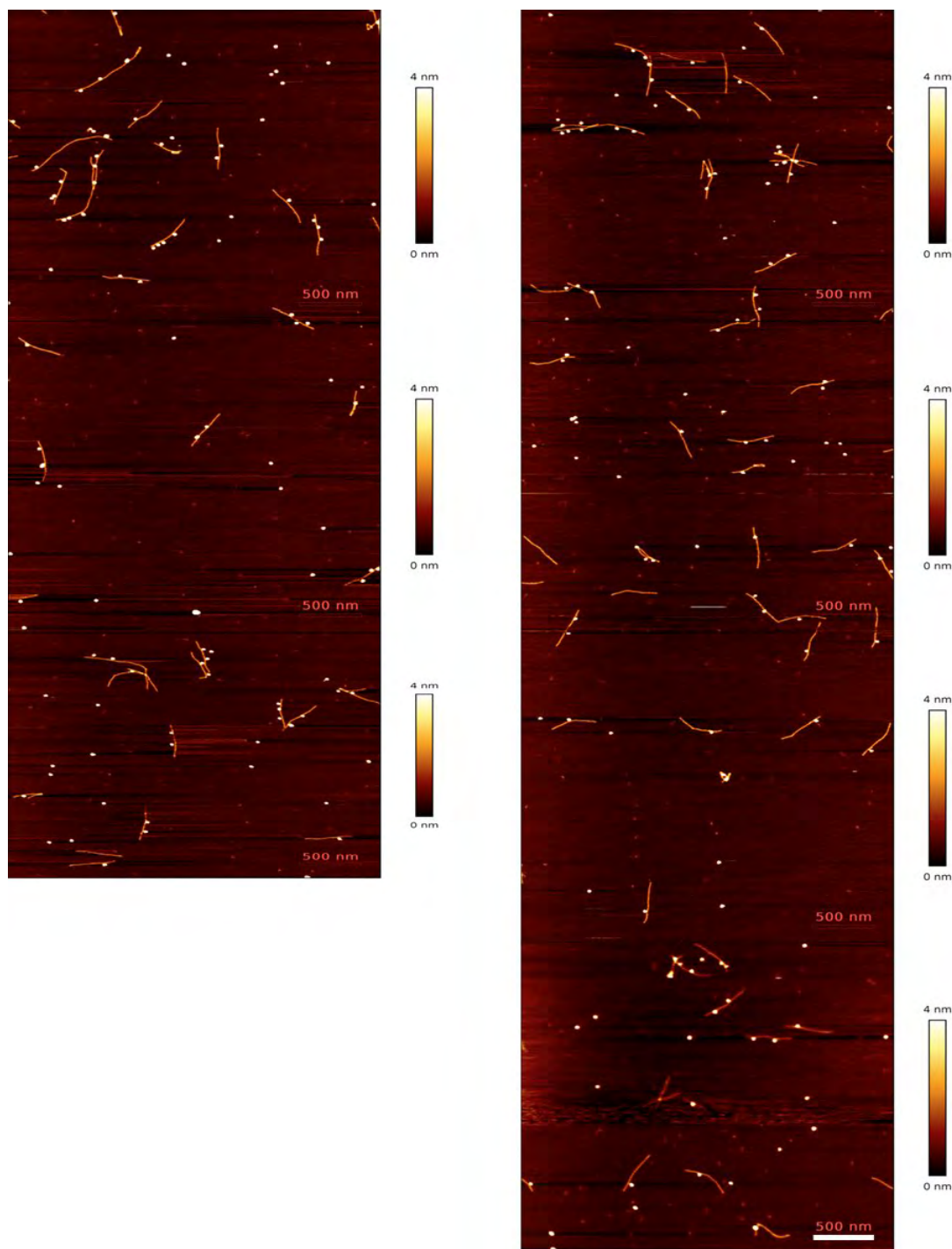
Supplementary Fig. 30. AFM images corresponding with the Qdot tagging of the bio-comp-iSteps on the DNA origami path upon transcription with Catenane walker (126-bp rotor). Time 0 min. The scans reflect a continuous surface, but images were measured subsequently and then re-aligned.
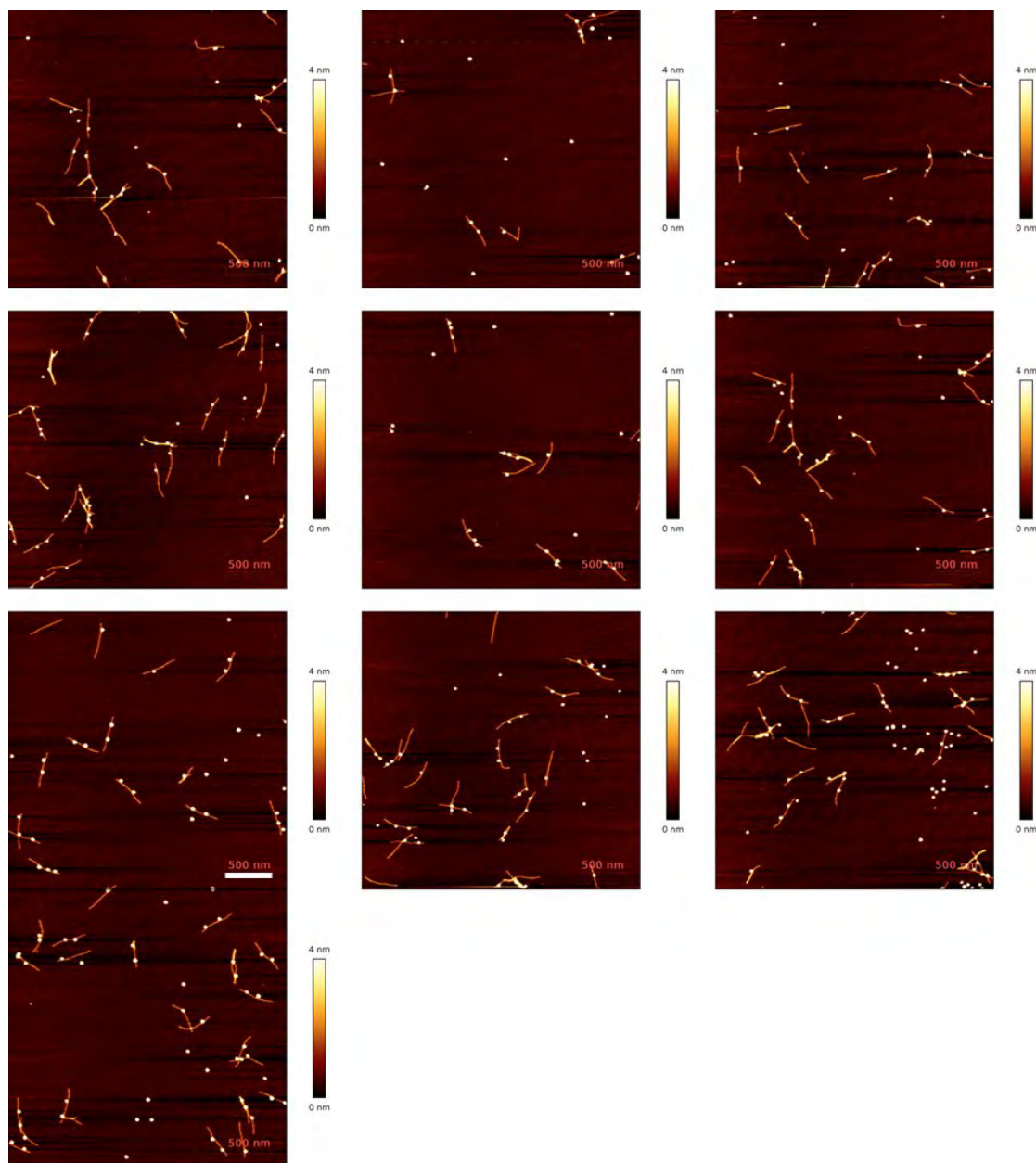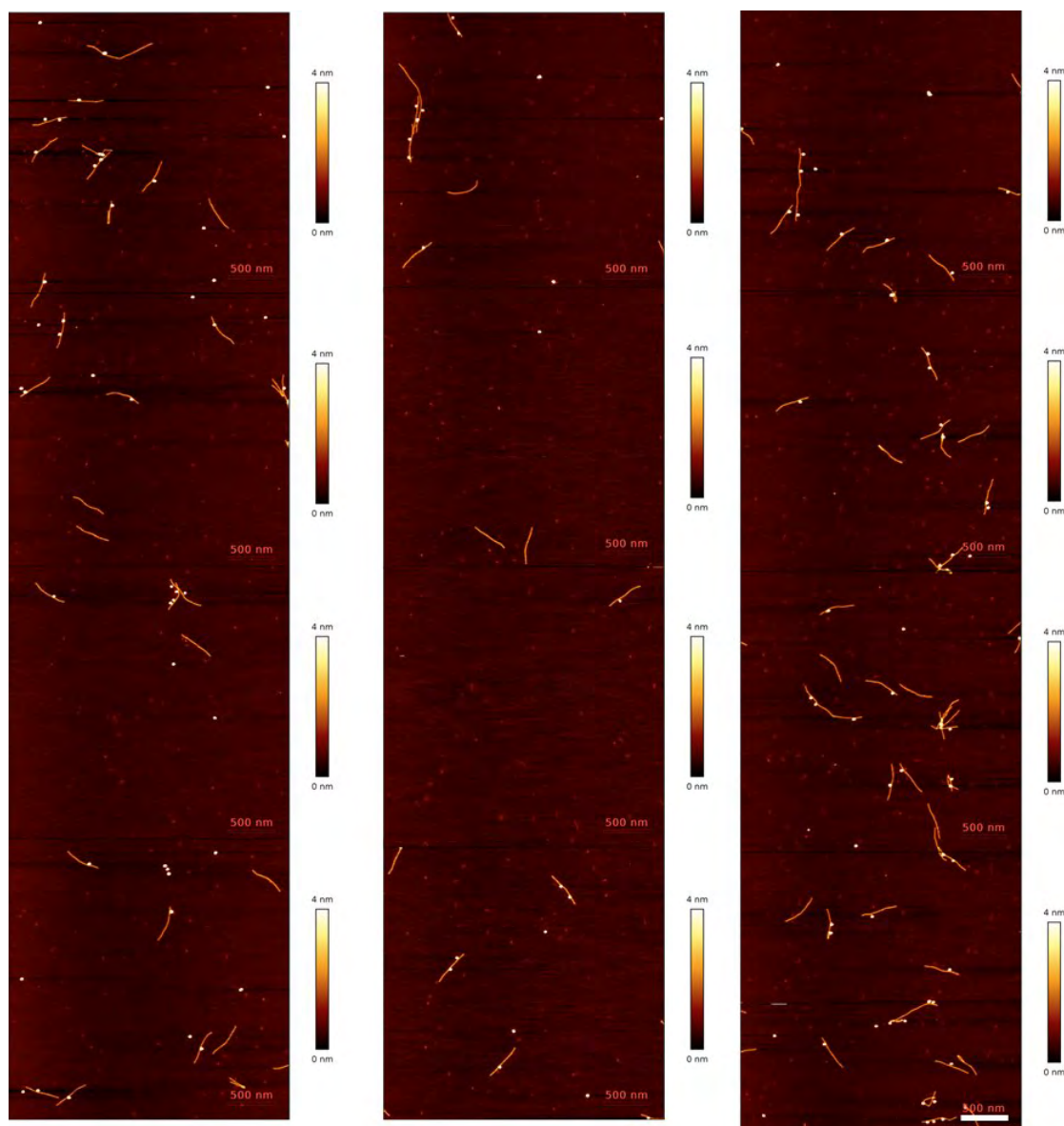
Supplementary Fig. 31. AFM images corresponding with the Qdot tagging of the bio-comp-iSteps on the DNA origami path upon transcription with Catenane walker (126-bp rotor). Time 20 min. The scans reflect a continuous surface, but images were measured subsequently and then re-aligned.
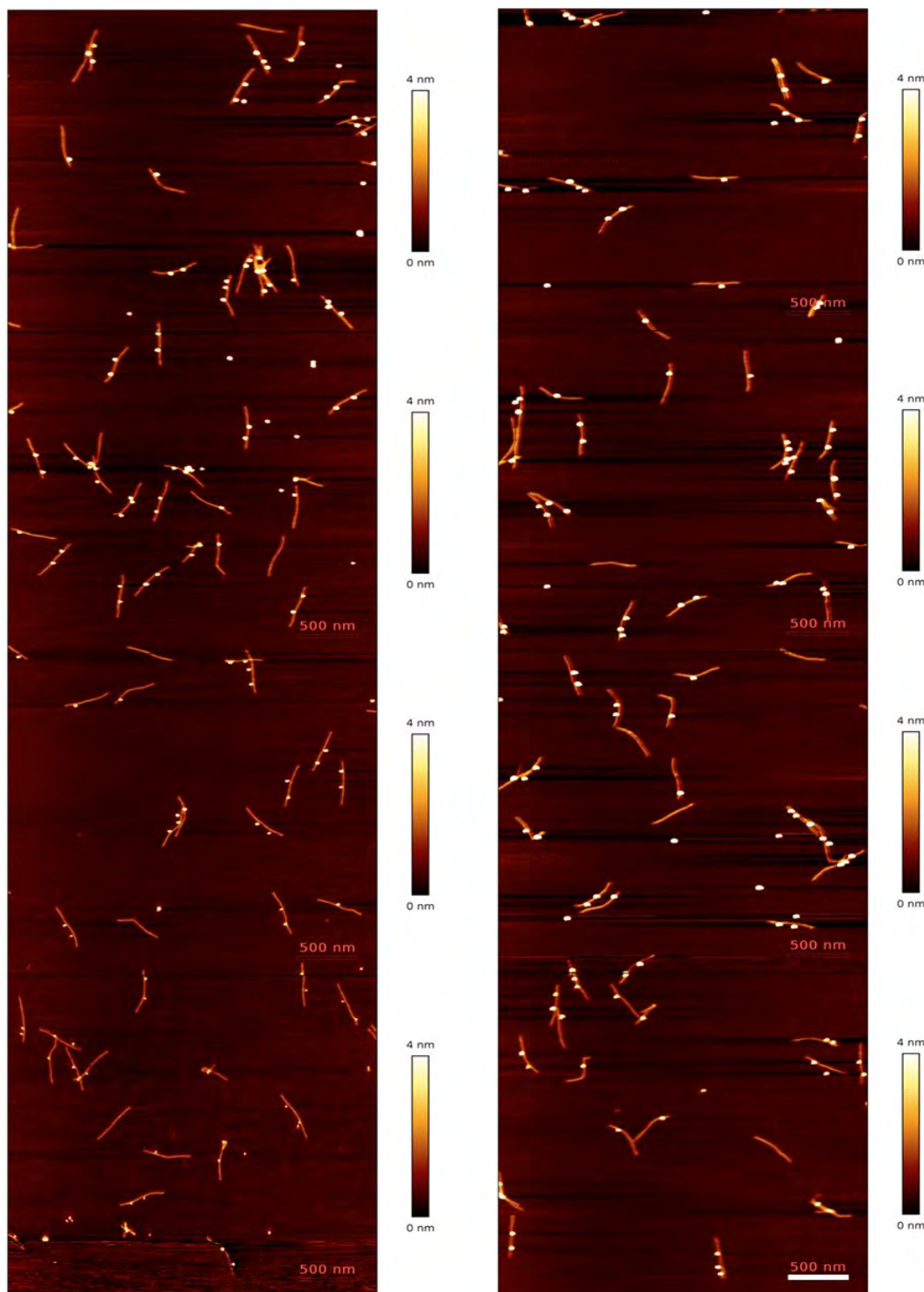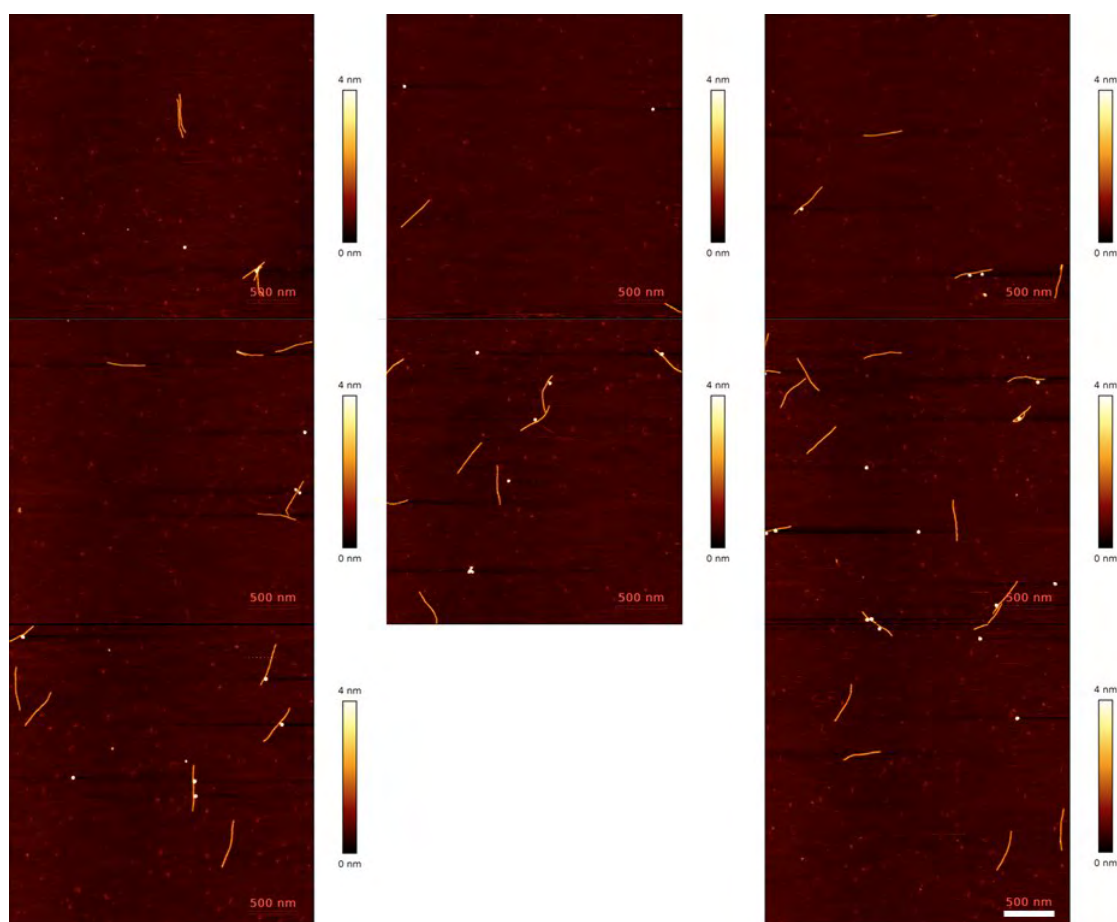
Supplementary Fig. 32. AFM images corresponding with the Qdot tagging of the bio-comp-iSteps on the DNA origami path upon transcription with Catenane walker (126-bp rotor). Time 40 min. The scans reflect a continuous surface, but images were measured subsequently and then re-aligned.
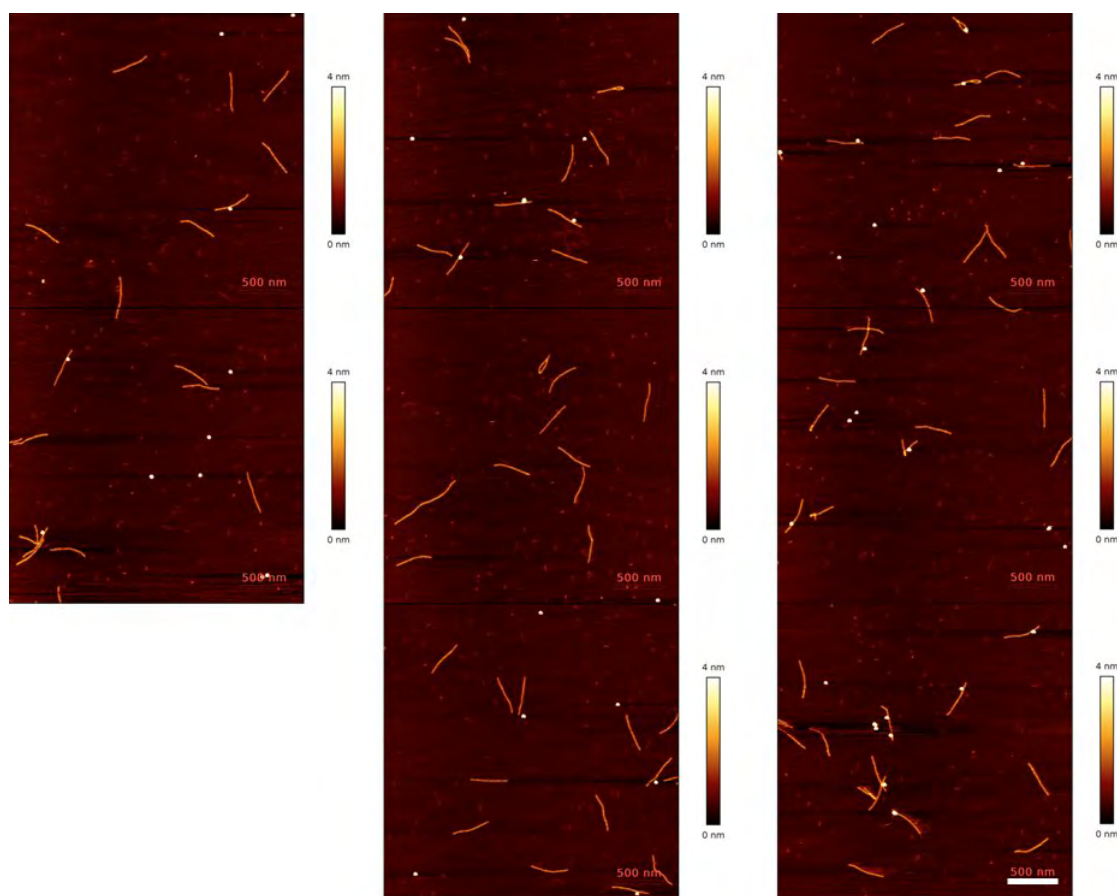
Supplementary Fig. 33. AFM images corresponding with the Qdot tagging of the bio-comp-iSteps on the DNA origami path upon transcription with Catenane walker (126-bp rotor). Time 150 min. The scans reflect a continuous surface, but images were measured subsequently and then re-aligned.

a

b

c
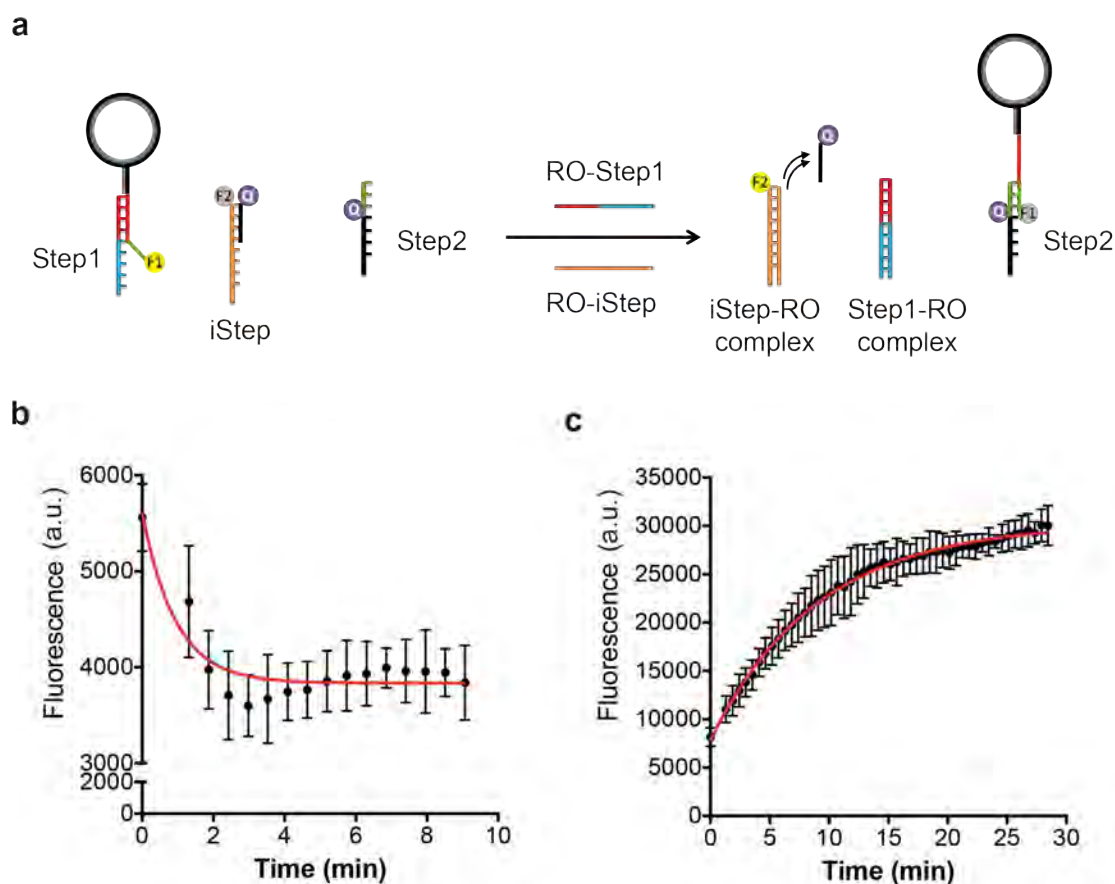
Supplementary Fig. 34. Strand-displacement and hybridization kinetics of the different reactions occurring during catenane walking (**a**) Schematic representation of the assay to measure the strand displacement and hybridization kinetics for Step 1 to 2 translocation of the modified 168bp stator ring and the release of comp-iStep from the iStep by addition of the corresponding release ODNs (RO-Step1 and RO-iStep). (**b** and **c**) Kinetic analysis by exponential fitting of the fluorescence signal resulting from Step 1g2 translocation (**b**) and the release of comp-iStep from the iStep. Error bars: (**c**) by adding RO-Step1 and RO-iStep. Error bars: n = 2, mean ±SD

Supplementary Table 1. List of ODNs used for the assembly of DNA rings and catenanes and origami Steps used in this study.

126-bp rotor ring	
ALGmb_f short	5'phos-AAAGCTGCAAAAAAGACTGAAAAATTCGCAAAA AACGGCGAAAAAGGC
ALgP_f	5'-Phos-AACCCACAAAAAAGTGACAAAAATGCGTAAAAA ATCTCCCTATAGTGAGTCGTATTAATTAA
JVgmblong	5'-Phos-ACTTTTTTGTGGGTTTTTGAGGCCGCGTTCAGCCT TTTTCGCCGTTTTTTGCGAATTTTTCAG
ALgP_r	5'-Phos- TCTTTTTTGCAGCTTTTTAATTAATACGACTCACT ATAGGGAGATTTTTTACGCATTTTTGTC
JVRO2short_f RO_rotor	5'-phosTGAACGCGGCCTCAAA
126-bp control ring (no MB)	
P-mb_r	5'-Phos-AGCTTTTTAATTAATACGACTCACTATAGGGAGA TTTTTTACGCATTTTTGTCACTTTTTTGT
Pt-mb_f	5'-Phos-GACAAAAATGCGTAAAAAATCTCCCTATAGTGA GTCGTATTAATTAAAAAGCTGCAAAAAAGA
nTh_f	5'-Phos-CCCAAAAAGACACAAAAAACGGCGAAAAAGGCT GAAAAAACCAGCAAAAACCCACAAAAAAGT
nTh_r	5'-Phos-GGGTTTTTGCTGGTTTTTTCAGCCTTTTTCGCCGTT TTTTGTGTCTTTTTGGGTCTTTTTGC
210-bp rotor ring	
JV210_r	5' Phos-TCTTTTTTGGTCCTTTTTGCGACTTTTTTCGGCGTTT TTCTGCCTTTTTTGCGTGTTTTTGACCCTTTTTTCGCAGTTTTTGGC
JV210_1f	5'Phos-AAAGCTGCAAAAAAGAGCCAAAAACTGCGAAAAAA GGGTCAAAAACACGCAAAAAAGGCAGAAAAA
JV210_2f	5'Phos-CGCCGAAAAAAGTCGCAAAAAGGACCAAAAAGAC TGAAAAATTCGCAAAAAACGGCGAAAAAGGC
ALgP_f	5'-Phos-AACCCACAAAAAAGTGACAAAAATGCGTAAAAAAT CTCCCTATAGTGAGTCGTATTAATTAA
JVgmblong	5'-Phos- ACTTTTTTGTGGGTTTTTGAGGCCGCGTTCAGCCTTTTTCGCCGTT TTTTGCGAATTTTTCAG
ALgP_r	5'-Phos- TCTTTTTTGCAGCTTTTTAATTAATACGACTCACTA TAGGGAGATTTTTTACGCATTTTTGTC
JVRO2short_f RO_rotor	5'-phosTGAACGCGGCCTCAAA
168-bp ring stator (with and without the Zif268 binding site)	
Alfa-b1zif	5'-phos-CGCCCACGCTGAACCCTTCGGAAAAAACGCGCAA AAAGCGCGAAAAAGGG
Alfa-b1 nozif	5'-phos-AAAAAAGTGCCAAAAGACGGAAAAAACGCGCAAA AAGCGCGAAAAAGGGTTTTGA
168Beta rc	5'phos-AACATTTTTTGACAGTTTTTCCGTCTTTTTTGCGCGT TTTTCCATATTTTTTGAACATTTTTCTCCGTT
168Alpha2 r	5'phos-CAGTTTTTGGCCCTTTTTTCGCGCTTTTTGCGCGTTTT

	TTCCG
Alfa-a1zif2 Threading ODN	5'-phos-AAGGGTTCAGCGTGGGCGCCGCGGCCTCAACCGTTT TTTACCGCTTTTTG
Beta f short	5'phos-CCAAAAACTGTCAAAAAACGGAGAAAAATGTTCAAA AAATAT
Alfa b3long	5-phos-GGAAAAACGCGCAAAAAAGACGGAAAAACTGTCAA AAAATGTTCAAAAAGCGGTAAAAAAC
RO CAT2 RO_stator	5'-phos-GGTTGAGGCCGCGG

168-bp ring stator for the DNA catenane walker (substitute 168Beta rc by:)

168beta rc_1short	5'-Phos-AACATTTTTTGACAGTTTTTCCGTCTTTTTTGGCTGACCTCCA
168beta rc2cshort	5'-Tamra- GCGATGAGGCCGCGTTCAGCCTGGAGGTCAGCTT TTTCCATATTTTTTGAACATTTTTCTCCGTTTTTTGA
Blocker rc2c	5'-ACGCGGCCTCATCGCATTACATCATGGT
RO_Blocker rc2c	5'-ACCATGATGTAATGCGATGAGGCCGCGT

ODNs for the catenane walker/Steps on DNA origami path and comp-iStep

Step1_6HB_JV34	5'-ACACCGCCTGCAACAAGATGATGAAACAAAACACCGGA ATCATTATTATTATTGGCTGAACGCGGCCTCAAAAACCCACAAAA AA
Step2b_6HB_JV40	5'-ATTAAATCCTTTGCCAATATAATCCTGACCTGTTTATCA ACATTTTATTTATGCCTCATCGCCT-BHQ2-3'
Step2b_6HB_JV51	5'-CAAACGGCGGATTGCATTCCATATAACATCAGTTGAGA TTTATTTTATTTATGCCTCATCGCCT-BHQ2-3'
iSteplong1_6HB_JV91	5'(Cy5)-AAAGACTGAAAAATTCGCAAAAAACGGCTTATATG TGATAAATAAGGATCCAAATAAGAAAAACGTAGAAAATAC
iSteplong2_6HB_JV92	5'(Cy5)-AAAGACTGAAAAATTCGCAAAAAACGGCTTATATA ATTACTAGAAAAAATTTGCCAGTTACAACGCAAAGACACC
iSteplong2_6HB_JV92 (HEX)	5'(HEX)-AAAGACTGAAAAATTCGCAAAAAACGGCTTATATA ATTACTAGAAAAAATTTGCCAGTTACAACGCAAAGACACC
iSteplong3_6HB_JV93	5'(Cy5)-AAAGACTGAAAAATTCGCAAAAAACGGCTTATAAA ATTCTTACCAGTTCCTGAATCTTACCATAGAAAATTCATA
iSteplong4_6HB_JV95	5'(Cy5)-AAAGACTGAAAAATTCGCAAAAAACGGCTTATAG GCAGAGGCATTTTGTTTTAGCGAACCTAAATTATTCATTAA
iSteplong5_6HB_JV98	5'(Cy5)-AAAGACTGAAAAATTCGCAAAAAACGGCTTATAA TAGATAAGTCCTGAACCAAGTACCGCAATAGCAGCACCGTA
iSteplong5_6HB_JV98 (FAM)	5'(FAM)-AAAGACTGAAAAATTCGCAAAAAACGGCTTATAAT AGATAAGTCCTGAACCAAGTACCGCAATAGCAGCACCGTA
iSteplong7_6HB_JV104	5'(Cy5)-AAAGACTGAAAAATTCGCAAAAAACGGCTTATAAG GCTTGCCCTGACAAGACTTTTTCATGACAGGAGGTTGAGG
iSteplong7_6HB_JV104(TxR)	5'(TexasRed)-AAAGACTGAAAAATTCGCAAAAAACGGCTTAT AAGGCTTGCCCTGACAAGACTTTTTCATGACAGGAGGTTGAGG
iSteplong8_6HB_JV107	5'-(Cy5)-AAAGACTGAAAAATTCGCAAAAAACGGCTTATACGTTGGGAAGA AAAAACCGATATATTCGGATGATACAGGAGT
Comp i-step new	5' AATTTTTCAGTCT (BHQ3) 3'
Comp i-step	5' CGAATTTTTCAGTCTTATTA (biotin)-3'

newbioE	
JVgmblong_RO	5' ACTTTTTTGTGGGTTTTTGAGGCCGCGTTCAGCCTTTTT
Displace_comp-i-step	5' TTTCGCCGTTTTTTGCGAATTTTTCAGTCTTT
ODNs for the catenanes used in smFRET experiments	
JVgmblong (icy3)	5'-Phos-ACTTTTTTGTGGGTTTTTGAGGCCGCGTTCAGCCT TT(icy3)TTCGCCGTTTTTTGCGAATTTTTCAG
Alfa-a1zif2(icy5)	5'-phos-AAGGGT(icy5)TCAGCGTGGGCGCCGCGGCCTCAACC GTTTTTTACCGCTTTTTG
168beta rc2cshort (biotin)	5'-Biotin-TTTGGAGGTCAGCTTTTTCCATATTTTTTGAACAT TTTTCTCCGTTTTTTGA
168beta rc_1short	5'-Phos-AACATTTTTTGACAGTTTTTCCGTCTTTTTTGGCTGA CCTCCA
Molecular beacon ODN (2'-OMe-RNA)	
MB	5'-FAM-UUUGCCUGAAAAAUUCGCAAA-Dabcyl-3'
ODNs used for SPR measurements	
Long N/Z_JV	5'-Biotin-TTTTTTTTTTTTTTTTCTGCAAGGGTTCAGGCG TGGGCGGTAAG-3'
N/Z_JV_rev	5'-CTTACCGCCCACGCCTGAACCCTTGCAGA

Supplementary Table 2: Gamma function fitting parameters for the full transcription cycle and the FRET transition times

Rotor	Shape factor or number of irreversible steps	Dwell time in each step (s)	Dwell time after correction for the limited time window (s)
126-bp rotor (Full transcription cycle)	2.7 ± 1.2	192 ± 87	220
210-bp rotor (Full transcription cycle)	3.2 ± 0.6	155 ± 29	172
126-bp rotor (high FRET to low FRET)	2.0 ± 0.4	0.69 ± 0.19	0.69
126-bp rotor (low FRET to high FRET)	2.3 ± 0.6	0.45 ±0.14	0.45
210-bp rotor (high FRET to low FRET)	2.0 ± 0.4	0.51 ± 0.14	0.51
210-bp rotor (low FRET to high FRET)	2.6 ± 0.5	0.29 ± 0.06	0.29

Supplementary Table 3. ODNs for the catenane walker/DNA origami path

Name	Sequence
6HB_JV1	TACATTTTGACGCTATCTTACCGAAGCCCGCTAATATCAGAG
6HB_JV2	ACCGCCAGCCATTGAACAAAGTTACCAGGAATTAACTGAACA
6HB_JV3	ACTCAAACTATCGGGGAATACCCAAAAGCAGAGAGAATAACA
6HB_JV4	ACTTCTTTGATTAGGCAGTATGTTAGCACGATTTTTTGTTTA
6HB_JV5	TAAAAGAGTCTGTCCAACATATAAAAGAAAAATAAACAGCCA
6HB_JV6	AGAATCCTGAGAAGTTTTGTCACAATCAAACGCTAACGAGCG
6HB_JV7	CAGGAGGCCGATTACAAAGACAAAAGGGTGCTATTTTGCACC
6HB_JV8	GTATAACGTGCTTTGTAAATATTGACGGCCCGACTTGCGGGA
6HB_JV9	GCGCCGCTACAGGGCGTCACCGACTTGACTTATCCGGTATTC
6HB_JV10	GCGGTCACGCTGCGCACCAGTAGCACCAATCATTACCGCGCC
6HB_JV11	AAGAAAGCGAAAGGCAATGAAACCATCGCTCATCGAGAACAA
6HB_JV12	GCTTGACGGGGAAAAATCAAGTTTGCCTTTCCTTATCATTCC
6HB_JV13	AAAGCACTAAATCGCGGCATTTTCGGTCGTCGAAATCCGCGA
6HB_JV14	GAACCATCACCCAATTTCATAATCAAAAACAAAGTACAACGG
6HB_JV15	ACGTCAAAGGGCGACGCCTCCCTCAGAGAAACACTCATCTTT
6HB_JV16	CAGTTTGGAACAAGAGCCACCACCCTCAGAAGGCACCAACCT
6HB_JV17	ATAAATCAAAAGAACGCCGCCAGCATTGAGGAAGTTTCCATT
6HB_JV18	AAATCCTGTTTGATGGCCTTGATATTCAGCAACGGCTACAGA
6HB_JV19	AGTTGCAGCAAGCGAATGGAAAGCGCAGTCGTCACCCTCAGC
6HB_JV20	ACGGGCAACAGCTGCATACATGGCTTTTGTCGCTGAGGCTTG
6HB_JV21	TGCGTATTGGGCGCTTTTAACGGGGTCAACAATGACAACAAC
6HB_JV22	AGCTGCATTAATGACAGTTAATGCCCCCGAGGTGAATTTCTT
6HB_JV23	TGCGCTCACTGCCCACATGAAAGTATTACAAAAGGAGCCTTT
6HB_JV24	CCTGGGGTGCCTAATAGGATTAGCGGGGATAATAATTTTTTC
6HB_JV25	CAATTCCACACAACCGTCGAGAGGGTTGCAGCGGAGTGAGAA
6HB_JV26	CATGGTCATAGCTGCACCGTACTCAGGAAATTTTCTGTATGG
6HB_JV27	CGACTCTAGAGGATCACCCTCAGAACCGAACGATCTAAAGTT
6HB_JV28	GGTTTTCCCAGTCACGACGTTGTAAAACGACGGCAGGGATAG CAAGCCAACGCCTGTAGCA
6HB_JV29	AGTCACACGACCAATTTATCA
6HB_JV30	GAGATAGAACCCTTTAGCGATAGCTTAGGCTTAGGTTGGGTT
6HB_JV31	ACAGACAATATTTTTCGTCGCTATTAATATCCAATCGCAAGA
6HB_JV32	ACTGATAGCCCTAACATAAATCAATATAATATTTTAGTTAAT
6HB_JV33	CCACCAGCAGAAGATTAACAATTTCATTTGAAATACCGACCG
6HB_JV34	ACACCGCCTGCAACAAGATGATGAAACAAAACACCGGAATCA
6HB_JV35	GAAAAATCTAAAGCCGCGCAGAGGCGAACATATGCGTTATAC
6HB_JV36	CCCTCAATCAATATTAACGGATTCGCCTCAACAGTAGGGCTT
6HB_JV37	AGGAATTGAGGAAGATGAATATACAGTACAACATGTAATTTA
6HB_JV38	ACAACTAATAGATTCAGAAATAAAGAAAGAGAATATAAAGTA
6HB_JV39	GATTTAGAAGTATTAAGGGTTAGAACCTGACGACGACAATAA
6HB_JV40	ATTAAATCCTTTGCCAATATAATCCTGACCTGTTTATCAACA
6HB_JV41	GTAACATTATCATTAATTATCATCATATTATCCCATCCTAAT
6HB_JV42	TCAACCGTTCTAGCAAAGGCCGGAGACAGCCGGAACGAGGCG

6HB_JV43	ATTTTTGAGAGATCCAATGCCTGAGTAATGACCAACTTTGAA
6HB_JV44	AGTCTGGAGCAAACCGCAAGGATAAAAAGGCGCATAGGCTGG
6HB_JV45	ACTAGCATGTCAATTATGACCCTGTAATAGAACCGGATATTC
6HB_JV46	AGCCCCAAAAACAGAAGCCTCAGAGCATTCATTCAGTGAATA
6HB_JV47	GTAAACGTTAATATAATCATACAGGCAACGAGTAGTAAATTG
6HB_JV48	TAAATCAGCTCATTTGGCATCAATTCTAATCATTGTGAATTA
6HB_JV49	TAATTCGCGTCTGGCCTGTTTAGCTATATATACCAGTCAGGA
6HB_JV50	TAAATGTGAGCGAGATTTAGTTTGACCAAACGAACTAACGGA
6HB_JV51	CAAACGGCGGATTGCATTCCATATAACATCAGTTGAGATTTA
6HB_JV52	AGATGGGCGCATCGCATGTTTTAAATATCATAACGCCAAAAG
6HB_JV53	CGACGACAGTATCGATGGCTTAGAGCTTTATCATAACCCTCG
6HB_JV54	TTTCCGGCACCGCTGTACCTTTAATTGCAGCGAGAGGCTTTT
6HB_JV55	ATTCGCCATTCAGGGAACCAGACCGGAATAGTAAAATGTTTA
6HB_JV56	TGCGGGCCTCTTCGCGAAAGACTTCAAACGTCATAAATATTC
6HB_JV57	GTGCTGCAAGGCGACAGAAGCAAAGCGGGTTCAGAAAACGAG
6HB_JV58	AAGAGTCAATAGTGAGTAATAAAAGGGAGGATTATTTACATTGGCAGATTCACC
6HB_JV59	AATCCTTGAAAACACTGACCTGAAAGCGCTCATGGAAATACC
6HB_JV60	CTTGCTTCTGTAAATGAATGGCTATTAGTCCAGAACAATATT
6HB_JV61	TAATGGAAACAGTAAACATCGCCATTAAGCCTGAGTAGAAGA
6HB_JV62	AAAATTAATTACATTAAAACAGAGGTGAACCGTTGTAGCAAT
6HB_JV63	TACCTGAGCAAAAGAGTGCCACGCTGAGGTGAGGCCACCGAG
6HB_JV64	CCAAGTTACAAAATATCACCTTGCTGAAAGGAACGGTACGCC
6HB_JV65	ATCGGGAGAAACAACTGGTCAGTTGGCAGAGCGGGAGCTAAA
6HB_JV66	AGGTTTAACGTCAGGTTATCTAAAATATGCTTTGACGAGCAC
6HB_JV67	ATTTGCACGTAAAAAGAGCCGTCAATAGCCGCCGCGCTTAAT
6HB_JV68	CTTCTGAATAATGGAGACTTTACAAACACGCTGGCAAGTGTA
6HB_JV69	TGATGGCAATTCATCCGAACGTTATTAACGAGAAAGGAAGGG
6HB_JV70	ACCAGAAGGAGCGGTTGCGGAACAAAGAGCCCCCGATTTAGA
6HB_JV71	TTCAAAAGGGTGAGTGATAAATTAATGCGGTCGAGGTGCCGT
6HB_JV72	ATATATTTTAAATGTACAAAGGCTATCAATGGCCCACTACGT
6HB_JV73	AGCCTTTATTTCAAAAGAGAATCGATGAGAACGTGGACTCCA
6HB_JV74	TGTACCAAAAACATCATATGTACCCCGGGTTGAGTGTTGTTC
6HB_JV75	AAAATTAAGCAATAGAAGATTGTATAAGCGGCAAAATCCCTT
6HB_JV76	ATTAACATCCAATATTTGTTAAAATTCGGCCCCAGCAGGCGA
6HB_JV77	GCGAGCTGAAAAGGTTTTAACCAATAGGCCTGGCCCTGAGAG
6HB_JV78	CAAATGGTCAATAACCTTCCTGTAGCCATTTTCACCAGTGAG
6HB_JV79	CTGCGAACGAGTAGTAACAACCCGTCGGGGGGAGAGGCGGTT
6HB_JV80	GTGTCTGGAAGTTTACCGTAATGGGATAAAACCTGTCGTGCC
6HB_JV81	ATGCTGTAGCTCAATAACCGTGCATCTGCACATTAATTGCGT
6HB_JV82	GGTCATTTTTGCGGGCCTCAGGAAGATCCATAAAGTGTAAAG
6HB_JV83	GTCAGGATTAGAGATCTGGTGCCGGAAATTGTTATCCGCTCA
6HB_JV84	TCGAGCTTCAAAGCCTGCGCAACTGTTGCTCGAATTCGTAAT
6HB_JV85	ATTAAGAGGAAGCCCTATTACGCCAGCTGCATGCCTGCAGGT
6HB_JV86	GTCTTTACCCTGACTATTATAGTTTAAGTTGGGTAACGCCAG
6HB_JV87	AAATCATAGGTCTGAGAGACTACAATTGAGTTAAGCCCAATA

6HB_JV88	ATATAACTATATGTAGAGGGTAATTGAGCTTTTTAAGAAAAG
6HB_JV89	CAAAGAACGCGAGACGCATTAGACGGGAAAGGAAACCGAGGA
6HB_JV90	TTCATCTTCTGACCAATAGCAGCCTTTAAACTGGCATGATTA
6HB_JV91	TGTGATAAATAAGGATCCAAATAAGAAAAACGTAGAAAATAC
6HB_JV92	TAATTACTAGAAAAAATTTGCCAGTTACAACGCAAAGACACC
6HB_JV93	AAATTCTTACCAGTTCCTGAATCTTACCATAGAAAATTCATA
6HB_JV94	AATTGAGAATCGCCAAATCAAGATTAGTCGACATTCAACCGA
6HB_JV95	GGCAGAGGCATTTTGTTTTAGCGAACCTAAATTATTCATTAA
6HB_JV96	CCGACAAAAGGTAATCAGATATAGAAGGGCCATTTGGGAATT
6HB_JV97	ACAACATGTTCAGCTTTTCATCGTAGGATTACCATTAGCAAG
6HB_JV98	ATAGATAAGTCCTGAACCAAGTACCGCAATAGCAGCACCGTA
6HB_JV99	TTACGAGCATGTAGATAATCGGCTGTCTTTAGCGTCAGACTG
6HB_JV100	CAGACGGTCAATCAGCCTGATAAATTGTATAGCCCCCTTATT
6HB_JV101	AGAGGACAGATGAAATACCAAGCGCGAATCACCGGAACCAGA
6HB_JV102	CTGACCTTCATCAAAAAGAATACACTACCGCCACCCTCAGA
6HB_JV103	ATTACCCAAATCAACGTAATGCCACTACGAGCCGCCACCAGA
6HB_JV104	AGGCTTGCCCTGACAAGACTTTTTCATGACAGGAGGTTGAGG
6HB_JV105	GGCTTGAGATGGTTTCGGAACGAGGGTACAAACAAATAAATC
6HB_JV106	CCTTATGCGATTTTCCGCTTTTGCGGGATCTCTGAATTTACC
6HB_JV107	CGTTGGGAAGAAAAAACCGATATATTCGGATGATACAGGAGT
6HB_JV108	ACAACATTATTACACGATAGTTGCGCCGGTGCCTTGAGTAAC
6HB_JV109	GGAATACCACATTCATCAGCTTGCTTTCTGCCTATTTCGGAA
6HB_JV110	GAATTACGAGGCATCAAAAAAAGGCTCAGAGGCTGAGACTC
6HB_JV111	TTTACCAGACGACGTAAAGGAATTGCGATTTTGCTCAGTACC
6HB_JV112	GCAAAGAAGTTTTACTTTCAACAGTTTATATAAGTATAGCC
6HB_JV113	GACTGGATAGCGTCGACGTTAGTAAATGGGTTTAGTACCGCC
6HB_JV114	ATTGAATCCCCCTCCTCATAGTTAGCGTCCACCCTCAGAGCC
6HB_JV115	AATGACCATAAATCACCAGTACAAACTACCAATAGGAACCCA TGTACCGTAACA
6HB_JV116	AGATAACCCACAAGCTTTTTAACCTCCGATTAAGACGCTGAG
6HB_JV117	CCCTGAACAAAGTCAAATGCTGATGCAATAATTTTCCCTTAG
6HB_JV118	TAAAAACAGGGAAGAAACTTTTTCAAATTGTGAGTGAATAAC
6HB_JV119	ACGTCAAAAATGAATAAATTTAATGGTTTGAATTACCTTTTT
6HB_JV120	TATTATTTATCCCACGTTAAATAAGAATAACATCAAGAAAAC
6HB_JV121	TCTTTCCAGAGCCTAGCCTGTTTAGTATTTATTCATTTCAAT
6HB_JV122	CAGCTACAATTTTAATAAAGCCAACGCTGATTGCTTTGAATA
6HB_JV123	GGTTTTGAAGCCTTATATTTAACAACGCACAGTACCTTTTAC
6HB_JV124	TAAGAACGCGAGGCCGAGCCAGTAATAATTGCGTAGATTTTC
6HB_JV125	CAATAGCAAGCAAAAGTAATTCTGTCCAACCATATCAAAATT
6HB_JV126	GCAAGCCGTTTTTATAATGCAGAACGCGTTGTTTGGATTATA
6HB_JV127	AAGAACGGGTATTAAACAAGAAAAATAATCCTGATTATCAGA
6HB_JV128	CCTGCTCCAAATCAAAACCTGTTACTTAGTCAAATCACCACC
6HB_JV129	AGATTTGTATCATCTAAGGGAACCGAACTGTGTAGGTAAAGA
6HB_JV130	GACCCCCAGCGATTCGGTGTACAGACCATTTTTAGAACCCTC
6HB_JV131	AAAACGAAAGAGGCGAGTAATCTTGACAACTTTTGCGGGAGA
6HB_JV132	AAACGGGTAAAATACGTAACAAAGCTGCAAAGCTAAATCGGT

6HB_JV133	GGCTTTGAGGACTAGAGAAACACCAGAAGGCAAAGAATTAGC
6HB_JV134	CAGGGAGTTAAAGGAAGAACTGGCTCATTTTTCATTTGGGGC
6HB_JV135	CATCGCCCACGCATATCTACGTTAATAATTAGATACATTTCG
6HB_JV136	AAACAGCTTGATACGGTAGAAAGATTCAGTTGATTCCCAATT
6HB_JV137	AATTGTATCGGTTTAACTAATGCAGATAGCAACTAAAGTACG
6HB_JV138	ACGTTGAAAATCTCAGTAAGAGCAACACAATTGCTGAATATA
6HB_JV139	TAGAAAGGAACAACATAAAAACCAAAATTCCTTTTGATAAGA
6HB_JV140	GATTTTGCTAAACAGCCAGAGGGGGTAAGCAAACTCCAACAG
6HB_JV141	TTGTCGTCTTTCCACAATACTGCGGAATTATCGCGTTTTAAT
6HB_JV142	TTCCACAGACAGCCAAATGCTTTAAACAATTGCATCAAAAAG
6HB_JV143	CTGAGTTTCGTCAAAAATCAG
6HB_JV144	AGCGAAAGACAGCATAATTTCAACTTTACTAATAGTAGTAGC
6HB_JV145	ATAAGAGCAAGAAACAATGAAATAGCAATAGCTCAATCG TCTGAAATCATTCTGGCCAACA
6HB_JV146	TAAGCAGATAGCCGCAACAGGAAAAACGTAAGAATACGTGGC
6HB_JV147	AACGCAATAATAACCCTTGCTGGTAATATCTTTAATGCGCGA
6HB_JV148	AGACTCCTTATTACTAATAACATCACTTAAATACCGAACGAA
6HB_JV149	ATACATAAAGGTGGCATCACGCAAATTAGGCGGTCAGTATTA
6HB_JV150	ACGGAATAAGTTTATGTTTTTATAATCAAGCCAGCAGCAAAT
6HB_JV151	TGGTTTACCAGCGCAAGGGATTTTAGACCCTCAAATATCAAA
6HB_JV152	TTGAGGGAGGGAAGCCTCGTTAGAATCAAATCAACAGTTGAA
6HB_JV153	AGGTGAATTATCACCGCGTACTATGGTTCTTTAGGAGCACTA
6HB_JV154	AGAGCCAGCAAAATCGTAACCACCACACATAATACATTTGAG
6HB_JV155	GCCGGAAACGTCACAGCGGGCGCTAGGGATTCGACAACTCGT
6HB_JV156	ATCAGTAGCGACAGGCCGGCGAACGTGGTTTTAAAAGTTTGA
6HB_JV157	TAGCGCGTTTTCATGAACCCTAAAGGGAAATCAATATGATAT
6HB_JV158	AGCGTTTGCCATCTATCAAGTTTTTTGGCGGAGAGGGTAGCT
6HB_JV159	GCCACCACCGGAACAAAACCGTCTATCAGGTCATTGCCTGAG
6HB_JV160	ACCGCCACCCTCAGAGTCCACTATTAAAACGGTAATCGTAAA
6HB_JV161	ACCACCACCAGAGCTAGCCCGAGATAGGTTGATAATCAGAAA
6HB_JV162	CAGGTCAGACGATTGGTGGTTCCGAAATCAAATATTTAAATT
6HB_JV163	CTCATTAAAGCCAGGTCCACGCTGGTTTCATTAAATTTTTGT
6HB_JV164	GTTCCAGTAAGCGTATTGCCCTTCACCGAACGCCATCAAAAA
6HB_JV165	GTACTGGTAATAAGCAGGGTGGTTTTTCGCTTTCATCAACAT
6HB_JV166	AGTGCCCGTATAAAATCGGCCAACGCGCATTCTCCGTGGGAA
6HB_JV167	CCTATTATTCTGAAGCTTTCCAGTCGGGGGTCACGTTGGTGT
6HB_JV168	CTCAAGAGAAGGATTGAGTGAGCTAACTCCAGTTTGAGGGGA
6HB_JV169	AGGCGGATAAGTGCATACGAGCCGGAAGGCACTCCAGCCAGC
6HB_JV170	CGGAATAGGTGTATTTTCCTGTGTGAAACCAGGCAAAGCGCC
6HB_JV171	ACCCTCAGAACCGCCCCCGGGTACCGAGGGAAGGGCGATCGG
6HB_JV172	ACCACCCTCATTTTCCAGTGCCAAGCTTGGCGAAAGGGGGAT

Supplementary Table 4. AFM analysis of Qdot attachment on the DNA origami path. Total number and percentage of DNA path structures with 0, 1, 2 and 3 Qdot attached at different time points (0, 20, 40 and 150 min) during the transcription of the catenane walkers with 210-bp and 126-bp rotors, as well as the non-transcription control.

	Time (min)	Nº of structures				% of structures			
		with 0 Qdots	with 1 Qdot	with 2 Qdots	with 3 Qdots	with 0 Qdots	with 1 Qdot	with 2 Qdots	with 3 Qdots
Transcription with Catenane walker (210-bp rotor)	**0**	4	17	30	8	6,8	28,8	50,8	13,6
	20	32	46	20	2	32,0	46,0	20,0	2,0
	40	36	28	7	0	50,7	39,4	9,9	0,0
	150	62	11	1	0	83,8	14,9	1,4	0,0
No transcription control	**0**	7	38	43	9	7,2	39,2	44,3	9,3
	20	9	29	49	9	9,4	30,2	51,0	9,4
	40	4	15	18	7	9,1	34,1	40,9	15,9
	150	6	45	79	13	4,2	31,5	55,2	9,1
Transcription with Catenane walker (126-bp rotor)	**0**	2	28	18	5	3,8	52,8	34,0	9,4
	20	19	33	10	1	30,2	52,4	15,9	1,6
	40	25	9	2	1	67,6	24,3	5,4	2,7
	150	56	15	1	0	77,8	20,8	1,4	0,0

Supplementary Table 5. Quantification of Qdot specific attachment on the different iSteps of the DNA origami path by AFM imaging analysis. Total number and percentage of Qdot attached on the different iStep positions at different time points (0, 20, 40 and 150 min) during the transcription of the catenane walkers with 210-bp and 126-bp rotors, respectively, as well as the non-transcription control.

	Time (min)	Nº of Qdots in position			% of Qdots in position		
		#1	#2	#3	#1	#2	#3
Transcription with Catenane walker (210-bp rotor)	0	35	26	40	59,3	44,1	67,8
	20	15	41	36	15,0	41,0	36,0
	40	4	21	11	5,6	29,6	15,5
	150	5	5	3	6,8	6,8	4,1
No transcription control	0	47	46	74	54,2	22,9	25,0
	20	50	48	56	52,1	50,0	58,3
	40	20	23	29	45,5	52,3	65,9
	150	56	95	91	39,2	66,4	63,6
Transcription with Catenane walker (126-bp rotor)	0	17	33	29	32,1	62,3	54,7
	20	9	30	17	14,3	47,6	27,0
	40	4	7	5	10,8	18,9	13,5
	150	6	8	3	8,3	11,1	4,2

References:

1   Zadeh, J. N. *et al.* NUPACK: Analysis and design of nucleic acid systems. *J Comput Chem* **32**, 170-173, doi:10.1002/jcc.21596 (2011).

2   Mathews, D. H., Sabina, J., Zuker, M. & Turner, D. H. Expanded sequence dependence of thermodynamic parameters improves prediction of RNA secondary structure. *J Mol Biol* **288**, 911-940, doi:10.1006/jmbi.1999.2700 (1999).

3   Douglas, S. M. *et al.* Rapid prototyping of 3D DNA-origami shapes with caDNAno. *Nucleic Acids Res.* **37**, 5001-5006, doi:10.1093/nar/gkp436 (2009).